Physics Library
QC1
.U56
APR 11 1961

Volume 65A
Number 2
Mar.–Apr. 1961

Physics and Chemistry

SECTION A

JOURNAL OF RESEARCH

NATIONAL BUREAU OF STANDARDS

Journal of Research

of the

National Bureau of Standards

A. Physics and Chemistry

MAR.–APR. • 1961

VOLUME • 65A

NUMBER • 2

Editor: U. Fano

Associate Editors: L. M. Kushner
J. M. Richardson

Publication dates:
Feb. 1, Apr. 1, June 1, Aug. 1, Oct. 1, Dec. 1, 1961.

JOURNAL OF RESEARCH

The National Bureau of Standards Journal of Research reports research and development in the fields of activity shown at right. Also included from time to time are survey articles on topics closely related to the Bureau's scientific and technical program.

The Journal is published in four separate sections as follows:

A. Physics and Chemistry

Contains papers of interest primarily to scientists working in these fields. Issued six times a year. Annual subscription: domestic, $4.00; foreign, $4.75.

B. Mathematics and Mathematical Physics

Presents studies and compilations designed mainly for the mathematician and the theoretical physicist. Issued quarterly. Annual subscription: domestic, $2.25; foreign, $2.75.

C. Engineering and Instrumentation

Reports research and development results of interest chiefly to the engineer and the applied scientist. Issued quarterly. Annual subscription: domestic, $2.25; foreign, $2.75.

D. Radio Propagation

Reports work in radio propagation, upper atmospheric physics, and communications. Issued six times a year. Annual subscription: domestic, $4.00; foreign, $4.75.

U.S. DEPARTMENT OF COMMERCE
Luther H. Hodges, Secretary

NATIONAL BUREAU OF STANDARDS
A. V. Astin, Director

Functions and Activities

The functions of the National Bureau of Standards are set forth in the Act of Congress, March 3, 1901, as amended. These include the development and maintenance of the national standards of measurement and the provision of means and methods for making measurements consistent with these standards; the determination of physical constants and properties of materials; the development of methods and instruments for testing materials, devices, and structures; advisory services to government agencies on scientific and technical problems; invention and development of devices to serve special needs of the Government; and the development of standard practices, codes, and specifications. The work includes basic and applied research, development, engineering, instrumentation, testing, evaluation, calibration services, and various consultation and information services. The Bureau also serves as the Federal technical research center in a number of specialized fields. The scope of activities of the National Bureau of Standards is suggested in the following listing of the divisions and sections engaged in technical work.

Washington, D.C.

Electricity. Resistance and Reactance. Electrochemistry. Electrical Instruments. Magnetic Measurements. Dielectrics.

Metrology. Photometry and Colorimetry. Refractometry. Photographic Research. Length. Engineering Metrology. Mass and Scale. Volumetry and Densimetry.

Heat. Temperature Physics. Heat Measurement. Cryogenic Physics. Equation of State. Statistical Physics.

Radiation Physics. X-ray. Radioactivity. Radiation Theory. High Energy Radiation. Radiological Equipment. Nucleonic Instrumentation. Neutron Physics.

Analytical and Inorganic Chemistry. Pure Substances. Spectrochemistry. Solution Chemistry. Analytical Chemistry. Inorganic Chemistry.

Mechanics. Sound. Pressure and Vacuum. Fluid Mechanics. Engineering Mechanics. Rheology. Combustion Controls.

Organic and Fibrous Materials. Rubber. Textiles. Paper. Leather. Testing and Specifications. Polymer Structure. Plastics. Dental Research.

Metallurgy. Thermal Metallurgy. Chemical Metallurgy. Mechanical Metallurgy. Corrosion. Metal Physics. Electrodeposition.

Mineral Products. Engineering Ceramics. Glass. Refractories. Enameled Metals. Crystal Growth. Constitution and Microstructure.

Building Research. Structural Engineering. Fire Research. Mechanical Systems. Organic Building Materials. Codes and Safety Standards. Heat Transfer. Inorganic Building Materials.

Applied Mathematics. Numerical Analysis Computation. Statistical Engineering. Mathematical Physics.

Data Processing Systems. SEAC Engineering Group. Components and Techniques. Digital Circuitry. Digital Systems. Analog Systems. Applications Engineering.

Atomic Physics. Spectroscopy. Radiometry. Solid State Physics. Electron Physics. Atomic Physics.

Instrumentation. Engineering Electronics. Electron Devices. Electronic Instrumentation. Mechanical Instruments. Basic Instrumentation.

Physical Chemistry. Thermochemistry. Surface Chemistry. Organic Chemistry. Molecular Spectroscopy. Molecular Kinetics. Mass Spectrometry. Molecular Structure and Radiation Chemistry.

• Office of Weights and Measures.

Boulder, Colorado

Cryogenic Engineering. Cryogenic Equipment. Cryogenic Processes. Properties of Materials. Gas Liquefaction.

Ionosphere Research and Propagation. Low Frequency and Very Low Frequency Research. Ionosphere Research. Prediction Services. Sun-Earth Relationships. Field Engineering. Radio Warning Services.

Radio Propagation Engineering. Data Reduction Instrumentation. Radio Noise. Tropospheric Measurements. Tropospheric Analysis. Propagation-Terrain Effects. Radio-Meteorology. Lower Atmosphere Physics.

Radio Standards. High Frequency Electrical Standards. Radio Broadcast Service. Radio and Microwave Materials. Atomic Frequency and Time Interval Standards. Electronic Calibration Center. Millimeter-Wave Research. Microwave Circuit Standards.

Radio Systems. High Frequency and Very High Frequency Research. Modulation Research. Antenna Research. Navigation Systems. Space Telecommunications.

Upper Atmosphere and Space Physics. Upper Atmosphere and Plasma Physics. Ionosphere and Exosphere Scatter. Airglow and Aurora. Ionospheric Radio Astronomy.

Order all publications from the Superintendent of Documents
U.S. Government Printing Office, Washington 25, D.C.

Use of funds for printing this publication approved by the Director of the Bureau of the Budget (June 24, 1958).

JOURNAL OF RESEARCH of the National Bureau of Standards—A. Physics and Chemistry
Vol. 65A, No. 2, March–April 1961

Mass Spectra of Some Deuteroethanes

Edith I. Quinn [1] and Fred L. Mohler [2]

(November 11, 1960)

Mass spectra of seven of the nine possible deuteroethanes have been measured. When the patterns are computed on a scale to make the sums of ions equal, it is found that the abundances of molecule ions differ nearly twofold in the different molecules, and there are large differences in the patterns of the two $C_2H_4D_2$ molecules. The peaks in the C_1 range are compared with the patterns predicted for simple breaking of the C—C bond and dissociation of the methyl radicals. The "weighting factors" for removing H and D, HD, and 2D, etc., from C_2HD_5 are computed and also the weighting factors for H^+ and D^+ for all the deuteroethanes are given.

1. Introduction

While there is a rather extensive literature on mass spectra of deuterohydrocarbons, published data on deuteroethanes are fragmentary. Schissler, Thompson, and Turkevich [1] [3] published mass spectra of four deuteroethanes in 1951 in the mass range 12 to 36 and Dibeler [2] published a mass spectrum of C_2D_6 of good purity.

We were able to obtain samples of seven of the nine possible deuteroethanes. Two of these were synthesized by M. deHemptinne of the University of Louvain and the others were purchased from Merck Inc. Mass spectra were recorded with a 180 ° Consolidated model 21-103 mass spectrometer following standard operating procedures. The ionizing voltage is 70 v except as noted below.

2. Results

The samples were all of good chemical purity and an isotopic analysis was made by recording the spectrum at an ionizing voltage low enough to give molecule ions but not fragment ions [3]. Table 1 lists the seven deuteroethanes, the isotopic analysis and the source of the samples. This is a difficult analysis for ethane as the appearance potentials of the fragment ions are close to the ionization potential of the molecule. Field and Franklin [4] give appearance potentials as follows: $C_2H_6^+$, 11.6 ev, $C_2H_5^+$, 12.8 ev; and $C_2H_4^+$, 12.1 ev. This makes the measurement insensitive. (The impurity with one less D atom than the sample may be uncertain by 10 percent of the stated amount.) The mole percent impurities listed are consistent with the purity reported by Merck in round numbers as 98 and 99 atom percent.

[1] Mrs. Lile F. Davis, State College of Technology, Beaumont, Texas.
[2] Consultant, National Bureau of Standards.
[3] Figures in brackets indicate the literature references at the end of this paper.

TABLE 1. *Mole percent impurities in deuteroethanes*

Sample	Impurity	Mole percent	Source
C_2H_5D	C_2H_6	3.6	deHemptinne.
	$C_2H_4D_2$	1.4	
$CHD_2{\cdot}CH_3$	C_2H_5D	3.2	Merck Inc.
$CH_2D{\cdot}CH_2D$	C_2H_5D	1.2	Merck Inc.
	$C_2H_3D_3$	.3	
$CH_3{\cdot}CD_3$	$C_2H_4D_2$	5.0	Merck Inc.
$CHD_2{\cdot}CHD_2$	$C_2H_3D_3$	2.7	Merck Inc.
	C_2HD_5	.2	
C_2HD_5	$C_2H_2D_4$	6.2	deHemptinne.
	C_2D_6	.4	
C_2D_6	C_2HD_5	4.0	Merck Inc.

Table 2 gives the mass spectra of C_2H_6 and the seven deuteroethanes. The contributions of ions containing C^{13} and of isotopic impurities from table 1 have been subtracted from the spectra. The patterns of the different molecules have been normalized in an unconventional manner. It seemed logical to present the spectra on a scale to make the parent ion abundances all equal but when this is done it is found that there is a wide variation in the sums of all the ions in the spectrum. It seems unlikely that there is a wide variation in the total ionization of molecules that differ only in the isotopic masses of the atoms although difference of mass distribution will change the pattern of dissociation. In table 2 the patterns are on a scale to make the sums of the ions equal to the sum for C_2H_6 with the conventional scale of abundances used for the C_2H_6 pattern.

It is evident that on this scale there is a wide variation of the abundances of the molecule ions. It ranges from 13.0 for $CH_3{\cdot}CD_3$ to 23.0 for C_2H_5D. Both of the highly unsymmetrical molecules $CH_3{\cdot}CD_3$ and $CH_3{\cdot}CHD_2$ give low values of the molecule ion. There are many other conspicuous differences between the mass spectra of the symmetrical and unsymmetrical molecules of $C_2H_4D_2$ in columns 4 and 5.

TABLE 2. *Mass spectra of deuteroethanes on a scale to make the sums of ions equal*

M/e	C_2H_6	C_2H_5D	CH_3D-CH_3D	CHD_2-CH_3	CH_3-CD_3	CHD_2-CHD_2	C_2HD_5	C_2D_6
1	4.11	5.04	3.98	4.63	3.72	2.26	1.13	------
2	.46	.84	.92	.95	1.24	1.56	1.98	2.61
3	------	.12	.27	.13	------	.22	.11	------
4	------	------	.04	.03	------	.07	.14	.18
12	.90	1.02	.95	1.39	1.31	1.03	1.18	1.16
13	1.74	1.55	1.04	1.92	1.41	.39	.27	------
14	4.12	2.26	2.07	3.60	2.96	1.86	2.32	2.60
15	5.87	5.12	3.41	3.16	3.17	2.28	1.12	------
16	------	3.19	5.43	1.19	1.87	2.63	3.53	5.63
17	------	------	.32	1.84	.88	5.60	2.79	------
18	------	------	------	------	1.69	.26	3.08	6.21
24	1.09	1.00	.92	1.63	1.33	.82	.76	.73
25	5.16	4.00	2.36	4.71	2.66	.84	.89	------
26	26.2	13.4	9.03	21.1	12.0	3.97	3.71	4.02
27	36.8	24.3	17.1	29.5	19.6	10.0	5.39	------
28	100	42.3	32.0	43.1	28.6	18.3	20.3	24.1
29	19.3	84.1	54.6	49.4	41.8	19.0	12.4	------
30	22.1	15.9	59.8	35.1	66.0	45.5	19.6	31.2
31	------	23.0	14.3	10.5	14.0	58.2	66.8	------
32	------	------	19.1	13.5	10.6	26.5	45.7	113.5
33	------	------	------	------	13.0	8.7	12.4	------
34	------	------	------	------	------	18.0	4.79	17.1
35	------	------	------	------	------	------	17.4	------
36	------	------	------	------	------	------	------	18.7
13.5	.06	.09	------	.09	.04	------	------	------
14.5	.54	.84	.47	.35	.26	.03	------	------
15.5	------	.01	.36	.24	.37	.59	.57	------
16.5	------	------	------	------	------	.20	.24	------

As a general rule the removal of D atoms from deuterohydrocarbons is less probable than the removal of H but C_2D_6 affords a notable exception. The $C_2D_4^+$ ion has an abundance of 113.5 as compared with 100 for $C_2H_4^+$ of C_2H_6. In the patterns of ethanes containing H and D two different ions contribute to many of the peaks. Thus $C_2H_2^+$ and C_2D^+ contribute to mass 26, $C_2H_3^+$ and C_2HD^+ to 27 etc. In the deuteroethane spectra there is no safe basis for computing the relative probability of removing H and D or several H and D atoms except in the C_2HD_5 spectrum. In that spectrum each peak comes from a single isotopic fragment ion.

Table 3 gives in the third column the pattern of C_2HD_5 with the peaks grouped in pairs of ions containing 1, 2, 3, etc., hydrogenic atoms. The sums of these pairs in column 4 give the relative probability of removing one to five atoms. This times the a'priori probability gives, in column 6, the pattern predicted if removal of H and D were random. The experimental values divided by the theoretical give the "weighting factors" for removing H and D atoms and all possible combinations of these. It is seen that except for the 25, 26 pair, ions involving loss of the H atom have a weight factor greater than one and the otners less than one. This is qualitatively consistent with experiments with other deuterohydrocarbons. The weighting factors for removing H and D, 1.67 and 0.86 are of the magnitudes found for CHD_3 [5] and C_2HD_3 [6]. There is, however, no regular trend in weighting factors for removing 1, 2, 3, etc., atoms from C_2HD_5 such as was found in the deuteroethylene spectra [6].

TABLE 3. *Pattern of C_2HD_5 and theoretical pattern in C_2 range*

M/e	Ions	Pattern	Sums of [a] pairs	a'priori probability	Theoretical [b]	Weight [c] factor	C_2D_6 pattern
24	C_2	0.76	(0.76)	1	0.76	------	0.73
25	C_2H	.89	------	1/6	.77	1.15	------
26	C_2D	3.71	4.60	5/6	3.83	.97	4.02
27	C_2HD	5.39	------	1/3	8.57	.63	------
28	C_2D_2	20.3	25.7	2/3	7.13	1.18	24.1
29	C_2HD_2	12.4	------	1/2	16.0	.78	------
30	C_2D_3	19.6	32.0	1/2	16.0	1.22	31.2
31	C_2HD_3	66.8	------	2/3	75.	.89	------
32	C_2D_4	45.7	112.5	1/2	37.5	1.22	113.5
33	C_2HD_4	12.4	------	5/6	14.3	.86	------
34	C_2D_5	4.79	17.2	1/6	2.87	1.67	17.1
35	C_2HD_5	17.4	(17.4)	1	17.4	1.00	------
------	------	------	------	------	------	C_2D_6	18.7

[a] The sums of the indicated pairs give the relative abundance of ions with 1 to 5 hydrogenic atoms.
[b] This column gives the a'priori probability, times the abundances of column 4.
[c] This gives the ratio of the observed pattern and the theoretical pattern.

The last column of table 3 the observed pattern of C_2D_6 is given and it is quite similar to the "sums of pairs" of C_2HD_5 in column 4. It is not surprising that C_2HD_5 is more like C_2D_6 than C_2H_6.

The ions in the mass 12 to 18 range (table 2) involve breaking the C—C bond and if this bond breaks without rearrangement of H and D atoms there will be a simple relation between patterns of unsymmetrical molecules and patterns of two symmetrical molecules. Thus the CH_3·CD_3 fragment ions in the C_1 range will involve contributions from CH_3 and from CD_3 as given by the C_2H_6 and C_2D_6 patterns. However the observed pattern shows a small 17 peak from CHD_2^+ so there is some rearrangement.

Table 4 compares the observed patterns for unsymmetrical molecules in the C_1 range and the patterns computed from the spectra of two symmetrical molecules. The last two rows give the basis of computation. Thus the CH_3·CH_2D pattern is compared with 0.59 times the patterns of CH_2D·CH_2D plus 0.53 times the pattern of C_2H_6. In some cases as in the CHD_2·CD_3 spectrum there is fairly good agreement between the observed and computed spectra while in CH_3·CHD_2 the agreement is poor. In the CH_3·CD_3 pattern there is a peak at 17 that comes from the rearrangement giving CHD_2^+ and CH_2D and the residual on the 16 peak comes from the same rearrangement with the charge on CH_2D.

TABLE 4. *Mass spectra in the C_1 range and computed values* [a]

M/e	C_2H_5D		CH_3·CHD_2		CH_3·CD_3		C_2HD_2·CD_3	
	exp.	comp.	exp.	comp.	exp.	comp.	exp.	comp.
12	1.02	1.04	1.39	0.71	1.31	0.81	1.18	1.06
13	1.55	1.54	1.92	.85	1.41	.94	.27	.19
14	2.26	3.41	3.60	2.31	2.96	2.94	2.32	2.16
15	5.12	5.12	3.16	3.16	3.17	3.17	1.12	1.13
16	3.19	3.19	1.19	.87	1.87	1.53	3.53	3.99
17	------	(.19)	1.84	1.84 *	.88	------	2.79	2.79
18	------	------	------	(.09)	1.69	1.69	3.08	3.08
Comp. from	.59×CH_2D .53×CH_3		.33×CHD_2 .41×CH_3		.272×CD_3 .540×CH_3		.475×CD_3 .50×CHD_2	

[a] Mass spectra of unsymmetrical molecules are computed from symmetrical molecules on the assumption that these ions come from breaking of the C—C bond without rearrangement of H atoms.

TABLE 5. *Hydrogenic ions*

	C_2H_6	C_2H_5D	CH_2D CH_2D	CHD_2 CH_3	CH_3 CD_3	CHD_2 CHD_2	C_2HD_5	C_2D_6
H^+	4.11	5.04	3.98	4.63	3.72	2.26	1.13	
D^+		.60	.72	.85	1.24	1.53	1.98	2.61
Weight Factor								
For H		1.07	1.27	1.26	1.50	1.79	2.17	
For D		.64	.46	.46	.50	.61	.76	(.63)

Table 5 gives the observed H^+ and D^+ ions and weighting factors for H^+ and D^+. A small but rather uncertain correction for H_2^+ has been made to the mass 2 peaks of table 2. The weighting factor is computed from the observed value divided by $H^+ + D^+$) times the apriori probability. In C_2D_6 it is simply the ratio of D^+ of C_2D_6 to H^+ of C_2H_6. There is a progressive increase in the weighting factor for H^+ as the number of D atoms in the atom increases. The factors for D^+ do not change progressively.

Table 2 includes some small half integer peaks that come from doubly charged ions of mass 27, 29, 31, and 33. Doubly charged ions of even mass number are masked by singly charged ions. The more abundant ions contain 4 and 5 hydrogenic atoms. In the case of C_2HD_5 the relative abundance of the pairs of ions containing 4 or 5 hydrogenic atoms can be computed if it is assumed that the same weighting factors apply in doubly and singly charged ions. Peak 15.5 of abundance 0.57 comes from $C_2HD_3^{++}$ and from table 3, $C_2D_4^{++}$ will have an abundance of about 0.39. The abundance of the pair is 0.96. The 16.5 peak of abundance 0.24 is $C_2HD_4^{++}$. $C_2D_5^{++}$ is about 0.09 and the abundance of the pair of ions with 5 hydrogenic ions is 0.33. The abundance of $C_2H_5^{++}$ of C_2H_6 is 0.54.

The doubly charged ions of C_2HD_5 make contributions of about 0.39 to the 16 peak and 0.09 to the 17 peak on the basis of the above assumptions. There is no good basis for computing contributions of doubly charged ions to the 14, 15, 16, and 17 peaks of other deuteroethanes but they are a source of experimental uncertainty in the data of table 4. In the case of C_2H_6 the abundance of $C_2H_4^{++}$ will be approximately like that of the pair of ions from C_2HD_5 of abundance 0.96.

(Paper 65A2–89)

3. Summary

The mass spectra of deuteroethylenes [6] and deuteromethanes [5] show a regular trend in the probability of removing H and D atoms from molecules with increasing numbers of D atoms in the molecule. In the C_2 range there is no appreciable difference between the patterns of symmetrical and unsymmetrical dideuteroethylenes. In these molecules it is logical to compute "weighting factors" on the basis of the C_2H_4 or CH_4 spectra. In the case of the ethanes there is no regular trend. There are large differences in the relative abundance of molecule ions and there are striking differences between symmetrical and unsymmetrical molecules. Only in the case of the C_2HD_5 pattern is there a logical basis for computing weighting factors for removing H and D.

It is consistent with the statistical theory of mass spectra of polyatomic molecules [7] that there will be some differences in patterns of deuteroethanes because of differences in vibration levels of D and H atoms. This is a complicated problem and beyond the scope of this paper.

It will be of interest to obtain the patterns of the other deuteroethanes, $CH_2D{\cdot}CHD_2$ and $CH_2D{\cdot}CD_3$ for these undoubtedly differ from the isomers available for this study. This is needed for analytical purposes. For instance there is a small uncertainty in this work because $C_2H_2D_4$ is the most abundant impurity in C_2HD_5 and $C_2H_3D_3$ is the most abundant in $CHD_2{\cdot}CHD_2$. We used the patterns of $CHD_2{\cdot}CHD_2$ and CH_3CD_3 for the corrections but it would be better to use the mean patterns of the two isomers if both were known.

The experimental material in this paper was used by Miss Quinn as a Master's thesis at the University of Alabama.

4. References

[1] Schissler, Thompson and Turkevich, Farad. Soc. Discussion **10** (1951).
[2] V. H. Dibeler, J. Res. NBS **44,** 489 (1950) RP2095.
[3] D. P. Stevenson and C. D. Wagner, J. Chem. Soc. **72,** 5612 (1952).
[4] F. H. Field and J. L. Franklin, Electron Impact Phenomena (Academic Press, New York, N.Y., 1957).
[5] Mohler, Dibeler, and Quinn, J. Research NBS **61,** 171 (1958) RP2896.
[6] Dibeler, Mohler, and deHemptinne, J. Research NBS 53, 107 (1954) RP2522.
[7] Rosenstock, Wallenstein, Wahrhaftig, and Eyring, Proc. Nat. Acad. Sci. **38,** 667 (1952).

JOURNAL OF RESEARCH of the National Bureau of Standards—A. Physics and Chemistry
Vol. 65A, No. 2, March–April 1961

Heats of Hydrolysis and Formation of Potassium Borohydride

Walter H. Johnson, Richard H. Schumm, Isa H. Wilson, and Edward J. Prosen

(November 29, 1960)

The heat of reaction of potassium borohydride with 0.060 molal HCl has been measured by solution calorimetry. The heat of solution of the hydrolysis products has also been measured and combined with certain literature values to calculate the process:

$$KBH_4(c)+HCl(g)+3H_2O(liq)\rightarrow KCl(c)+H_3BO_3(c)+4H_2(g),$$
$$\Delta H°(25\ °C)= -354.06\pm 1.84\ \text{kj/mole}\ (-84.62\pm 0.44\ \text{kcal/mole}).$$

A combination of this value with literature values for the heats of formation of HCl(g), H_2O(liq), KCl(c), and H_3BO_3(c) gives for KBH_4(c):

$$\Delta Hf°(25\ °C)=-228.86\pm 2.30\ \text{kj/mole}\ (-54.70\pm 0.55\ \text{kcal/mole}).$$

Other data on the heats of formation of the alkali-metal borohydrides are discussed briefly.

1. Introduction

The metallic borohydrides constitute a unique class of chemical compounds that contain the borohydride group, BH_4^-. A number of borohydrides have been prepared; some are ionic in character and others are covalent. The alkali-metal borohydrides have ionic structures and are much more stable toward oxygen and moisture than are the covalent compounds.

The reactivity of the alkali-metal borohydrides toward moisture decreases with increase in the atomic weight of the metal. Potassium borohydride does not form a hydrate as does the sodium salt, and, although quite soluble, it hydrolyses very slowly in water. In dilute acid, however, the hydrolysis is rapid and quantitative, with the liberation of 4 moles of hydrogen per mole of the hydride.

Combustion-calorimetric methods are generally not applicable to the borohydrides because of uncertainties in the composition and thermodynamic states of the combustion products. Nathan, Stegeman, and Mason [1] [1] investigated the combustion of $LiBH_4$ and found that the products included $LiBO_2$ together with significant amounts of elemental boron, Li_2O, and B_2O_3. For this reason, we have used solution reactions to obtain the heat of formation of potassium borohydride.

2. Materials

The KBH_4 was obtained from Metal Hydrides, Inc. Analysis by R. A. Paulson of the Analytical Chemistry Section of the Chemistry Division gave 98.79, 99.28, and 99.33 weight percentages (± 0.09) of theoretical hydrolyzable hydrogen, boron, and potassium, respectively. Thus, the molar ratio of KBH_4 to total B was 0.9951. The impurities were probably KBO_2 and H_2O or their equivalent in partially hydrolyzed sample. Douglas and Harman [2], who measured the heat content of samples taken from the same lot of material, have given details of the analytical procedures and the results of exposure to moist air.

The KCl and H_3BO_3 were reagent-grade materials, dried in vacuo over anhydrous magnesium perchlorate. The hydrochloric acid solution was prepared by dilution of reagent-grade acid; the concentration was determined by titration with a standard alkali solution.

3. Apparatus and Procedure

The calorimeter was similar to that previously described [3], except that the liquid capacity was 400 ml and the resistance of the calorimeter heater was 228 ohms. The cooling constant was 0.0010 °C min^{-1} (°C of thermal head).$^{-1}$ The rise in temperature attributed to stirring energy and bearing friction was 0.0003 °C/min.

The thermometric system and the apparatus for measurement of electrical energy were similar to those previously described [4, 5], except that a White double potentiometer was used for the potential measurements.

Samples of approximately 0.01 mole of KBH_4 were placed in thin-walled, soft-glass bulbs and dried for 16 hours at room temperature over anhydrous magnesium perchlorate in an evacuated desiccator. The sample bulbs were then removed, connected to a suction tube, and sealed under a partial vacuum.

[1] Figures in brackets indicate the literature references at the end of this paper.

The KCl-H_3BO_3 mixtures were prepared by weighing 0.010 mole of each of the air-dry materials into glass bulbs, which were then dried and sealed as described above.

The calorimetric solution, 398 g of 0.0597 molal HCl, was adjusted to 23.5 °C and weighed in the calorimeter. The stirrer, the calorimeter heater, the KBH_4 sample, and the bulb-crushing apparatus were lowered into the calorimeter, and the platinum resistance thermometer was inserted. The assembled calorimeter was placed in a water bath which was thermostatically controlled at 25.2 °C within ±0.04 °C. Calorimeter temperatures were observed at 2-min intervals during a 20-min initial rating period, after which the sample bulb was broken. Observations of calorimeter temperature were continued at 1-min intervals during a 15-min "reaction" period and at 2-min intervals during a 20-min final rating period.

The hydrogen, which evolved quite rapidly, passed through a vent in the calorimetric vessel and was collected in a collapsed rubber balloon that had previously been flushed with dry helium. The balloon distended without causing any appreciable increase in pressure. The vapor mixture in the balloon was next drawn slowly through a weighed water-absorption tube containing anhydrous magnesium perchlorate and phosphorus pentoxide. The balloon was then refilled with dry helium and emptied through the water-absorption tube. The increase in weight of the tube gave a fairly accurate measure of the quantity of water which vaporized from the calorimetric solution.

The quantity of boric acid in the resulting solution was determined by neutralization followed by titration with standard alkali solution in the presence of D-mannitol; a Beckman *p*H-meter was used to determine the end-point of the titration. The amount of reaction is based on this titration.

The calorimetric system was calibrated with electrical energy, over approximately the same temperature interval, as previously described [4, 5].

The calorimetric system used for the heat of solution of the KCl-H_3BO_3 mixture differed slightly from that used for the KBH_4 hydrolysis experiment in that the concentration of HCl was changed to 0.0298 molal, the calorimeter vent was closed, and the initial calorimeter temperature was 25.0 °C.

4. Results and Calculations

All atomic weights are taken from the 1957 International Table of Atomic Weights [6]. The unit of energy employed is the joule; for conversion to the conventional thermochemical calorie, one calorie is taken as 4.1840 joules. All instruments were calibrated with reference to standards maintained at NBS.

The results of the electrical calibration experiments are given in table 1. The energy equivalent of the system, E_s, is obtained as the ratio of the electrical energy, E, to the corrected temperature rise, ΔRc [7]. A correction, Δe, is applied to correct the energy equivalent of the actual calorimetric system to a selected "standard" system. The deviations from the standard calorimetric system were due to small variations in the mass of solution.

The results of the experiments on the hydrolysis of KBH_4, table 2, are calculated by

$$-\Delta H(25°\ C)=\frac{\Delta Rc(E_s+\Delta e)+q_v}{\text{mole } H_3BO_3\times 0.9951}-0.29.$$

The quantity 0.9951 is the molar ratio of B hydrolyzable as KBH_4 to total H_3BO_3 produced as calculated from the analytical data. The quantity 0.29 kj/mole is the estimated heat liberated,

$$\frac{(0.9928-0.9879)(14.1)(4.1840)}{0.9879}\ \text{kj/mole},$$

TABLE 1. *Results of the electrical calibration experiments*

Experiment No.	ΔRc	E	Δe	E_s
	Ohm	*j*	*j/ohm*	*j/ohm*
1	0.155645	2813.14	35.2	18038.9
2	.155159	2810.21	35.2	18076.6
3	.155531	2805.02	−13.7	18048.8
4	.154673	2797.75	19.1	18069.0
Mean				18058.3
Standard deviation of the mean				±8.7

TABLE 2. *Results of the experiments on the hydrolysis of* KBH_4

Experiment No.	ΔRc	Δe	q_v	H_3BO_3	$-\Delta H$(25 °C)
	Ohm	*j/ohm*	*j*	*Mole*	*kj/mole*
1	0.137899	−2.5	104.44	0.01074	242.47
2	.162020	8.4	111.62	.01255	243.04
3	.124036	3.5	173.55	.01015	238.67
4	.131172	47.8	189.77	.01074	239.70
5	.120168	41.2	133.89	.009619	240.94
Mean					240.96
Standard deviation of the mean					±0.82

by the KBO_2 impurity accompanying one mole of KBH_4. The ΔH of reaction of KBO_2 under the conditions of the experiment, −14.1 kcal/mole, is obtained from its heat of formation, −233 kcal/mole [9], and other appropriate data [8]. The correction, q_v, applied for the vaporization of water from the calorimeter solution, is calculated from the mass of water collected in the absorption tube, using 2440 j/g for the heat of vaporization. The heat capacity of crystalline KBH_4 is taken as 23.03 cal/mole °C [2].

Thus, for the process:

$$KBH_4(c)+[2.20HCl+2053\ H_2O](soln)\rightarrow$$

$$[KCl+H_3BO_3+1.20\ HCl+2050\ H_2O](soln)+4H_2(g)$$

$$\Delta H(25\ °C)=-240.96\pm 1.76\ \text{kj/mole}$$
$$(-57.59\pm 0.42\ \text{kcal/mole}). \quad (1)$$

TABLE 3. *Results of the experiments on the solution of the* $KCl-H_3BO_3$ *mixtures*

Experiment No.	ΔRc	Δe	$KCl-H_3BO_3$	$-\Delta H(25\ °C)$
	Ohm	*j/ohm*	*Mole/each*	*kj/mole*
1	−0.021580	−0.9	0.01000	−39.03
2	− .021260	−6.1	.01000	−38.44
3	− .021146	−5.0	.01000	−38.23
Mean				−38.57
Average deviation from the mean				±0.31

The results of the experiments on the heat of solution of a mixture of .01 mole each of KCl and H_3BO_3 in 2206 moles H_2O containing 1.18 moles HCl are given in table 3. A correction of 27.9 j/ohm in the energy equivalent of the calorimetric system is made for the change in concentration of the hydrochloric acid solution. Ignoring the negligible heat effect accompanying small changes in concentration [8], we have:

$$KCl(c)+H_3BO_3(c)+[1.20\ HCl+2050\ H_2O](soln)\rightarrow$$
$$[KCl+H_3BO_3+1.20\ HCl+2050\ H_2O](soln),$$
$$\Delta H(25\ °C)=38.57\pm0.64\ \text{kj/mole}\quad(9.22\pm0.15\ \text{kcal/mole}). \quad (2)$$

The heats of solution of gaseous HCl, in water, are calculated from existing data [8] for the following processes:

$$2.20\ HCl(g)+2053\ H_2O(liq)\rightarrow [2.20\ HCl+2053\ H_2O]\ (soln),$$
$$\Delta H(25\ °C)=-39.261\pm0.040\ \text{kcal/mole} \quad (3)$$

$$1.20\ HCl(g)+2050\ H_2O(liq)\rightarrow [1.20\ HCl+2050\ H_2O]\ (soln),$$
$$\Delta H(25\ °C)=-21.448\pm0.020\ \text{kcal/mole}. \quad (4)$$

The appropriate combination of equations 1, 2, 3, and 4 yields the process:

$$KBH_4(c)+HCl(g)+3H_2O(liq)\longrightarrow KCl(c)+H_3BO_3(c)+4H_2(g),$$
$$\Delta H°(25\ °C)=-354.06\pm1.84\ \text{kj/mole}\ (-84.62\pm0.44\ \text{kcal/mole}).$$

The heat of formation of crystalline boric acid is taken as -262.16 ± 0.32 kcal/mole [9]. This value, combined with the literature values [8] for the heats of formation of KCl(c), HCl(g), and H_2O(liq), gives for KBH_4(c):

$$\Delta Hf°(25\ °C)=-228.86\pm2.30\ \text{kj/mole}\quad(-54.70\pm0.55\ \text{kcal/mole}).$$

The uncertainties assigned to the experimental values given in this paper are determined by combining twice the standard deviation of the mean of the experimental data with reasonable estimates of all other known sources of error.

5. Summary

No previous experimental data on the heat of formation of KBH_4 have been reported. Altshuller [10] estimated the heats of formation of KBH_4, $RbBH_4$, and $CsBH_4$ to be −58, −59, and −63 kcal/mole, respectively, from lattice-energy calculations. Davis, Mason, and Stegeman [11] measured the heats of hydrolysis of $LiBH_4$ and of $NaBH_4$ in aqueous hydrochloric acid, using a closed system, and obtained −44.15 and −43.83 kcal/mole, respectively, for the standard heats of formation. The available data on the heats of formation of the alkali-metal borohydrides are summarized in the following tabulation in kcal/mole at 25 °C:

$LiBH_4$	−44.15	[11]
$NaBH_4$	−43.83	[11]
KBH_4	-54.70 ± 0.55	This investigation
$RbBH_4$	−59	[10]
$CsBH_4$	−63	[10]

6. References

[1] C. C. Nathan, G. Stegeman, and L. S. Mason, Univ. of Pittsburgh Technical Report on Contract No. N6ori-43, T.O. 1, February 1950.
[2] T. B. Douglas and A. W. Harman, J. Research NBS **60,** 117 (1958) RP2828.
[3] W. H. Johnson, A. A. Gilliland, and E. J. Prosen, J. Research NBS **63A,** 161 (1959).
[4] E. J. Prosen and F. D. Rossini, J. Research NBS **33,** 255 (1944) RP1607.
[5] E. J. Prosen, W. H. Johnson, and F. Y. Pergiel, J. Research NBS **62,** 43 (1959) RP2927.
[6] E. Wichers, J. Am. Chem. Soc. **80,** 4121 (1958).
[7] E. J. Prosen, Chapter 6 in Experimental thermochemistry, F. D. Rossini, ed. (Interscience Publishers, Inc., New York, N.Y., 1956).
[8] F. D. Rossini, D. D. Wagman, W. H. Evans, S. Levine, and I. Jaffe, Selected values of chemical thermodynamic properties, NBS Circ. **500** (U.S. Government Printing Office, Washington 25, D.C., 1952).
[9] W. H. Evans, D. D. Wagman, and E. J. Prosen, (unpublished data, 1958).
[10] A. P. Altshuller, J. Am. Chem. Soc. **77,** 5455 (1955).
[11] W. D. Davis, L. S. Mason, and G. Stegeman, J. Am. Chem. Soc. **71,** 2775 (1949).

(Paper 65A2–90)

JOURNAL OF RESEARCH of the National Bureau of Standards—A. Physics and Chemistry
Vol. 65A, No. 2, March–April 1961

Heat of Combustion of Borazine, $B_3N_3H_6$

Marthada V. Kilday, Walter H. Johnson, and Edward J. Prosen

(November 25, 1960)

The heat of combustion of liquid borazine has been determined according to the following equation:

$$B_3N_3H_6(liq)+15/4\ O_2(g)+3/2\ H_2O\ (liq)=3H_3BO_3(c)+3/2N_2(g),$$
$$\Delta H^\circ\ (25\ ^\circ C)=-2313.3\pm12.6\ kj/mole\ (-552.90\pm3.0\ kcal/mole).$$

From this value the heat of formation of liquid borazine may be calculated as $\Delta Hf^\circ(25\ ^\circ C)=-548.5\pm13.4$ kj/mole (-131.1 ± 3.2 kcal/mole), and for the gas, $\Delta Hf^\circ(25\ ^\circ C)=-519.2\pm13.4$ kj/mole (-124.1 ± 3.2 kcal/mole).

1. Introduction

The determination of the heat of combustion of borazine, or borazole, was undertaken as part of the Bureau's program for determining thermochemical properties of boron compounds. Several compounds containing the borazine ring have been prepared [1, 2, 3, 4, 5],[1] but few thermochemical data have been reported for them [6, 7, 8, 9]; no data on the heat of formation of borazine itself have been reported.

Liquid borazine of high purity was burned in an oxygen atmosphere in a bomb, forming boric acid, boron nitride, and gaseous nitrogen as products. From the results of these combustion experiments a value for the heat of formation of borazine was calculated.

2. Materials and Apparatus

The borazine sample, supplied by the Naval Research Laboratory, was prepared by reducing trichloroborazole with lithium borohydride in ether solution. Details of the method are described by Shaeffer and coworkers [10]. The purity[2] of the sample was 99.5 mole percent. No attempt was made to correct the calorimetric results for the 0.5 percent impurity in the sample; the impurity was not identified, but was believed to be a derivative of ether with a boiling point near that of borazine.

The calorimeter was the isothermal-jacket type generally used for bomb calorimetry; the temperature of the jacket was maintained within ±0.001 °C at approximately 28 °C. A general description of the jacket, thermometric system, and bomb is given in [11]. Temperature measurements were made with a platinum resistance thermometer in conjunction with a Mueller G–2 bridge. The modified Parr bomb (vol. 376 ml) was sealed with a gold gasket and equipped with twin valves for convenience in flushing before filling with oxygen and in removing the gaseous products of combustion. Commercial oxygen used in filling the bomb was purified by passing through a furnace containing copper oxide at 600 °C to remove combustible materials, and then through an absorber containing Ascarite to remove carbon dioxide.

3. Experimental Procedure

The borazine samples, 0.5 to 1.0 g, were transferred in the vapor phase at room temperature into spherical soft-glass bulbs cooled to about −5 °C with an ice-salt mixture. The filled bulbs were sealed under vacuum, weighed carefully, and stored at −15 °C. In the first experiment, the sample was enclosed in a Pyrex-glass bulb and ignited by means of a platinum fuse wire instead of the usual iron wire, to eliminate possible complications from the iron oxides during analysis of the products; thereafter, iron fuse wire was used. Pyrex-glass bulbs were unsatisfactory for this work because only a small area of the glass was softened upon ignition, and incomplete combustion resulted. Soft-glass bulbs usually shattered upon ignition and the sample burned with free access to oxygen.

In assembling the bomb, the sample bulb was placed in a quartz crucible, 3 cm in diameter and 1.5 cm deep, which was supported a little below the center of the bomb. The carefully weighed fuse-wire of pure iron, 5 cm long and 5 mils in diameter, used for igniting the sample was placed in direct contact with the sample bulb. After 2 ml of distilled water had been added to the bomb, it was closed and flushed to displace air before filling with oxygen to a pressure of 30 atm. The bomb was placed in a calorimeter can containing 2968 g of water, the standard amount for the system.

The energy equivalent of the calorimetric system was determined in calibration experiments in which benzoic acid, NBS Standard Sample 39g, was burned. The heat evolved in the combustion of this sample is certified to be 26.4338 ±0.0026 kj/g at the standard bomb conditions.

Temperature observations during the experiments were divided into four groups, an initial rating period (20 min), a combustion period (5 min), an equilibration period (11 min), and a final rating

[1] Figures in brackets indicate literature references at the end of this paper.
[2] Determined from freezing-point measurements by the Pure Substances Section of the Chemistry Division.

period (20 min). The rapid temperature change during the combustion period was recorded by means of a chronograph (Gaertner Scientific Co.) having a synchronous motor and two pens marking a waxed tape which advanced uniformly at 10 mm per sec. One pen recorded time in seconds as obtained from standard signals transmitted by the National Bureau of Standards, the other recorded the times when a telegraph key was tapped indicating when the resistance of the thermometer in the calorimeter passed certain previously selected values. Temperatures were recorded at 1-min intervals during the equilibration period, and at 2-min intervals during the rating periods.

The gaseous products of the experiments reported here were not analysed since nitrogen oxides were not detected in any of the preliminary experiments in which the product gases were bubbled through distilled water and the solution titrated with 0.1-*N* sodium hydroxide.

The solid products remaining in the bomb were washed with hot distilled water; the washings were filtered to remove fragments of the shattered crucible, glass bulb, and undissolved products of combustion. The filtrate, containing nitric and boric acids, was titrated with 0.1-*N* sodium hydroxide, using a Beckmann *p*H meter to determine the end points. The amount of nitric acid present was determined from the first titration curve; D-mannitol was then added to the solution to form a complex with the boric acid and a decrease in the *p*H resulted; the amount of boric acid was determined from the second titration curve. No method was found for making a quantitative separation of the insoluble products and glass fragments.

4. Data and Discussion

The atomic weights used are given in the International Table of Atomic Weights [12]. All heat capacity data were taken from [13] except that of borazine. No values for the density and heat capacity of liquid borazine were available, so the corresponding values for liquid benzene were used, i.e., $d_{28}=0.871$ g/cm^3 [14] and $Cp(28\ °C)=32.5$ cal/mole °C or 16.7 j/g-ohm [15]. The unit of energy was the joule, and for conversion to the thermochemical calorie the following relation was used: 1 thermochemical calorie = 4.1840 joules.

The products of combustion of borazine contained grey-white material which was insoluble in water and which was not attacked during digestion in aqua regia; the material was assumed to be boron nitride. This assumption was supported by an X-ray diffraction analysis [3] although positive identification was not possible because the X-ray powder pattern was not clearly defined.

Elemental boron was not present in the products of combustion in detectable quantity. The insoluble residue of combustion was digested in aqua regia for several hours to oxidize the boron to boric acid. The solution was then filtered, and the filtrate was neutralized with sodium hydroxide, made slightly acid, and titrated to the first end point. When D-mannitol was added, no significant decrease in *p*H occurred indicating that boric acid (or boron) was not present. Since elemental boron was not found, it was assumed that any boron in the sample which was not titrated as boric acid in the water soluble products remained in the insoluble residue as boron nitride; furthermore, it was assumed that any nitrogen in the borazine sample which was not accounted for as nitric acid or boron nitride, was present in the products as gaseous nitrogen. Nitrogen oxides were not found in the gaseous products of preliminary experiments.

Data for the borazine combustion experiments are given in table 1. The amounts of nitric acid and of boric acid found in titrations are given in the second and third columns. The ratio of boric acid titrated to the boric acid calculated from the weight of sample may be used as an indication of completeness of combustion. BN is the amount of boron nitride in the products (by assumption); it is the difference between the number of moles of boron in the sample and the number of moles of boron titrated as boric acid.

[3] Made by the Constitution and Microstructure Section of the Mineral Products Division.

TABLE 1. *Data for borazine combustion experiments*

Expt. No.	HNO_3 titrated	H_3BO_3 titrated	H_3BO_3 titr. / H_3BO_3 calc.	BN	Δt	E_o	ΔRc	q_i	q_n	W.C.	q_{BN}	S	$-\Delta E°(28°\ C)$
	Mole	*Mole*		*Mole*	*j/ohm*	*j/ohm*	*Ohm*	*j*	*j*	*j*	*j*	*Gram*	*kj/mole*
1	0.000980	0.02016	0.9920	0.000163	16.2	141,731.3	0.109885	[1] 0.0	56.6	[2] 6.1	67.6	0.54555	2301.52
2	.000935	.02662	.9818	.000493	34.6	141,749.7	.145888	36.3	54.0	8.8	204.6	.72782	2301.79
3	.001073	.02362	.9885	.000274	41.7	141,756.8	.130025	38.2	62.0	[2] 7.8	113.7	.64141	2316.90
4	.001567	.03452	.9866	.000468	43.4	[3] 141,726.8	.189172	37.1	90.6	11.5	194.2	.93923	2305.51
5	.000996	.02745	.9850	.000419	34.1	141,749.2	.150439	37.0	57.6	9.1	173.9	.74811	2305.05
6	.000878	.01809	.9904	.000175	38.5	141,753.6	.099485	37.5	59.7	6.1	72.6	.49030	2314.75
7	.000838	.01908	.9856	.000278	32.5	141,747.6	.104598	37.4	48.4	6.4	115.4	.51966	2303.26
8	.000749	.02308	.9656	.000821	41.6	141,756.7	.128189	37.4	43.3	7.8	340.7	.64159	2314.50
Mean													2307.91
Standard Deviation of the Mean													±2.26

[1] Platinum wire used for ignition.
[2] Includes a small correction to the isothermal reaction for deviation of the final temperature from 28° C.
Used $E_o=141{,}683.4\pm10.4$ j/ohm for a 2° temperature rise.

The energy equivalent for the calorimetric system was 141,715.1±9.2 j/ohm for a temperature rise of 1 °C. Heat-capacity corrections for deviations from the calibrated system are included in Δe (table 1); E_a is the energy equivalent of the actual system used; and ΔRc is the temperature rise corrected for cooling and stirring energies as described by Prosen [16]. The ignition energy, q_i, is equal to 7.50 kj/g of iron fuse-wire. (The ignition energy for the platinum fuse-wire used in expt. 1 was too small to measure.) The correction for the formation of nitric acid, q_n, is 57.8 kj/mole; W.C., the Washburn correction, was calculated as described in [16, 17]. W.C. for experiments 1 and 3 also includes corrections of $-0.7\ j$ and $-0.1\ j$, respectively, for deviations from 28 °C, the temperature of the isothermal reaction. In table 1, S is the weight in vacuo of the sample.

The energy for converting the boron nitride to boric acid and gaseous nitrogen, q_{BN}, was calculated from the value for the combustion of boron nitride [18, 19], according to equation (1).

$$BN(c)+\tfrac{3}{4}O_2(g)+\tfrac{3}{2}H_2O(liq)=H_3BO_3(c)+\tfrac{1}{2}N_2(g),\quad \Delta H(25\ °C)=-99.3\ \text{kcal/mole}. \qquad (1)$$

This is equivalent to 415 kj/mole of BN for the constant volume process at 28 °C.

The heat of combustion of borazine for the constant-volume process in which the products and reactants are in their thermodynamic standard states was calculated according to the following equation:

$$-\Delta E°(28\ °C)=\frac{E_a(\Delta Rc)-q_i-q_n+\text{W.C.}+q_{BN}}{80.532\ S}.$$

The mean heat of combustion, $\Delta E°(28\ °C)$, was -2307.91 ± 2.26 kj/mole or -551.60 ± 0.54 kcal/mole for the reaction given in equation (2).

$$B_3N_3H_6\ (liq)+/^{15}\!/_4\ O_2(g)+3/2\ H_2O\ (liq)=3H_3BO_3(c)+{}^3\!/_2\ N_2\ (g) \qquad (2)$$

The heat of combustion at constant pressure, or enthalpy change, is obtained by adding $\Delta nRT=-1.35$ kcal/mole; thus, $\Delta H°(28\ °C)=-552.95$ kcal/mole. By adding a correction of 0.05 kcal/mole for the change in temperature, we obtain $\Delta H°(25\ °C)=-552.90\pm3.0$ kcal/mole. The uncertainty assigned to this value is the square root of the sum of the squares of the individual uncertainties. Included in this uncertainty are twice the standard deviations of the means of the combustion experiments and of the calibration experiments, an estimated uncertainty of 0.1 percent for weights and for titrations, and 0.5 percent estimated error from sample impurity and from the uncertainty in final state of boric acid. The latter value was assigned arbitrarily because the impurity in the sample was not identified and the amount of boric oxide in the products of combustion was not determined. It is believed that the boron in the sample is burned to boric oxide which is then hydrated to boric acid. Two-thirds of this hydration probably occurs with water formed by combustion of the hydrogen in the sample. The remaining water of hydration must be supplied from the water vapor in the bomb atmosphere which is saturated at the beginning and end of the experiment; an error of as much as 7 kcal/mole would be introduced if no water reacted with the boric oxide. However, the amount of boric oxide remaining at the end of an experiment was probably very small because the solid products were quite evenly distributed over all the inner surfaces of the bomb providing maximum surface for the hydration reaction to take place. A relatively small uncertainty exists regarding the amount and concentration of boric acid in solution. This error is in the opposite direction and tends to cancel the error due to incomplete hydration of boric oxide.

The heat of formation of crystalline boric acid, -262.16 ± 0.32 kcal/mole [19], and of liquid water, -68.3174 ± 0.0100 kcal/mole [13], were used to calculate the heat of formation of liquid borazine,

$$\Delta Hf°(25\ °C)=-548.5\pm13.4\ \text{kj/mole or}\ -131.1\pm3.2\ \text{kcal/mole}.$$

The heat of vaporization of borazine was obtained from the data of Stock, Wiberg, and coworkers [7, 8, 9]. A least squares fit of their data yields the following equation for the vapor pressure,

$$\log p_{mm}=6.39278-\frac{919.131}{(T-67.198)};$$

this may be used with the Clausius-Clapeyron equation to obtain

$$\Delta H_v(25\ °C)=7.01\ \text{kcal/mole}.$$

Thus, the heat of formation of borazine gas is

$$\Delta Hf°(25\ °C)B_3N_3H_6(g)=-519.2\pm13.4\ \text{kj/mole or}\ -124.1\pm3.2\ \text{kcal/mole}.$$

5. Summary

The heat of combustion at constant pressure was determined by burning liquid borazine in oxygen in a bomb calorimeter. For the reaction,

$$B_3N_3H_6(liq)+{}^{15}\!/_4\ O_2(g)+{}^3\!/_2\ H_2O(liq)=3H_3BO_3(c)+{}^3\!/_2\ N_2(g),$$

it was found that $\Delta H°\ (25\ °C)=-552.90\pm3.0$ kcal/mole. From this value the heat of formation of liquid borazine was calculated to be $\Delta Hf°(25\ °C)=-548.5\pm13.4$ kj/mole or -131.1 ± 3.2 kcal/mole, and that for gaseous borazine to be

$$\Delta Hf°(25\ °C)=-519.2\pm13.4\ \text{kj/mole or}\ -124.1\pm3.2\ \text{kcal/mole}.$$

We wish to thank R. R. Miller of the Naval Research Laboratory for supplying the sample of borazine used in these determinations.

6. References

[1] E. Wiberg and K. Hertwig, Z. anorg. u. allgem. Chem. **255,** 141 (1947).
[2] H. I. Schlesinger, D. M. Ritter, and A. B. Burg, J. Am. Chem. Soc. **60,** 1296 (1938).
[3] W. V. Hough, G. W. Schaeffer, M. Dzurus, and A. C. Stewart, J. Am. Chem. Soc. **77,** 864 (1955).
[4] A. B. Burg and E. S. Kuljian, J. Am. Chem. Soc. **72,** 3103 (1950).
[5] G. W. Schaeffer and E. R. Anderson, J. Am. Chem. Soc. **71,** 2143 (1949).
[6] E. R. van Artsdalen and A. S. Dworkin, J. Am. Chem. Soc. **74,** 3401 (1952).
[7] A. Stock, E. Wiberg, and H. Martini, Ber. **63,** 2927 (1930).
[8] A. Stock and E. Pohland, Ber. **59,** 2215 (1926).
[9] E. Wiberg and A. Bolz, Ber. **73,** 209 (1940).
[10] R. Schaeffer, M. Steindler, L. Hohnstedt, H. S. Smith, Jr., L. B. Eddy, and H. I. Schlesinger, J. Am. Chem. Soc. **76,** 3303 (1954).
[11] W. H. Johnson, E. J. Prosen, and F. D. Rossini, J. Research NBS **35,** 141 (1945) RP1420.
[12] E. Wichers, J. Am. Chem. Soc. **80,** 4121 (1958).
[13] F. D. Rossini, D. D. Wagman, W. H. Evans, S. Levine, and I. Jaffe, Selected values of chemical thermodynamic properties, NBS Circ. **500** (U.S. Government Printing Office, Washington 25, D.C., 1952).
[14] F. D. Rossini, K. S. Pitzer, R. L. Arnett, R. M. Braun, K. Li, H. J. Ries, P. A. Cowie, J. Mitchell, L. A. Parcella, M. B. Epstein, A. L. McClellan, M. H. Sarao, C. R. DeCelles, and H. M. Flanagan, Selected values of physical and thermodynamic properties of hydrocarbons and related compounds (Carnegie Press, Pittsburgh, Pa., 1953).
[15] G. D. Oliver, M. Eaton, and H. M. Huffman, J. Am. Chem. Soc. **70,** 1502 (1948).
[16] E. J. Prosen, Chapter 6, Experimental thermochemistry, F. D. Rossini, ed. (Interscience Publishers, Inc., New York, 1956).
[17] E. W. Washburn, BS J. Research **10,** 525 (1933) RP546.
[18] A. S. Dworkin, D. J. Sasmor, and E. R. van Artsdalen, J. Chem. Phys. **22,** 837 (1954).
[19] E. J. Prosen, W. H. Johnson, and F. Y. Pergiel, J. Research NBS **62,** 43 (1959) RP2927.

(Paper 65A2–91)

JOURNAL OF RESEARCH of the National Bureau of Standards—A. Physics and Chemistry
Vol. 65, No. 2, March–April 1961

Thermodynamic Properties of Thorium Dioxide From 298 to 1,200 °K

Andrew C. Victor and Thomas B. Douglas

(November 26, 1960)

As a step in developing new standards of heat capacity applicable up to very high temperatures, the heat content (enthalpy) of thorium dioxide, ThO_2, relative to 273 °K, was accurately measured at ten temperatures from 323 to 1,173 °K. A Bunsen ice calorimeter and a drop method were used to make the measurements on two samples of widely different bulk densities. The corresponding heat-capacity values for the higher density sample are represented within their uncertainty (estimated to be ±0.3 to 0.5%) by the following empirical equation [1] (cal $mole^{-1}$ deg^{-1} at T °K):

$$C_p^\circ = 17.057 + 18.06(10^{-4})\ T - 2.5166\ (10^5)/T^2$$

At 298 °K this equation agrees with previously reported low-temperature measurements made with an adiabatic calorimeter. Values of heat content, heat capacity, entropy, and Gibb's free energy function are tabulated from 298.15 to 1,200 °K.

1. Introduction

Current practical and theoretical developments have increased the need for accurate heat capacities and related thermal properties at high temperatures, yet the values reported for the same material from different laboratories often show large differences. In some cases the precision is correspondingly poor, but in other cases the disagreement is so largely attributable to systematic errors that the availability of suitable heat standards to monitor the accuracy is almost imperative. It is one of the fundamental functions of NBS to develop such standards as the need arises.

A material chosen for such a standard must meet certain requirements. In the temperature range of its use it must exist in a definite reproducible physical state, have a fixed chemical composition, and not be subject to appreciable spontaneous decomposition. In addition it is highly desirable that it not react chemically with the gases of the atmosphere (oxygen, nitrogen, carbon dioxide, and water vapor) nor undergo appreciable fusion, volatilization, or transition. Its cost should not be prohibitive, and its heat capacity should not be too small.

α-Aluminum oxide (corundum) meets these specifications excellently up to approximately 1,800 °K, and was therefore recommended by the Third Calorimetry Conference, which met in 1948, as a high-temperature heat-capacity standard. The Bureau obtained and conditioned a highly pure sample of a synthetic grade of this substance, and established its heat capacity accurately from 10 to 1,200 °K [1]; [2] using new apparatus recently constructed, these measurements are soon to be extended up to approximately 1,800 °K.

However, at higher temperatures aluminum oxide is impractical as a heat standard, for it becomes increasingly volatile, and melts at approximately 2,300 °K. A more refractory solid is needed at these temperatures, and preferably a substance which could serve as a standard at the lower temperatures also. There are approximately a dozen well-known substances of definite chemical composition whose melting points lie above 2,800 °K. Of these, almost the only ones which appear to have all the above desirable properties are thorium dioxide, beryllium oxide, and magnesium oxide.

As a standard, thorium dioxide would have the minor practical disadvantage that many impurities commonly present in it have specific heats which are considerably higher than its own. The latter fact causes the heat capacity per unit mass to be correspondingly sensitive to the exact chemical composition of the sample used. Advantages outweighing this fact, however, are the unusually high melting point of thorium dioxide (reported to be 3,300 °K [2]), its monomorphism, and its high chemical stability and inertness.

The temperatures to which beryllium oxide and magnesium oxide could be used as a standard are somewhat lower because their melting points (reported to be about 2,800 °K and 3,000 °K respectively [2]) are not as high. However, compared with thorium dioxide, their heat capacities per unit mass are much less sensitive to the influence of common impurities, and also, they are less expensive. The accurate knowledge of the heat capacities of all three substances over long temperature ranges would have added value because their favorable high-temperature properties lead to their very frequent use as structural materials in many installations operated at elevated temperatures.

[1] Using the defined calorie=4.1840 absolute joules.
[2] Figures in brackets indicate literature references at the end of this paper.

Recent accurate measurements at the Bureau of the heat capacity of ThO_2 from 298.15 to 1,200 °K are reported in this paper. The Bureau plans to extend these measurements up to 1,800 °K in the near future, and probably up to 2,800 °K within the next few years. Since it is difficult to melt such a refractory substance without incurring undesirable contamination, the present investigation was carried out on two pressed and sintered samples of widely different bulk densities, in order to test the sensitivity of the thermal values to variations in this property.

A paper describing similar measurements on beryllium oxide and magnesium oxide will be published shortly. The authors believe that these papers will present evidence supporting the advisability of higher temperature heat-content measurements on ThO_2, BeO, and MgO, which may eventually lead to the adoption of one of them as a calorimetric standard at temperatures above 1,800 °K.

2. Samples and Containers

Each sample consisted of two cylinders, each 2 cm long and 1 cm in diameter, which were prepared in the Engineering Ceramics Section of the Bureau by pressing, firing and sintering fine powder of high purity. Variations of firing temperatures made it possible to obtain samples of different bulk densities so as to be able to investigate any existing dependence of heat capacity on density.

The thorium dioxide in the form of powder was supplied by Lindsay Chemical Company, of Chicago, Illinois. By firing to different high temperatures, samples of 9.7 g cm^{-3} and 7.2 g cm^{-3} bulk density were obtained. The density calculated from X-ray diffraction data is 10.04 g cm^{-3}. These two samples have densities which are 97 and 72 percent of this density, and will hereafter be called thorium dioxide samples 1 and 2 respectively.

Specimens of each of the two densities of thorium dioxide were analyzed spectrochemically at the Bureau. The results of these analyses are given in table 1.[3] The samples were analyzed for the 44 chemical elements listed in table 1, 30 of which were determined by the use of synthetic standards made from ThO_2. Although the alkali metals, U, La, Ce, and Y were not detected, neither analytical standards for these elements nor the techniques of using them were available.

Assuming each element detected to be present in the form of its highest stable oxide, the thorium dioxide samples were calculated to be 99.95 percent ThO_2 by weight.

Published values of the heat capacities of the contaminating oxides were used to correct, on an additive basis, all the heat measurements to the basis of pure ThO_2. These heat measurements were sufficiently precise that application of the corrections for the impurities, which never exceeded 0.1 percent, should reduce the systematic error significantly.

The samples were enclosed in sealed containers of annealed pure silver (999.5 fine, cylinders 1.8 in. long and of $\frac{5}{8}$ in. diam). After introducing the

[3] To grind the thorium dioxide specimens in preparation for their analysis, mills of different composition (boron carbide, alundum, and plastic) were used to check the possibility of appreciable contamination. Of the nine specimens analyzed, the two which had been ground in alundum showed fifteen times as much silicon (0.05 percent) as the others, and were discounted. This difference in silicon would correspond to two specimens of ThO_2 whose relative heat contents at the same temperature should differ by approximately 0.5 percent; however, several thermal measurements made on both types of specimen indicated an actual difference of 0.05±0.05 percent. There was no discrepancy with respect to the percentage of any other chemical element.

TABLE 1. *Impurities in the samples of thorium dioxide* [a]

Element	Sample 1	Sample 2	Lower limit of detection	Element	Sample 1	Sample 2	Lower limit of detection
	Weight %	*Weight %*	*Weight %*		*Weight %*	*Weight %*	*Weight %*
Ag	(?)	(?)		Mg	<0.0002	<0.0002	0.00005
Al	0.01	0.008		Mn	<.0005	<.0005	.0001
As			0.01	Mo			.02
Au			.0001	Nb			
B	[b] <.001	[b] <.001	.0005	Ni	.009	.007	
Ba				P			.01
Be			.0002	Pb	.0001	$.0002_5$	
Bi			.001	Pt			
Ca	.005	.005		Sb			.0002
Cd				Si	.003	$.003_5$	
Ce				Sn	(?)	(?)	.001
Co			.001	Sr			.005
Cr	<.0005	<.0005	.0002	Ta			
Cu	.005	.003		Ti			.01
Fe	.004	$.001_5$		Tl			.0001
Ga				U			.1
Ge			.0001	V			.01
Hf				W			
Hg			.001	Y			
In			.0001	Yb			
Ir				Zn			.002
La				Zr			

[a] A dash indicates that the element was not detected.
[b] The other elements were determined from specimens ground in a boron carbide mortar. The estimates of boron were made from separate specimens not so treated.

sample and enough extra silver to adjust the total final mass of this metal to a standard value (exactly 12 g), the protruding edges of the two end caps (each 0.02 in. thick), which were shaped to fit the cylinder, were flame-welded to the ends of the cylinder (wall thickness, 0.015 in.). Since the sample and container had an average temperature of approximately 700 °C when the final sealing was accomplished, the amount of air sealed in was insufficient to distort the container by internal pressure at the highest temperatures subsequently used. A Pt—10 percent Rh wire of known mass encircled a groove around the silver cylinder and served to suspend the latter in the furnace and calorimeter.

In accurate work, there are certain advantages in using containers composed of silver instead of a hard base metal such as 80 Ni–20 Cr, which the authors have often used. Unlike silver, the alloy mentioned undergoes a transition near 550 °C, shows small but detectable changes in heat capacity attributed to minor annealing effects, and through traces of oxidizing gases accumulates surface coatings of oxides that must be measured by frequent reweighing and be corrected for. The mechanically sealed base-metal containers frequently develop leaks. It appears that during the short time such a silver container is falling into the calorimeter the radiation at the highest temperatures, which must be constant to avoid error in the heat measurements, decreases slowly but measurably from run to run. This effect presumably occurs through grain growth and consequent lowering of the emissivity of the silver surfaces, but the error appears to be negligible if the container is conditioned by being held for several hours in the furnace at 900 °C before the heat measurements are begun. Silver containers sealed as described above would be inapplicable to samples which, unlike thorium dioxide, must be kept cold during the sealing to prevent volatilization or must be kept in an inert atmosphere to prevent reaction with air. This disadvantage could be avoided by substituting the superior sealing technique of induction welding.

3. Heat Content Measurements

The "drop" method employed in the heat-content measurements has been described in detail in a previous publication [1]. In brief, the method was as follows. The sample, sealed in a container, was suspended in a silver-core furnace until it had time to come to a constant known temperature. It was then dropped (with almost free fall) into the Bunsen ice calorimeter, which measured the heat evolved by the sample plus container in cooling to 0 °C. In order to account for the heat content of the container and the heat lost during the drop, a similar experiment was made with the empty container (or an identical one) at the same furnace temperature. The difference between the two values of heat is a measure of the heat-content change of the sample between 0 °C and the temperature in the furnace.

Up to and including 600 °C [4] a strain-free platinum resistance thermometer was used to measure the temperature of the central portion of the furnace. A platinum—platinum-10 percent rhodium thermocouple was used over the whole temperature range of the furnace: below 600 °C it did not compete with the more precise resistance thermometer, but only served to detect any otherwise unsuspected large change in either measuring instrument. Above 600 °C the thermocouple alone was used.

Table 2 gives the measured heat values obtained in individual runs for the empty container in calories (one defined calorie being equivalent to 4.1840 joules). The chronological order of the furnace temperatures for the experiments was as follows: 900°, 700°, 100°, 200°, 300°, 500°, 600°, 800°, 400°, 50°. The 900 °C experiments were made first in order to condition the surface of the capsule so that its emissivity, and hence its heat loss during a drop into the calorimeter, would be little affected by subsequent heat treatment. Results on another container (having the same masses of parts), which were obtained three years earlier, were higher than those of table 2 by 0.6 cal at 100 and 200 °C. However, at and above 300 °C there was no systematic difference between the two sets, the average discrepancy in this temperature range being only ±0.12 cal. The earlier container was run at all temperatures without preliminary heat treatment at 900 °C. This agreement, as well as the conditioning of the present empty container before its use, increased the authors' confidence in the reproducibility of the empty-container heat values. Since in determining the heat content of the samples it was not convenient to use the same containers as those in which the samples were measured, it was important to verify the assumption that this substitution of containers caused inappreciable error.

TABLE 2. *Individual heat measurements on an empty container*

Furnace temperature, t	Measured heat	Mean heat	Furnace temperature, t	Measured heat	Mean heat
°C	cal	cal	°C	cal	cal
50.00	36.61 36.61	36.61	500.00	387.56 387.71	387.64
100.00	73.62 73.63	73.62	600.00	469.79 469.60	469.70
200.00	149.35 149.79	149.57	700.0	554.20 554.60	554.40
300.00	227.87 228.10	227.98	800.0	641.94 642.21	642.08
400.00	306.99 306.86	306.92	900.0	731.04 730.99	731.02

[4] Temperatures are on the International Temperature Scale of 1948 as modified in 1954. This assigns the temperature 273.16 °K to the triple point of water and defines zero on the Celsius scale as 0.0100 degree below this [3].

TABLE 3. *Relative heat content of thorium dioxide,* $(H_t - H_{0\,°C})$

Furnace temperature, t	Individual heat-content measurements		Mean sample 1	Calculated eq. (1)	Mean sample 1 minus calculated
	Sample 1	Sample 2			
°C	cal g^{-1}	cal g^{-1}	cal g^{-1}	cal g^{-1}	cal g^{-1}
50.00	2.780 2.776		2.778	2.792	−0.014
100.00	5.763 5.749		5.756	5.745	+.011
200.00	11.946 11.944	11.999 11.953	11.945	11.954	−.009
300.00	18.428 18.399 18.401		18.409	18.420	−.011
400.00	25.056 25.066		25.061	25.058	+.003
500.00	31.810 31.813 31.827	31.928 31.841 31.826	31.817	31.829	−.012
600.00	38.718 38.722		38.720	38.709	+.011
700.0	45.727 45.737 45.716		45.727	45.687	+.040
800.0	52.754 52.748		52.751	52.755	−.004
900.0	59.888 59.876	59.914 59.940	59.882	59.906	−.024

In table 3, the second and third columns contain fully corrected heat-content values, in defined calories per gram, for thorium dioxide samples 1 and 2 (masses 37.1217 g and 22.8781 g respectively). These values were obtained with the furnace temperatures in random order. The listed individual heat contents were obtained by subtracting the empty container values, using the mean at each temperature, from the observed heat contents for sample plus container and dividing the resulting heat contents by the sample mass. Corrections had been applied for the calorimeter heat leak, the deviations of the sample container from standard conditions, weighing in air instead of vacuum, the extra air in the empty container because no sample was present, and for the heat contributions of analyzed impurities in the sample as described in section 2. The largest correction, that for impurities, was −0.1 ±0.005 percent of the net heat content of the sample at all temperatures. The sum of all other corrections amounts to approximately 0.01 percent of the net heat content. The calculated values of heat content in table 3 are smoothed values arrived at as described in section 4.

4. Smoothed Thermodynamic Functions

The mean heat content values in table 3, column 4, are for ThO_2 sample 1 alone. Because this sample is closer in density to the X-ray value, and hence presumably a more reproducible state, than sample 2, the authors felt that the values from this sample alone would be more meaningful. Using the method of least squares, the values in column 4 were used to determine the constants in eq (1) for thorium dioxide (in cal g^{-1} at t °C):

$$H_t^\circ - H_{0\,°C}^\circ = 0.0664596 + 3.418(10^{-6})t^2 - 3.488t/(t+273.15) \quad (1)$$

This form of equation was found to fit the low-temperature measurements (50 and 100 °C) better than an equation with the third term proportional to $\log_{10}[(t+273.15)/273.15]$, which has commonly been used in representing high-temperature metal-oxide heat contents obtained in this laboratory.

Using the following thermodynamic relations

$$C_p^\circ = (\partial H/\partial T)_p \quad (2)$$

$$S_T^\circ - S_{0\,°K}^\circ = \int_0^T C_p^\circ \, dT/T \quad (3)$$

$$-(F_T^\circ - H_{0\,°K}^\circ)/T = S_T^\circ - S_{0\,°K}^\circ - (H_T^\circ - H_{0\,°K}^\circ)/T \quad (4)$$

equations were derived from eq (1) for the molar heat content, heat capacity, entropy, and Gibbs-free-energy function for ThO_2 (molecular weight, 264.12). The values of thermodynamic functions at 298.15 °K were evaluated from Osborne and Westrum's values for $(H_{298.15}^\circ - H_{0\,°K})$ and $(S_{298.15}^\circ - S_{0\,°K})$ [4]. Osborne and Westrum's measurements on ThO_2 (10 to 305 °K) gave heat-capacity values identical at 298.15° and different (higher) by only 0.3 percent at 273.15 °K than those given by eq (1). Furthermore, their adiabatic calorimeter has shown excellent agreement (in general, within ±0.1% in heat capacity) with Bureau adiabatic calorimeters, as demonstrated by work in both laboratories on standard-sample benzoic acid [5, 6]. Their heat capacities of ThO_2 are believed to be more reliable between 273° and 298 °K than those given by eq (1). The following final equations for ThO_2 (in terms of cal mole^{-1} at T °K and one atm pressure) may therefore be considered strictly applicable only over the temperature range 298°–1,200 °K:

$$H_T^\circ - H_{0\,°K}^\circ = 17.0601\ T + 9.028(10^{-4})T^2 + 2.5166(10^5)/T - 3486.55 \quad (5)$$

$$C_p^\circ = 17.060 + 18.06(10^{-4})T - 2.5166(10^5)/T^2 \quad (6)$$

$$S_T^\circ - S_{0\,°K}^\circ = 39.2826\ \log_{10} T + 18.056(10^{-4})T + 1.2583(10^5)/T^2 - 83.5645 \quad (7)$$

$$-(F_T^\circ - H_{0\,°K}^\circ)/T = 39.2826\ \log_{10} T + 9.028(10^{-4})T - 1.2583(10^5)/T^2 + 3486.55/T - 100.6246 \quad (8)$$

Values for ThO_2 calculated from eqs (5) to (8) at selected temperatures are given in table 4.

TABLE 4. *Thermodynamic properties of thorium dioxide*

T	C_p°	$H_T^\circ - H_{0\,°K}^\circ$	$S_T^\circ - S_{0\,°K}^\circ$	$-\frac{F_T^\circ - H_{0\,°K}^\circ}{T}$
°K	*cal/mole-deg*	*cal/mole*	*cal/mole-deg*	*cal/mole-deg*
298.15	14.76	2524.4	15.593	7.126
300	14.81	2551.6	15.683	7.178
320	15.18	2851.6	16.651	7.740
340	15.50	3158.4	17.581	8.292
360	15.77	3471.1	18.474	8.834
380	16.00	3788.9	19.334	9.363
400	16.21	4111.1	20.160	9.882
420	16.39	4437.1	20.955	10.390
440	16.55	4766.6	21.721	10.888
460	16.70	5099.2	22.461	11.376
480	16.84	5434.6	23.174	11.852
500	16.96	5772.5	23.864	12.319
550	17.22	6627.2	25.493	13.444
600	17.44	7494.0	27.001	14.510
650	17.64	8371.1	28.405	15.526
700	17.81	9257.4	29.719	16.494
750	17.97	10151.9	30.953	17.417
800	18.11	11053.9	32.117	18.299
850	18.25	11962.9	33.219	19.145
900	18.37	12878.4	34.266	19.957
950	18.50	13800.2	35.263	20.736
1000	18.61	14728.0	36.214	21.486
1050	18.73	15661.6	37.125	22.209
1100	18.84	16600.7	37.999	22.907
1150	18.95	17545.4	38.838	23.582
1200	19.05	18495.3	39.648	24.235

Figure 1 represents the heat capacity from 0 to 1,200 °K. The two independent curves for C_p represent the smooth values of Osborne and Westrum and of the present work respectively, and join very smoothly, as noted above. The points indicate mean unsmoothed high-temperature values, as they correspond to successive differences in the column of mean heat contents of table 3 but embodying the small curvature corrections indicated by eq (6).

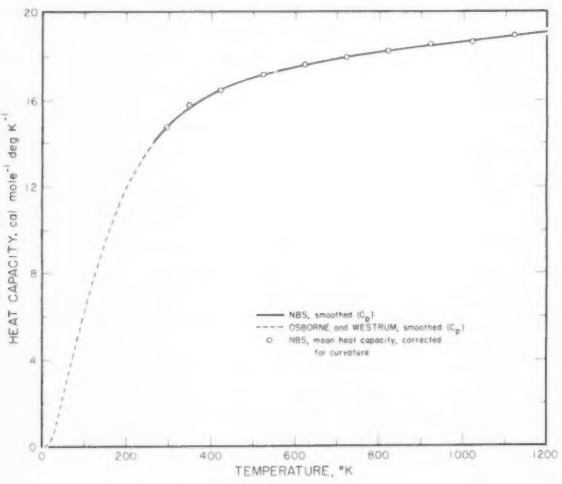
HEAT CAPACITY, cal mole⁻¹ deg K⁻¹
TEMPERATURE, °K
NBS, smoothed (C_p)
OSBORNE and WESTRUM, smoothed (C_p)
NBS, mean heat capacity, corrected for curvature

FIGURE 1. *Heat capacity of thorium dioxide.*

5. Discussion of Experimental Results

Evidence as to the probable accuracy of the heat-content values given by eq (1) and of heat capacity given by the derivative of this equation can be obtained from three sources: (1) The reproducibility or precision of the measurements, (2) an examination of the likely systematic errors, and (3) the agreement among different observers.

Taking into account only the effect of the precision at a given temperature in the individual runs on the empty container and also those on the container with sample, the probable error of the mean unsmoothed net heat content of thorium dioxide sample 1 at a given temperature, relative to that at 0 °C, can be shown from table 3 to average ± 0.004 cal g^{-1}. This corresponds to a variation from ± 0.10 percent or less between 50 and 300 °C to ± 0.01 percent or less from 400 to 900 °C. The average deviation of the mean experimental heat-content values from the values given by eq (1) is ± 0.014 cal g^{-1}. This corresponds to a variation from ± 0.21 percent up to and including 300 °C to ± 0.04 percent between 400 and 900 °C. The reproducibility of the ice calorimeter was as good during the thorium-dioxide measurements as with the most precise measurements with the same apparatus in the past. A careful analysis of all possible sources of error, systematic as well as accidental, led to the conclusion that the largest uncertainty is that due to the amount of sodium present in the thorium-dioxide sample. The qualitative spectrochemical analysis reported in section 2 indicated less than 0.05 percent sodium, but even this upper limit contributes an uncertainty of ± 0.2 percent in both heat-content and heat-capacity values. All other possible sources of error were estimated to contribute ± 0.05 percent at 400 °C and ± 0.1 percent at 900 °C. Therefore the total probable error in heat-content and heat-capacity values reported here is estimated to be approximately ± 0.2 percent between 400 and 900 °C. Below 400 °C the uncertainties in heat content are probably closer to ± 0.3 or ± 0.4 percent, owing in large part to the decreased percentage reproducibility of the calorimeter because of low heat contents. Measurements of the heat-content of standard-sample α-aluminum oxide, made immediately after the present thorium dioxide experiments, indicate agreement at 400 and 700 °C with smoothed reported values [5] within the estimated accuracy of the latter.

The heat-content values obtained for low-density thorium dioxide sample 2 have not been included in this discussion. Because sample 1 was much closer to the X-ray density, had more reproducible heat-content values, and did not show as good agreement with sample 2 as had been expected, the heat-content values of sample 2 were neglected. A complete series of heat-content measurements, not recorded in this paper, was made on thorium dioxide samples 1 and 2 before the reported results were obtained. The subsequent discovery of a leak in the mercury

line of the ice calorimeter indicated the advisability of repeating the measurements after the leak was repaired. The results reported here for sample 1 agree well with those obtained earlier, with the exception of those at 200 and 900 °C, which were both higher in the earlier than in the later series of measurements. The measurements on sample 2 made before the leak was repaired indicated that this sample, in general, showed a higher heat content than sample 1 at all temperatures. This trend is indicated by a comparison of the heat-content values in the second and third columns of table 3 although the values agree within the poorer precision on sample 2. This lower precision seems to be due to the sample itself and not to the experimental proceedure.

Figure 2 affords a comparison of the present measurements with previously reported values, in the form of percentage deviation of individual unsmoothed measurements of $(H_t^\circ - H_0^\circ{}_{°C})$ from eq (1). The present measurements fill a previous gap in ThO_2 heat-content data from 25 to 250 °C. The agreement with Osborne and Westrum is outstanding considering the very small values of heat content involved. Southard [7] used the same form of equation as eq (1) to represent his results, but some of his individual heat-content values deviate from his equation by comparatively large amounts. Southard's smoothed results above 500 °C are nearly parallel to eq (1), indicating nearly the same heat-capacity values from 500 to 900 °C as obtained in the present work. Because figure 2 represents percentage deviations, this fact is not immediately apparent. Jaeger and Veenstra [8] obtained heat-content values which vary from eq (1) by comparatively large, irregular amounts. Because of the superior precision of the present measurements and previous experience with this calorimeter, the authors believe that the smoothed values in this paper are the most accurate yet reported for ThO_2 in the high-temperature region.

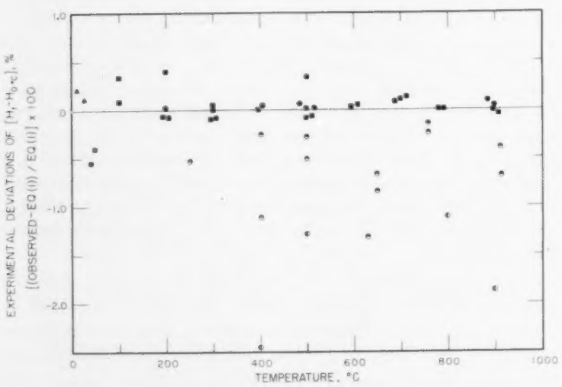

FIGURE 2. *Comparison of the heat content, relative to* 0 °C, *of thorium dioxide obtained from equation 1 with the values obtained in other investigations.*

(Some of the observed points have been displaced horizontally by small amounts in order to avoid the confusion of overlapping. For each of the two sets of NBS data, all observed points for a given temperature are based on the *mean* empty-container value observed for that temperature.) ————, NBS equation 1; ■, NBS sample 1; ●, NBS sample 2; ▲, Osborne and Westrum; ◓, Southard; ◐, Jaeger and Veenstra.

6. Summary

This paper has presented precise measurements of the heat content of high-density sintered thorium dioxide. As anticipated, no transitions which might mar the suitability of this material as a heat-capacity standard were found to occur below 900 °C. Measurements on a lower-density sample showed poorer precision than those on the high-density sample. The two sets of measurements agree within the precision of the former.

Further precise studies should be made to determine the thermal behavior of high-purity ThO_2 powder and of high-purity samples obtained independently of the batch described in this paper. The authors believe that further heat measurements on pure thorium dioxide should be made to the highest possible temperatures to determine its suitability as a heat-capacity standard for temperatures which exceed the useful range of α-Al_2O_3. If thorium dioxide is to be used as a standard it should be useful as such from room temperature to temperatures in excess of 2,000 °K.

An important advantage of α-Al_2O_3 as a standard is the uniformity of the macroscopic crystals used. Macrocrystalline ThO_2 was not available for the measurements described in this paper. If high-density pressed thorium dioxide is to be a suitable standard it must be shown that different specimens of the same purity and of approximately the same density are close enough in thermal behavior that differences are undetectable within the precision of the best high-temperature calorimetric apparatus.

One important condition which α-Al_2O_3 is assumed to meet as a heat-capacity standard is that different specimens from the same large batch have nearly identical thermal properties. This assumption has generally been accepted, although the National Bureau of Standards has published data on only two specimens [1,9]. Several other specimens have been checked at one or two temperatures only without observing any significant differences from published values. Such a test is frequently used to monitor the performance of the apparatus used in the present work (see sec 5 of this paper).

Measurements at 600 and 900 °C were made on a second high-density ThO_2 specimen from the same batch of powder. At the same temperature, all measurements on both specimens agreed within 0.1 percent of the heat content relative to 0 °C. Although this does not definitely prove the suitability of pressed samples as standards, it does support the authors' belief that within the precision of present-day high-temperature calorimetric measurements, individually pressed, fired, and sintered specimens from the same homogeneous batch of

powder should have the same reliability as heat-capacity standards as the macrocrystalline α-Al_2O_3 now used.

7. References

[1] G. T. Furukawa, T. B. Douglas, R. E. McCoskey, and D. C. Ginnings, J. Research NBS **57,** 67 (1956) RP2694.
[2] F. D. Rossini, D. D. Wagman, W. H. Evans, S. Levine and I. Jaffe, Selected values of chemical thermodynamic properties, NBS Circ. 500 (U.S. Government Printing Office, Washington, D.C., 1952).
[3] H. F. Stimson, Am. J. Phys. **23,** 614 (1955).
[4] D. W. Osborne and E. F. Westrum, Jr., J. Chem. Phys. **21,** 1884 (1953).
[5] D. C. Ginnings and G. T. Furukawa, J. Am. Chem. Soc. **75,** 522 (1953).
[6] Private communication between D. W. Osborne and G. T. Furukawa.
[7] J. C. Southard, J. Am. Chem. Soc. **63,** 3142 (1941).
[8] F. M. Jaeger and W. A. Veenstra, Proc. Acad. Sci. Amst. **37,** 327 (1934).
[9] D. C. Ginnings and R. J. Corruccini, J. Research NBS **38,** 593 (1947) RP1797.

(Paper 65A2–92)

JOURNAL OF RESEARCH of the National Bureau of Standards—A. Physics and Chemistry
Vol. 65A, No. 2, March–April 1961

Calculated Energy Dissipation Distribution in Air by Fast Electrons From a Gun Source [1]

John E. Crew [2]

(November 22, 1960)

Results of calculations on the energy dissipation distribution for electrons from a point collimated (gun) source in an infinite air medium are presented. The calculation has been made for a monoenergetic source of 0.4 Mev electrons. The method of moments has been employed, fitting the two spatial variables separately.

1. Introduction

Calculations of the energy dissipation distributions for fast electrons in infinite and homogeneous media have been reported for the simplest source geometries.[3,4] The problem of electron penetration is considered to be the following: given a source of electrons in a material, calculate the energy deposited by the electrons in a small spherical volume as a function of its position in the material. Spencer has calculated the energy dissipation distributions for the plane perpendicular source and the point isotropic source,[3,4] using the moment fitting technique which has proved successful in treating X-ray penetration.[5] His calculations were made for a variety of materials and for a range of source energies from 25 kev to 10 Mev. Agreement with available experimental data has been good.

The present work is concerned with a source geometry involving two spatial variables, namely that of the point collimated (gun) source, and corresponds to the following experimental situation: A collimated beam of monoenergetic electrons originates at a point in the medium. As the electrons move about, they dissipate energy. The quantity we determine, $J(r,\alpha)$, is basically the energy dissipated in a small volume at a distance r from the source point, at an obliquity angle α with respect to the initial line of fire, and at an azimuthal angle ϕ relative to an arbitrary reference plane.

2. Calculation of the Moments

Following the notation of footnote (4), the electrons are assumed to be generated at energy E_0, with residual range r_0 and stopping power $(-dE/dr)_{E0}$. If N electrons are produced by the source, then the energy dissipated in a small volume $dV=r^2 drd\phi d(cos\alpha)$ at the position (r,α,ϕ) is

$$\frac{dE}{dV}=\frac{N(dE/dr)_{E0}}{r_0^2}J(r,\alpha). \tag{1}$$

Determination of the function $J(r,\alpha)$ is our objective. This is accomplished by fitting moments of the closely related function

$$F(r,\alpha)=2\pi(r/r_0)^2J(r,\alpha). \tag{2}$$

$F(r,\alpha)$ is proportional to the energy dissipated per unit volume in a narrow ring of the material, whose symmetry axis is the initial line of fire, at a position (r,α). The moments

$$F_{n,l}=\frac{1}{r_0}\int_0^{r_0}(r/r_0)^n dr\int_{-1}^{1}d(\cos\alpha)\,P_l(\cos\alpha)\,F(r,\alpha). \tag{3}$$

Thus for total energy production by the source NE_0, the lowest order coefficient is

$$F_{0,0}=\frac{1}{r_0^3}\int J(r,\alpha)dV=\frac{E_0}{r_0(dE/dr)_{E0}}. \tag{4}$$

The $F_{n,l}$ may be represented as linear combinations of a set of basic coefficients

$$I_{n,l}^{m,l_0}=\int_0^1 dt\left[\frac{(1+\alpha)t}{t+\alpha}\right]^{m-n-\frac{1}{2}}$$
$$2\pi\int_{-1}^{1}dx\,x^n\int_{-1}^{1}d(\cos\alpha)\,P_l(\cos\alpha)\,I_{l_0}(t,\alpha,x) \tag{5}$$

obtained by solution of the differential equation

$$-\frac{\partial I_{l_0}}{\partial t}+\cos\alpha\frac{\partial I_{l_0}}{\partial x}=\int_0^{2\pi}d\varphi'\int_{-1}^{1}d(\cos\alpha')S(t,\Theta)$$
$$\{I_{l_0}(t,\alpha',x)-I_{l_0}(t,\alpha,x)\}+\frac{(l_0+\frac{1}{2})}{2\pi}\,\delta(x)\delta(t-1)\,P_{l_0}(\cos\alpha). \tag{6}$$

[1] Supported in part by U.S. Atomic Energy Commission.
[2] Now at Physics Department, University of Illinois, Urbana, Illinois.
[3] L. V. Spencer, Phys. Rev. **98**, 1597, (1955).
[4] L. V. Spencer, NBS Mono. **1**, (1959).
[5] Fano, Spencer, and Berger, *Encyclopedia of Physics* (Springer-Verlag, Berlin, 1959) vol. **38**, pt. 2.

This equation describes penetration by electrons originating on a plane, with intensity in different directions given by a Legendre polynomial. The parameter t is the remaining fraction of the electrons' initial range, x is the distance from the source plane in units of the initial electron range, and the scattering kernel $S(t,\Theta)$ has an energy dependence expressed by a factor $[t(t+\alpha)]^{-1}$. (See footnote [4].)

Using the stopping power representation of eq. (14) of footnote (4) together with eq. (12.19) of footnote (5), which by symmetry applies also to the case of isotropic detector and collimated source, we write

$$F_{n,l}=\frac{\left(\frac{n-l}{2}\right)!\left(\frac{n+l+1}{2}\right)!2^n}{(2l+1)n!\,(\frac{1}{2})!}\sum_{i=1}^{4}A_i I_{n,0}^{(n+i-\frac{3}{2}),\,l} \quad (7)$$

where the A_i's are given in footnote (4).

Spencer has kindly made available to us tabulations of $I_{n,0}^{m,l_0}$ obtained with a generalized version of the machine program described in footnote (4). We have calculated from these a triangular set of $F_{n,l}$ values with $l\leq n\leq 12-l$, $0\leq l\leq 6$. The spatial moments $F_{n,l}$ were used to compute a set of functions $F_l(r)$ by the function fitting procedure of footnote (4). These moments are listed in table 1. Computations have been carried to six digits throughout for the sake of internal consistency.

TABLE 1. *Spatial moments for a point collimated source of 0.4 Mev electrons in air*

The entries written as $N(m)$ are to be interpreted as $N\times 10^m$

n	l	$F_{n,l}$	n	l	$F_{n,l}$
0	0	0.143977 (1)	9	1	0.232118 (−1)
1	1	.512249 (0)	9	3	.838418 (−2)
2	0	.383407 (0)	9	5	.157837 (−2)
2	2	.176665 (0)	9	7	.173430 (−3)
3	1	.182270 (0)	9	9	.123226 (−4)
3	3	.558737 (−1)	10	0	.217520 (−1)
4	0	.156178 (0)	10	2	.116838 (−1)
4	2	.741548 (−1)	10	4	.309866 (−2)
4	4	.162271 (−1)	10	6	.457991 (−3)
5	1	.827478 (−1)	10	8	.414279 (−4)
5	3	.265519 (−1)	10	10	.200647 (−5)
5	5	.436366 (−2)	11	1	.134557 (−1)
6	0	.744594 (−1)	11	3	.511519 (−2)
6	2	.369759 (−1)	11	5	.103639 (−2)
6	4	.854666 (−2)	11	7	.123527 (−3)
6	6	.109575 (−2)	11	9	.937227 (−5)
7	1	.422286 (−1)	11	11	.539047 (−6)
7	3	.144003 (−1)	12	0	.127403 (−1)
7	5	.251286 (−2)	12	2	.706332 (−2)
7	7	.258849 (−3)	12	4	.199041 (−2)
8	0	.389695 (−1)	12	6	.317900 (−3)
8	2	.201798 (−1)	12	8	.312289 (−4)
8	4	.500374 (−2)	12	10	.201874 (−5)
8	6	.683193 (−3)	12	12	.922263 (−7)
8	8	.578889 (−4)			

3. Construction of the Energy Dissipation Function

The fitting of the moments $F_{n,l}$ in r yields a set of functions

$$F_l(r)=2\pi\int_{-1}^{1}F(r,\alpha)\,P_l(\cos\alpha)\,d(\cos\alpha). \quad (8)$$

The same asymptotic form for the trial function for $F_l(r)$ was used as for the plane perpendicular source calculation in footnotes 3 and 4. The function $F_l(r)$ is normalized to unity at the origin, this boundary condition being assured by choosing the trial function

$$F_l(r)=\left(1-\frac{r}{r_0}\right)^{\gamma}\exp\left[-A_l r/(r_0-r)\right]$$
$$+\frac{r}{r_0}\sum_i\frac{\alpha_i}{\beta_i^{l+2}}\left(1-\frac{r}{\beta_i r_0}\right)^{\gamma}\exp\left[-A_l r/(\beta_i r_0-r)\right]$$
$$\text{for } 0\leq\frac{r}{r_0}\leq\beta_i$$
$$=0 \qquad \text{for } \frac{r}{r_0}>1. \quad (9)$$

The asymptotic constant A_l is calculated from the two highest moments of $F_{n,l}$, and the coefficients α_i,β_i are computed by fitting moments according to the procedure of footnote (4). The parameter γ was set equal to zero for $0\leq l\leq 3$. The choice $\gamma=1$ gave a better fit for $l=4$. The results of the fitting in r are shown in figure 1. The results for $l=0$ correspond to the case of a point isotropic source and are in close agreement with the previous calculation by Spencer.[4]

To obtain $F(r,\alpha)$ it is necessary to sum the Legendre series

$$F(r,\alpha)=\sum_{l=0}^{\infty}(l+\tfrac{1}{2})\,F_l(r)\,P_l(\cos\alpha) \quad (10)$$

using the set of $F_l(r)$'s known for $0\leq l\leq 4$. However, the series has very poor convergence unless terms with $l>>4$ are included; hence it was necessary to perform an extrapolation to higher l values. By fitting the F_l to a suitable form and making use

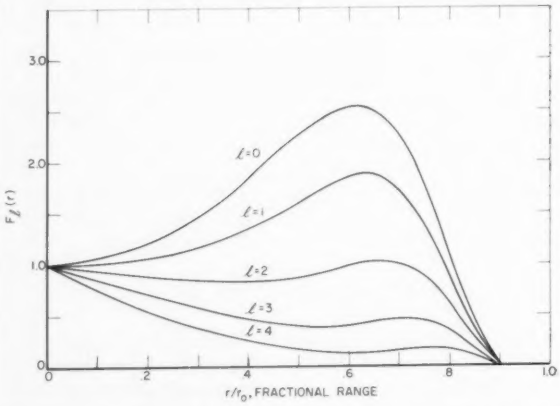

FIGURE 1. *First five partial moments in r versus radial distance from the source in units of the fractional range,* r/r_0.

$F_l(r)$ is in units of stopping power of 0.4 Mev electrons in air per unit range per electron.

[4] L. V. Spencer, NBS Mono 1, (1959).

of the generating function for Legendre polynomials, it was possible to sum the series.[6] The following form was used over an appreciable portion of the electron range:

$$F_l=\sum_i a_i(l+\tfrac{1}{2})^n \exp\left[-b_i(l+\tfrac{1}{2})\right] \tag{11}$$

for n an integer. If in the generating function for Legendre polynomials

$$(1-2xz+z^2)^{-1/2}=\sum_{l=0}^{\infty} z^l P_l(x) \tag{12}$$

the substitutions $z=e^{-a}$ and $x=\cos\alpha$ are made, it is easy to show that

$$F(r,\alpha)=\sum_i a_i \frac{(-1)^{n+1}}{\sqrt{2}} \frac{\partial^{n+1}}{\partial b_i^{n+1}} (\cosh b_i-\cos\alpha)^{-1/2}. \tag{13}$$

[6] L. V. Spencer, private communication.

This method was used for $r<0.5r_0$ with $n=1$. For larger values of r the series converges more rapidly, so that a simpler method of extrapolating to higher F_l values was used. A plot of $\log[F_l/(l+1/2)^m]$ versus l was made. A value of m yielding a straight line for the last three or four calculated F_l was chosen by trial and error and the higher values obtained by extrapolating this line. The series was then summed explicitly with only a moderate number of higher l terms required. From $F(r,\alpha)$ the desired energy dissipation function $J(r,\alpha)$ was obtained according to eq (2). A plot of the energy dissipation function versus α for different penetrations r/r_0 is presented in figure 2. A plot of $J(r,\alpha)$ versus r/r_0 for different angles α is given in figure 3. A polar diagram showing contours of constant energy dissipation is given in figure 4.

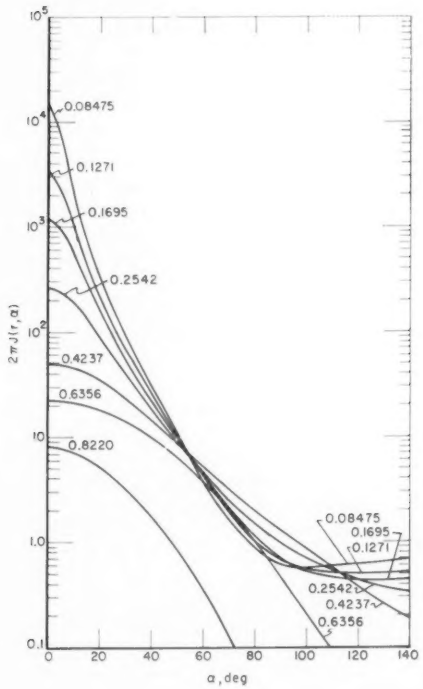

FIGURE 2. *Energy dissipation function versus angle with respect to initial beam direction for various radial penetrations,* r/r_0.

$J(r,\alpha)$ is in units of stopping power of 0.4 Mev electrons in air per sterradian per unit range per electron.

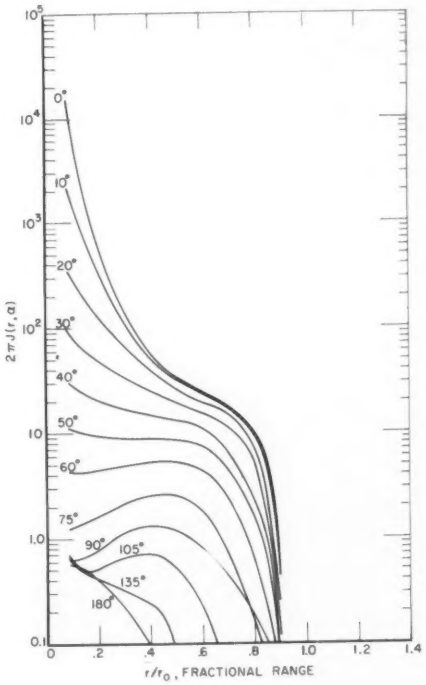

FIGURE 3. *Energy dissipation function versus radial penetration for various angles with respect to initial beam direction.*

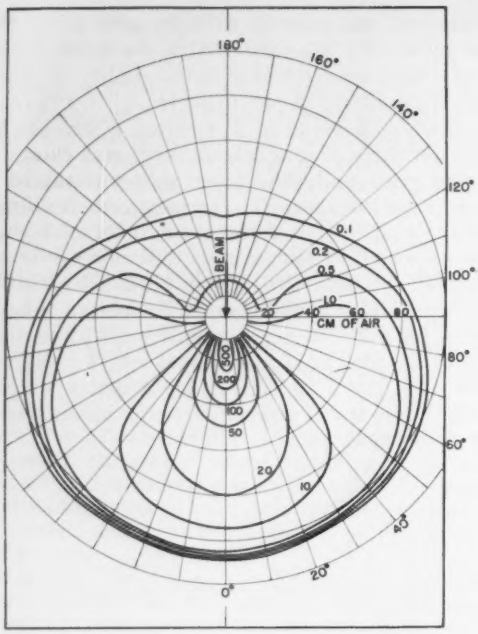

FIGURE 4. *Contours of constant energy dissipation in air for 0.4 Mev electrons.*

Contours of $2\pi J(r,\alpha)$ are shown, with the radial distances giving the penetrationi n cm of air at 76 cm of Hg and 25 °C.

(Paper 65A2–93)

4. Discussion

At present there are no experimental data with which to compare our results. Results of calculations for the one-dimensional problem have yielded results in good agreement with experiment. Calculations with slightly different trial functions generally reproduce results within about 3 percent. Since we are fitting twice, the errors can be expected to multiply, and our results cannot be expected to be better than about 10 percent. The exact value of the asymptotic constant A_l is not very critical. A variation of 10 percent in A_l affects the fit by more than the expected 3 percent error in fitting only on the tail of the distribution. The results in this region are not expected to be very precise anyway due to neglecting the range straggling. The values of the energy dissipation function near the source are of low precision because of the very slow convergence of the Legendre series in this region and also of low precision in the backward hemisphere for all penetrations because these values result from taking differences of nearly equal numbers.

An alternative double-fitting procedure would be to use the spatial moments in cylindrical coordinates (z, ρ). This presents an additional difficulty due to the fact that while the fitting in z is straightforward the asymptotic form to use in the fitting in ρ is not known.

The author expresses his appreciation to Dr. H. O. Wyckoff for suggesting this calculation. He is greatly indebted to Dr. L. V. Spencer for providing the plane source moments used as a starting point for this work and for valuable discussions. He also wishes to acknowledge the excellent work of Mrs. Sally Peavy of the NBS Computation Laboratory in performing certain calculations.

JOURNAL OF RESEARCH of the National Bureau of Standards—A. Physics and Chemistry
Vol. 65A, No. 2, March–April 1961

Vitrons as Flow Units in Alkali Silicate Binary Glasses[1]

Leroy W. Tilton

(November 23, 1961)

Two volume-changing processes found useful in studying the mechanism of viscous flow in glasses are: (a) stress-induced variation in fissuring near vitrons at their peripheries where the Si–O bonds are tensed and weakened, and (b) distention and modification of all silica network by added oxides. These idealized processes, readily derivable from the vitron concept of pentagonal ring structure in glass [1],[2] are sensitive to both temperature and composition and have previously been found useful [1, 2, 3, 4, 5] for understanding other properties of glasses.

Viscous flow of vitrons as units in annealing ranges, and at higher processing temperatures for silica-rich glasses, is here viewed as permitted primarily by the breaking of tensed and weakened Si–O bonds in shell-like stressed tissues surrounding vitrons. For modifier-rich glasses at high temperatures, where the activation energy of flow is known to be low for alkali silicates but slightly higher for alkaline earths, the shearing of cation-to-oxygen bonds may also be involved. The fissures between vitrons and matrix network may provide free volume for cooperative maneuvers among the vitrons.

At high processing temperatures, both viscosity and activation energy of flow are known to decrease monotonically and at first with extreme rapidity as the content of modifiers increases. This is understandable if even slight modification materially decreases the local pliability of the matrix network and oxide-volume expansion progressively widens the fissures that must be created at vitron peripheries where the radial contraction of vitron growth potential is checked by tangential Si–O bond stresses.

On cooling toward annealing temperatures, the observed rapid increases in viscosity and in activation energy of flow are here ascribed to a general tendency toward narrowing of *peripheral* fissures, with stronger bonds therein, as the distorted dodecahedral cages return toward symmetry in response to the increases in O–O repulsions. Such repulsions increase with extreme rapidity if ionic separations become smaller than equilibrium distances.

Near the annealing ranges where it becomes necessary to hold glasses at constant temperatures for appreciable times in order to observe flow of the high-temperature type, it is noticeable that the activation energy of flow *increases* as the content of modifiers increases. This suggests that the closure of fissures at these very low processing temperatures may be more effective in preventing cooperative maneuvers than in resealing the weak and broken Si–O bonds.

Below annealing temperatures, where the readily observed viscosities become somewhat higher while the activation energies decrease very rapidly, it is suggested that the character of flow is changing until finally there are possible only volume relaxations with such small relative movements as are permitted by the bending rather than breaking of bonds.

1. Introduction

Little is known about the mechanism of viscous flow in silica-rich glasses and the random network theory has been inadequate for describing units of flow. According to the vitron concept [1] of modulated microregularity of structure which the writer [1, 2, 3, 4, 5] has applied in studies of simple silicate glasses, nearly one-third of the silica forms small and limited clusters of dodecahedral cages called vitrons (computed density 1.99 g/cm^3 for (Si–O)=1.60 A) within which central bonds are strong, the structure nearly regular, and the cavities large. Only oblately deformed cages can completely unite with neighbors on all sides. These microregions, the vitrons, are necessarily surrounded by relatively thin peripheral tissues or channels within which most bonds are weak and some are broken, and the structure is much less regular and partially collapsed. The vitrons and their surrounding weak tissues must be well distributed, immersed or imbedded, in what may be a matrix of "random network" in the usually accepted sense but necessarily somewhat denser than vitron structure. The thin channels and the random network are assumed to have an average density approximating 2.30 g/cm^3 like neutron-irradiated silica as reported by Simon [6]. The random network is assumed to be stress-free with a short-range order resembling that in vitrons but with the average cavity size somewhat smaller.[3]

1.1. Fissuring

Vitrons as postulated are necessarily noncrystal (having five-fold symmetry) and therefore their growth is automatically limited by stresses and the peripheral bonds are necessarily weak. Consequently a corrollary of the vitron concept is a bal-

[1] Part of an invited paper read at the Pittsburgh meeting of the American Ceramic Society, 1958. Abstract 1G, Bull. Am. Ceram. Soc. **37**, 43 (1958).

[2] Figures in brackets indicate the literature references at the end of this paper.

[3] This vitron conception of the structure of silicate glasses is in accord with tentative conclusions reached by Warshaw from his electron microscopy of glass surfaces (J. Am. Ceram. Soc. **43**, 4, 1960), and is well illustrated by his fig. 14 which is a schematic representation of the bulk glass showing the possible origin of the fractured surface which would yield the structure shown in the electron micrographs of his study.

anced system of stresses and strains involving (a) intra-tetrahedral attractive and repulsive forces tending to promote symmetry within the tetrahedra, and (b) tensed Si–O bonds maintaining the peripheral bridging contacts between tetrahedra so that the outer dodecahedral cages can exist. When temperature changes, stress-induced variations should occur in the average effective thicknesses of the thin peripheral regions where many bonds are weak and broken. In discussions of vitron theory, the occurrence of such thin regions and volume variations therein is called *fissuring*.

Fissuring may occur *laterally*, as intravitron defective regions between the outer cages of vitrons, or *peripherally* as defective links between the outer cages of vitrons and the surrounding silica network. The idea of fissuring, in general, has already been found useful in understanding the mechanical weakness of bulk specimens of silica glass and some second-order abnormal effects of temperature and pressure on its volume [1, p. 149].

Lateral intravitron fissuring is probably the chief cause of the increases (1.5 percent) in the partial molar volumes of silica found at low modifier content by Callow [7]. This lateral type is more important, volumetrically, than the peripheral type, but may have little or no effect on viscosity because lateral fissures are inclosed within the vitrons as units. In general, the peripherical fissures, which seem predominantly related to viscosity, should tend to close somewhat on cooling (whereas those of lateral type should be expected to open) under the increasing symmetrical tendencies incident to the cooling. No references to lateral fissuring will be intended in this paper unless specifically so stated.

1.2. Modifiers and Fissuring

According to circumstances, peripheral fissures created at high temperatures by the oblate distortions [4] of dodecahedra necessary for vitron growth may be hampered in extent of their creation by the steric hindrance of modifiers present within the dodecahedra, and limited in their growth or maintenance by the symmetrical strength of tetrahedral units as supported by 0–0 repulsions.

Empty dodecahedra of silica glass probably deform elastically more easily than such cages with oxides therein and the dodecahedra grow together in clusters to form vitrons more easily (possibly into larger clusters). The surrounding network being also empty, its cavities likewise deform easily. Thus the distribution of stresses at vitron peripheries may be more general and greater in radial depth so that the effective peripheral shells or fissures, in which exist the critical stresses and strains, may be thicker but the individual bonds remain stronger than in modified silica glasses. Thus the viscosity of silica glass at very high temperatures becomes only moderately higher than in somewhat modified glasses at comparably high temperatures, but the activation energy remains very much higher.

In modified glasses the presence of oxides in the nonvitron cavities of the network makes the cages less pliant and deformable and thus less able to maintain good contacts with adjacent surfaces of vitrons. In other words, modified cavities of the matrix network are less adapted for closing the peripheral fissures that open as vitrons grow. This effect should be greater for oxides having large volumes or longer total extent. These views regarding the relative abilities of empty and modified cavities to influence the closure of fissures are somewhat consistent with Smyth's [5] mathematical analysis concerning the work done when glass is externally deformed.

According to these views, the more pliable a glass is with respect to local distortion, the greater its tendency to close peripheral fissures created by vitron growth and thus retard viscous flow of vitrons as units. Even slight modification stiffens vitron cages and matrix cavities, and especially the fissures, so that the fissures cannot so easily be closed. Hence vitron flow may be increased very rapidly and effectively by initial modification as compared with subsequent additions.

1.3. Temperature and Fissuring

The sensitivity of peripheral fissuring to temperature should be primarily a narrowing of fissures on cooling because of progressive return of the deformed dodecahedra and tetrahedra toward their natural symmetry as repulsions increase with extreme rapidity between the closely adjacent oxygen atoms within the tetrahedra. The narrowing of fissures should mean restoring of bond strengths. Such expectations are in general accord with the observed increase of about 50 cm^{-1} in frequency of the "valence-stretching" infrared peak near 1100 cm^{-1} upon cooling of fused silica from 1270 °C to room temperature, as reported by Neurath [8]. This contrasts with his similar finding that the cooling of two well-modified glasses from 1300 °C to room temperature causes increases of only about 25 cm^{-1} in frequency. This indicates that the fissures in well-modified glasses do not close easily and accords with the discussion above in section 1.2. on the relative properties of empty and modified cages and network cavities.

The narrowing of peripheral fissures on cooling would seem to mean increases in viscosity as well as in strength of bonds, although not necessarily so. For example, the conversion of wide gross fissures into many narrow ones, all in parallel, might eliminate critical channels for flow at low activation energy but have only moderate or small effect in increasing viscosity.

---

[4] Only dodecahedra that are radially decreased in diameter and elongated tangentially are usefully deformed for furthering growth of (spherical-type) vitrons in which all except a central cage must be so deformed as to touch and be integral with neighbor cages of the same shell, such as 12 around one.

[5] H. T. Smyth (J. Am. Ceram. Soc. **42**, 276, 1959) found that for silica-rich glasses, which have very low values of Poisson's ratio, work must also be done in internal distortion of the network; whereas for some well-modified glasses, with largest values of Poisson's ratio, it is necessary to assume that even more work is done in distorting the inclosed modifiers than in internal distortion of the network.

1.4. Oxide-Volume Expansion

As modifiers are added to silica glass there is a large structural expansion because of the added volumes that can only in part be included inside unstressed and undamaged cages of vitrons and similarly in other network cages. The mere presence of modifiers in the channels around vitrons expands these critically fissurable tissues and should be expected further to reduce Si–O bond strengths. This is in general accord with the observed decreases of about 50 cm^{-1} in frequency of the "valence-stretching" infrared peak near 1100 cm^{-1} when silica glass is very well-modified, as reported by Simon and McMahon [9] and also by Neurath [8]. There is also a structural expansion of the whole lattice or network attributable to the conventional and accepted concept of "broken bridges." Each additional ionized oxygen means one broken Si–O bridge and two oxygens each bonded to only one rather than two silicons. This process in its initial stages is conducive to a looser and more easily distendable network. These types of gross expansion are predominently structural and together they may appropriately be termed *oxide-volume expansion* [5]. This expansion in the peripheral shells subject to fissuring is here considered as an important factor contributing to the initial precipitate decrease in viscosity and activation energy of flow as modifiers are increased.

1.5. Proposed Flow Mechanism

It seems very plausible that differential volume changes among diverse components of structure should affect viscosity and particularly so for a modulated regularity in structure such as is entailed by the vitron concept. The object of this paper is to see if the vitron concept and corrollary ideas readily derivable therefrom are compatible with known data on the viscosity of glasses. The data that invite analysis in this structural study are chiefly viscosities and activation energies of flow expressed as functions of temperature and of degree of modification at comparable temperatures.

Preliminary surveys of such data indicate that, in general, both viscosity and activation energy of flow increase very rapidly as temperatures are lowered in the liquid glass fields, and it has already been surmised that cooling should be expected to narrow peripheral fissures and increase viscosity and activation energy of flow. The data also indicate that at high temperatures both viscosity and activation energy of flow fall rapidly as modification is increased. In contrast, at temperatures below annealing, viscosities remain very high while activation energies of flow fall to very low values.

A remarkable point is that at high temperatures (low viscosities) the activation energy for most silicate glasses is less than half that required to break Si–O bonds (estimated at 106 to 165 kcal/mole). Because of inability to account for this in a uniformly unstressed and strong network, Bockris and Lowe [10] and White [11] have postulated the presence in molten silica of large randomized discrete ions or "islands" and White suggests that they "permit viscous flow at lower activation energies by an ionic mechanism involving shear in the weak ionic links between anions (analogous to cleavage in crystalline silicates)".

In accord with their postulate, but in terms of vitron theory the processes operative in the viscous flow of silicate glasses would be largely localized in, or explainable because of, such weakened connective tissues as are being suggested in this paper for uniting vitrons with a comparatively stress free matrix of a more random network. In vitreous silica these tissues may be thought of as relatively thin—an irregular series of stressed bonds from Si^{+} of one vitron to an O^{-} of a neighbor network, etc. The peripheral or "surface" bonds of the vitrons are all under very considerable tension and thus below normal strength. Small impurities of any nature, including cation oxides, could interfere seriously with these connecting links and prevent sealing of some bonds. Even such cation or oxygen (or both) as may be trapped inside the network cavities may result in fissure tissues of greater abruptness—more localized stresses and consequently fewer weaker bonds for given total strain—than for unmodified silica. Vitron cages containing oxides will have less favorable (oblate) deformability at temperatures of formation and thus the average growth in size of vitrons may be lower as compared with conditions in unmodified and more pliable fused silica.

The flow mechanism for vitrons as units can be considered in similar manner to that sometimes given for atoms or molecules as flow units. In this case, however, many or perhaps all of the Si–O bonds near the peripheries of vitrons are already defective or very much below normal strength. Every vitron is somewhat of an island very imperfectly and perhaps somewhat loosely imbedded in a matrix of slightly denser but more pliable material.

The barriers to flow are chiefly the thin portions of the matrix network that intervene between vitrons to prevent their tangency. These portions are probably defective, little thicker than one or two tetrahedra, and they probably average between 6 and 12 vulnerable spots around the periphery of each vitron.[6]

The statistical processes continually taking place in the absence of applied stress and owing to the random energy of thermal motion, can be the making and breaking of the Si–O bonds in these vulnerable spots. The action of the externally applied stress makes it somewhat more likely for bonds to break in a direction parallel to local components of the stresses.[7] The innumerable fissures may supply free

[6] Very interesting possibilities are suggested by a comparison of this idea of fissuring with the concept of "fluctuating fissures" as proposed and illustrated by Jerzy Zarzycki (J. de Physique et le Radium **19**, 13A, 1958) to accord with his analysis of radial distribution curves for molten salts.

[7] This gives a slight flow corresponding to any stress, however small—a Newtonian flow. See H. T. Smyth, Glastechn. Berichte Sonderband **32K**, III, 28, 1959.

volume to such an extent that the activation energy of flow need not be much larger than the bond energy, except in unmodified silica glass and at low temperatures.

This idea of the nature of the barriers makes it easy to understand why the activation energy of flow can vary so widely with temperature and decrease so suddenly upon the addition of very small proportions of modifiers. If one thinks of about 5 tetrahedra involved in each peripheral vulnerable spot, then it follows that all such barriers may be effectively lowered by 16.7 mole percent modification.[8]

If the vitrons are approximately alined as in the "open packing" of spheres, a shear force on one plane of vitrons pushes it over another such plane. The free volume of the innumerable fissures allows cooperative lateral movements of adjacent vitrons that minimize the cohesive forces between the hypothetical planes.[9] For a closer packing of vitrons the required cooperative maneuvers are more extensive but of the same nature.

2. Viscosity Data

Measurements of viscosity of silicate glasses have been made over a range from a fraction of 1 poise to 1×10^{20} poises.[10] This remarkably wide range in this property is often overlooked because we usually plot viscosity on a logarithmic scale, or use only the logarithm of viscosity. The rapid *thermal* decrease in viscosity with increase in temperature, especially for molten glasses, is well known, but there is also an extremely rapid structural decrease in viscosity as modifier oxides are added to silica glass and particularly so for the initial additions. This is shown in figure 1 where isocomposition curves for 0, 15, 30, and 60 mole percent Na_2O are plotted from the data of Heidtkamp and Endell [12] and of Solomin [13].

2.1. Temperature Effects

The concomitant effects of temperature should be eliminated before plotting viscosity as a function of composition in order to study possible effects of fissuring and oxide-volume expansion. It is evident that temperature effects are not removed satisfactorily for comparisons of different glasses merely by using a constant temperature. It is sometimes suggested that equality of $d\eta/dt$ is a reasonable basis for the selection of "corresponding temperatures" where η represents viscosity and t is temperature. Such a criterion may be satisfactory for a comparison of structurally similar glasses. But

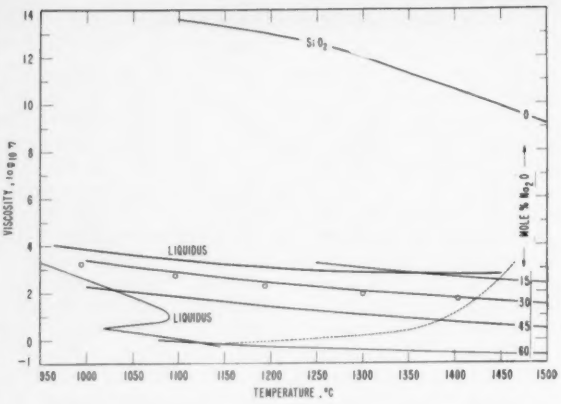

FIGURE 1. *Isocomposition curves of viscosities of molten glasses in the soda silicate system.*

The decrease in viscosity for the addition of the first 15 mole percent Na_2O is extremely large compared to subsequent equal additions. Curves for 15, 30, 45, and 60 mole percent Na_2O are taken from data by Heidkamp and Endell [12]; circles show data by Shartsis, Spinner, and Capps [31] for 30.1 mole percent Na_2O; the SiO_2 curve is from Solomin [13].

whether one uses a constant temperature (ordinates in fig. 1) or temperatures of equal slope (see for example, dashed line in fig. 1), it seems that the very great differences in viscosity between silica glass and one containing only a few percent of Na_2O must be chiefly of structural rather than thermal origin.

Another possibility for comparing the viscosities of compositionally different glasses involves use of the exponential equation

$$\eta = A \exp (B/RT) \qquad (1)$$

which has been much used for viscosities, also for ionic conductivities and diffusion phenomena in glasses. In this equation, A is a constant relating to frequency of the reaction, B is the activation energy for the process (R being the gas constant), and T is absolute temperature. This equation has been found valid for viscosities of nonpolymerized liquids over wide ranges of temperature.

For glasses this equation has been much used over short temperature intervals, especially at and near annealing regions where viscosities range from 1×10^{15} to 1×10^{13} poises. It is used also at the much higher molten-glass temperatures, but different constants are necessary in these two temperature regions. This will be evident from figure 2 if it be remembered that the straight-line equation

$$\log \eta = \log A + (B/RT) \qquad (2)$$

which relates viscosity and reciprocal of absolute temperature is equivalent to eq (1), and consequently

[8] See footnote, sec. 2.2.
[9] This type of flow for glass is mentioned by W. A. Weyl, Rheology Vol. **III**, p. 338; Academic Press, Inc., New York. 1960.
[10] A poise is the C.G.S. unit of absolute viscosity. In a liquid having unit viscosity a shearing force of 1 dyne will move a cm² surface with a velocity of 1 cm per second relative to and parallel with a similar surface distant 1 cm transversely.

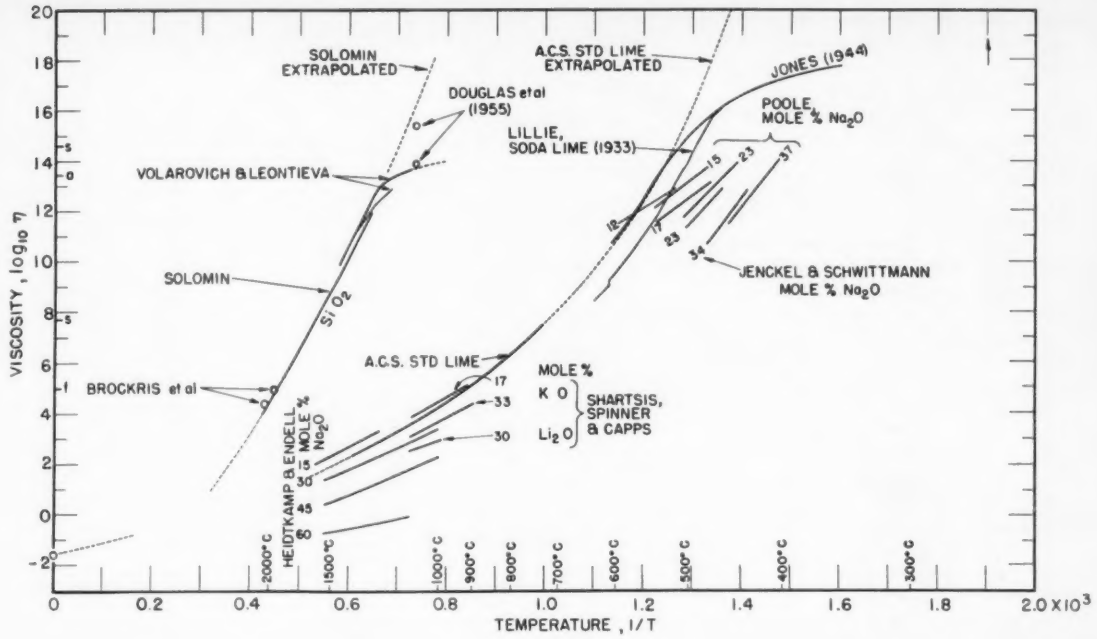

FIGURE 2. *Effect of modifiers on viscosities of silicate glasses.*

Note that modifiers reduce temperatures for isoviscous flow; that curves converge toward points at very low viscosities and high temperatures; also toward points at very high viscosities and low temperatures. The best formula for representing the viscosities of the American Ceramic Society's standard lime glass in fluid condition extrapolates to log $\eta = -1.6$ at infinite temperature, and to infinite viscosity at 250 °C. The same form of equation was used by Solomin [13] for SiO_2. (For data see literature ref [12, 13, 18 19, 24, 25, 26, 31, 33, 36].)

$d \log \eta/d(1/T) = B/R$. Figure 2 emphasizes the great difference between viscosities of molten glasses and so-called viscosities of glasses below their annealing ranges.

Several investigators, including Douglas [14], Cox [15], and Hodgdon and Stuart [16] have discussed equations for relating viscosity and temperature, but, as pointed out by Anderson and Stuart [17], these equations in each case reduce to 4-constant equations comparable with a dual writing of eq (1), once for high temperatures and again for low temperatures.

Others including Lillie [18] have sought to regard the constant, A, as a function of temperature, and Jones [19b] has suggested a continuous distribution of activation energies. Plumat [20] finds evidence of a step-wise distribution and "critical temperatures." An important clue for clarification may be recognition of the dominant role of the volume in determining the internal mobility of simple nonpolar liquids. One might follow Fox and Flory [21] in supposing that viscosity changes with temperature through two distinct effects: (1) the thermal energy available, and (2) the contribution of free volume to height of barrier. According to this idea one might seek to understand the inflections on some curves such as those of figure 2 at or near lower annealing [11] temperatures (where $\log \eta = 13$ approximately) if during cooling the bond-angle (3,4,5) configurational decreases in volume [11] are rapidly checked and an expansion by lateral fissuring between cages of vitrons is increased because of enforced quasi-rigidity and the stress-symmetry relationships.

Possibly all such views are more nearly consistent than their formal presentations indicate. However, there seems little assurance that the use of eq (1) can be entirely satisfactory for eliminating all temperature effects in the general comparison of glasses having different compositions.

Still another expedient for a survey of structural relationships, perhaps at approximately comparable

[11] The broad regions (unfortunately sometimes called transformation points) where such bond-angle decrease in volume would be checked are prominent on the curves of volume versus temperature as plotted for well modified glasses. It should be noted, however, that no traces of such a region have been reported for pure silica glass. Moreover White [11] and Tomlinson et al. [22] have reported data from which one may infer that such configurational changes in volume may be absent also in binary silicates, both alkali and alkaline earth, having less than 10 to 15 percent nonsilica. Such a threshold for bond-angle sensitivity accords with the idea that some oxides, as such, can be inclosed in the cages and that only metal ions can deform the electron clouds and occasion bond-angle sensitivity. Existence of this threshold is evidenced by the continuous decrease in the partial molar volume of silica in silicate glasses with more than 12 or 13 percent R_2O as reported by Callow [7]. See also lit. ref. 5, p. 16.

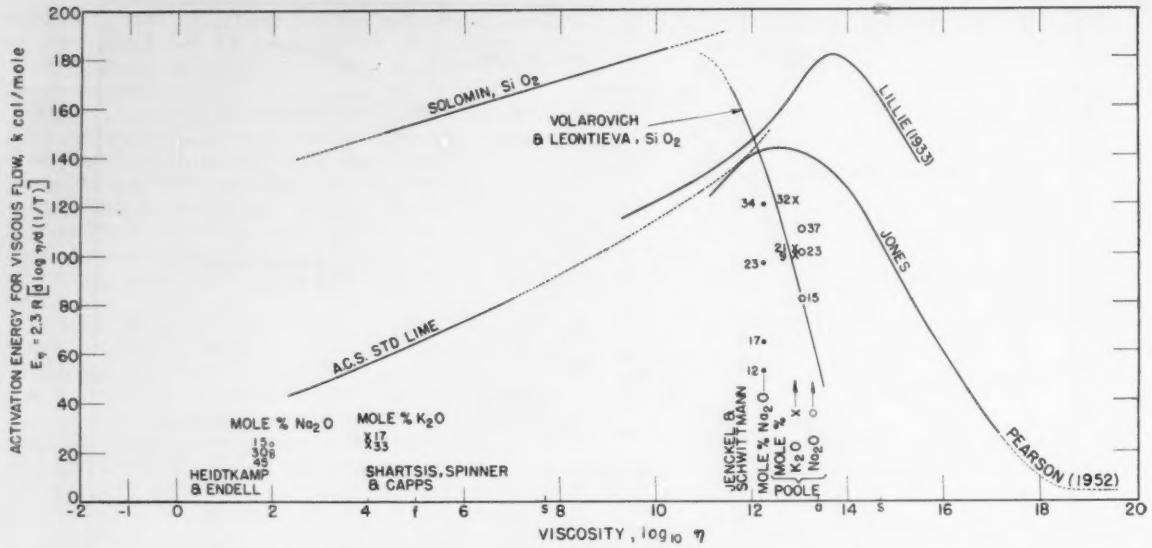

FIGURE 3. *General effect of modifiers on activation energy for viscous flow in molten and quasi-rigid silicate glasses.*

At temperatures where glasses are molten the activation energies are decreased by addition of modifiers but at lower temperatures the energies are raised by addition of modifiers. It is suggested that the high-temperature process of fissuring at the peripheries of vitrons is reversed on cooling by restored symmetry that is progressively enforced by the 0-0 repulsions, especially on near approach to quasi-rigid conditions. (For data see literature ref [12, 13, 18, 19, 24, 25, 26, 31, 34].)

temperatures, is exhibited in figure 3 where a number of computed values of activation energies have been plotted against log η to emphasize or accentuate the differences in flow properties above and below those regions where glasses change from predominantly fluid to quasi-rigid materials. That maximum values of the activation energy of flow occur in or near the annealing range (log $\eta = 13$ in fig. 3) has been explicitly noticed by Jones [19a] and by Stanworth [23c]. The maxima, of course, correspond with the inflections that are prominent in figure 2. The decrease to very low values at much lower temperatures, while viscosity remains high, suggests that the type of flow, if any, that occurs at very low temperatures is probably very different from that at high temperatures.

In figure 3 a number of points are plotted for several degrees of modification of various glasses, some for high temperatures and some for annealing temperatures. It will be noticed that higher oxide content correlates with lower activation energy of flow in liquid silicates but with higher activation energy in quasi-rigid glasses very near the annealing temperatures.[12] Similar data have been plotted in figure 4 to confirm this constrast between annealing and much higher temperature.

This reversal in structural effect seems, to a first approximation, to occur regardless of the type of modifier. At the lower temperatures it is especially difficult to explain the higher activation energy with higher oxide content on the basis of a continuous random network because modifiers are supposed to disrupt and weaken the structure as compared with that in pure fused silica. On a vitron basis, however, the processes of fissuring and oxide-volume expansion can serve to explain the reversal if it be remembered that the flow of vitrons requires not only that bonds between vitrons and matrix be broken but also that free volume be made available for the necessary cooperative maneuvers. At high temperatures the modifiers by their mere presence can cause extra tension and weaker bonds in critical fissures while free volume can be available by widely extended cooperative maneuvers. At low temperatures the modifiers are trapped in the fissures while they are being closed by the O-O repulsion effect and Si-O bond-angle contractions—a closure that may be much more effective in preventing cooperative maneuvers than in resealing weak and broken bonds. Thus the E_η curves for different modifications could cross and the correlation between E_η and degree of modification be reversed from decidedly negative at very high temperatures to decidedly positive at and near annealing.

[12] It will be noticed in figure 3 that the curve for E_η of fused silica at and below annealing should be shifted to *lower* viscosities by 1 or 2 units in log η in order to be entirely consistent with the plotted values corresponding to the work of Jenckel and Schwittmann [24] and of Poole [25]. That the locus may be imprecise for fused silica will be realized from the dual results reported for log η by Volarovich and Leontieva [26] as plotted in figure 2. On the other hand, the rapid descent of E_η for fused silica in figure 3 should correspond to a quasi-rigid condition such as is suggested by the other descending curves at somewhat *higher* viscosities on the right of the nominal annealing viscosity at log $\eta = 13.4$. To the extent that these data are reliable, it is indicated that glasses very rich in silica have their maximum activation energies of flow at viscosities appreciably lower than those for well modified glasses; that is at temperatures relatively higher in their annealing ranges.

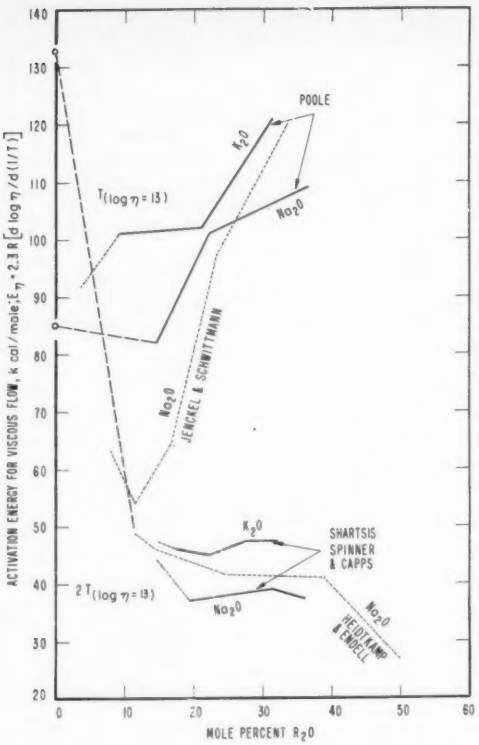

FIGURE 4. *Activation energies for isoviscous flow near annealing temperatures contrasted with those at twice annealing temperatures (absolute scale).*

For quasi-rigid glasses note the rising trends. For fluids there is a very sudden drop until cages are approximately filled with oxides; then a near steady state until cages are completely saturated. This confirms the reversal in structural effects noted in figure 3 and text. (For data see literature ref [12, 24, 25, 31].)

Such a reversal effect, if any, in respect to log η is not apparent from available data. Indeed, its existence for E_η may be partly an evidence of a change from high-temperature to low-temperature types of flow in silica-rich glasses that takes place gradually at temperatures between the softening and strain regions where values of E_η have their maxima.

This analysis of viscosity data, as presented in figures 2 and 3, suggests that there are both similarities and well-marked differences in the phenomena that have been designated as viscous, especially near annealing temperatures, in silicate glasses. Here it seems pertinent to recall that Lillie [18] prefers the equation

$$\log \eta = A + B/(T - T_0) \qquad (3)$$

for viscosities between 10 and 10^{12} poises, and says it is the only relationship between viscosity and temperature that fits high temperature data "within the expected limits of experimental error."

Although Lillie transforms eq (3) so that A becomes a function of temperature, the equation can be written also as

$$\eta = A' \exp\left(\frac{B}{T - T_0} \cdot \frac{T}{T}\right)$$

showing that the activation energy can be considered to increase as temperature is lowered. The values of T_0 required for this equation are well below temperatures in the annealing ranges. Possibly these T_0 temperatures can be regarded as ultra lower limits for viscous flow of a high-temperature type in which bonds at vitron peripheries are broken; limits where activation energy for such flow might become extremely high (because of position barriers) provided requisite, impossibly long periods could be taken for observations. Actually, Isard and Douglas [36] have reported for fused silica at 1080 °C both a low-temperature type of (high) viscosity immediately observed, and a high-temperature type of (even higher) viscosity observed after a holding time of 30 hours. Both points are shown in figure 2, the first agreeing with an extrapolation of results by Volarovich and Leontieva, the other with an extrapolation by eq (3) as used by Solomin with $T_0 = 455$ °K.

In contrast with the high and increasing activation energies of flow at equilibrium, according to eq (3), the activation energies of "flow" immediately observable in the really low-temperature region decrease and become of the order of magnitude for bending or stretching rather than breaking of bonds, and the number of such bonds that bend or stretch probably becomes extremely large. As mentioned above, this low-temperature flow could be the volume relaxation connected with the closure of peripheral fissures and the opening of lateral fissures consequent on the enforced further symmetry as cooling progresses. Such relaxation [13] during cooling has previously been mentioned by the writer [1, p. 149] and its minor contractive aspect through (peripheral) fissuring associated with the decrease in activation energy of flow near annealing temperatures. Also, its major expansive aspect through (lateral) fissuring was suggested [1, p. 150] as chiefly responsible for the very small and abnormal negative coefficient of equilibrium expansion as observed by Douglas and Isard [37] between 1000 ° and 1500 °C.

2.2. Structure Effects

The isotherms of activation energy of flow as plotted against mole percentage of various oxide

[13] There are on record two series of unexplained experiments which indicate that the dominating expansional aspect of this relaxation during cooling is temperature sensitive down to about 200 °C in fused silica. The first series, by Douglas and Isard [37] consists of measured differences between the expansivities for specimens of quenched silica glass after heat treatments to equilibrium at several different temperatures from 990 ° to 1480 °C. At 200 ° to 1000 °C the expansivities are numerically greater for the specimens which had higher-temperature heat treatments (and yielded greater values of densities). Below 175 ° or 200 °C the differences are negligible.

The second series, the compressibilities of silica glass at various temperatures from 0 to 400 °C and for 5 different pressure steps (F. Birch and R. B. Dow, Bull. Geol. Soc. Amer. **47,** 1235, 1936) shows not only that compressibilities become higher at increased pressures [1, p. 149], and that they decrease with increasing temperature, but that the decrease with temperature is most rapid near 175 ° to 200 °C. (See lit. ref. 1, p. 149; also C. L. Babcock, Stephen W. Barber, and Kasimir Fajans, Ind. and Eng. Chem. **46,** 161, 1954.)

modifiers in series of binary glasses have received only moderate attention. Stanworth [23a] gives activation energy data on a few glasses by Taylor and Dear [27] and by Taylor and Doran [28] for the transformation range, and MacKenzie [29] gives data for, or near, 1400 °C. Stanworth [23b] also reproduces such a curve published by Preston and Seddon [30] based on the viscosity measurements by Heidtkamp and Endell [12] at 1000 to 1500 °C. The Preston and Seddon energy curves agree more or less with MacKenzie's curve. Other data by Shartsis, Spinner, and Capps [31] are used by White [11] in similar curves that include the MacKenzie and other data.

From figure 5 and from figure 6 (which is reproduced from figure 5 of White's [11] thesis), it is noticeable that the respective curves for K, Na, and Li complete their rapid descent and cross each other in the region near 16.7 mole percent where one oxide molecule is available for each dodecahedral cage, or every 5 SiO_2.[14] Then it seems from the curves for the activation energy of flow (which descend only a little further) that the glass structure remains relatively constant until further addition of modifiers

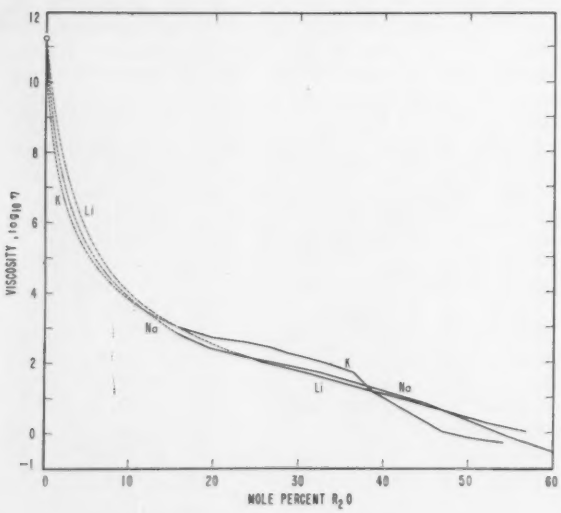

FIGURE 5. *Differential effects of modifier oxides on isothermal viscous flow of molten glasses. (Averages of data by Endell and Hellbrügge [35] at 1,250 to 1,450 °C.)*

Even slight oxide-volume expansion in the imperfect and denser network surrounding vitrons may localize and expand the peripheral fissures created by vitron growth. The largest K_2O oxide is most effective. The rapid decrease in viscosity is checked before 16.7 mole percent R_2O where one oxide molecule is available for every 5 of SiO_2. Thereafter all cages can offer some resistance to the distortion necessary for vitron growth and the formation of wider peripheral fissures.

[14] See table 1 and fig. 13 of paper cited in lit. ref. 2. Although table 1 was proposed for a silica glass structure consisting predominantly of vitrons, the principal of equidistribution of modifier oxide throughout the silica permits the table to to apply also to the vitron clusters immersed in denser network, to the residual denser network itself, and to the whole glass.

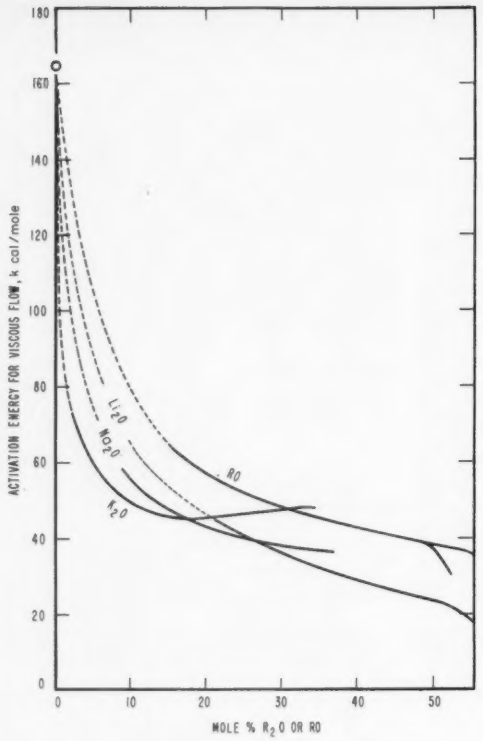

FIGURE 6. *Differential effects of modifier oxides on activation energies for isothermal viscous flow of molten glasses (1,400 °C). (From White's thesis [11].)*

Note the sudden drop increasing in the order Li, Na, K of increase in size of the oxides. After oxide saturation the descent is much less rapid, perhaps because fissures remain relatively constant and the activation energy is chiefly that for the breaking of cation-to-oxygen bonds.

up to at least 28.6, 37.5, and 50.0 mole percentages of K_2O, Na_2O, and Li_2O, respectively, which are the effective saturation limits for cation in the cages as previously deduced by the writer [3] from the data of Preston and Turner [32] on 20 hour volatilization losses at temperatures from 1100 to 1400 °C.

The marked changes in slope of the curves of figures 5 and 6 may indicate that two structural processes or factors are operating to advance viscous flow at high temperatures. One predominates in the high silica glasses with low modifier content, and the other process predominates after modification progresses beyond 16.7 mole percent.

The first factor, which acts very precipitately, may be fissuring combined with oxide-volume expansion in the fissures. This process, connected with or evidenced by structural changes in volume, predominates where the activation energies are sufficiently high to include the breaking of some Si–O bonds, especially those not of full strength because of (1)

fissuring and (2) fissures enlarged by oxide-volume expansion. In this low-modifier composition range, the viscosity and the activation energy for viscous flow fall more and more rapidly in the order Li, Na, and K (fig. 5), corresponding to the increasing volumes of the oxides that could be trapped in the fissures to prevent their normal closure, or trapped in the nonvitron cavities to make the network less pliable locally and less conducive to fissure closure.

At a concentration of 16.7 mole percent modifier, there will be one oxide molecule for every 5 tetrahedra. All cavities should be less deformable; the vitrons might cease growing at smaller diameters; the fissures should be wider; and the viscosity therefore could be much lower than for unmodified glass. From figure 5 (see also fig. 1) it can be estimated that the initial rapid structural-change process is essentially completed. The decreases of viscosity and of activation energy of viscous flow in the higher modifier range of composition are very gradual and may be caused by broken oxygen bridges and by steric hindrance of many modifiers trapped in the fissures.

In figure 6 it seems that at all degrees of modification the activation energy of flow falls appreciably slower for the alkaline earth oxides, which have smaller molar volumes and smaller maximum dimensions than any of the alkali oxides. This agrees with expectations that in silica-rich glasses the smaller sizes and volumes would make the earths less effective in promoting and maintaining fissuring. In the well-modified glasses (where flow may be effected by the shearing of weakened cation-to-oxygen bonds), it should be expected that divalent cations, each bonded to two unshared oxygens, can offer somewhat greater barriers to flow than the monovalent cations.

These structural interpretations accord with and tend to clarify the meaning implied by Shartsis, Spinner, and Capps [31] when they showed conclusively that "to a first approximation viscosity in these [alkali silicate] systems is a function of the number of alkali ions *per unit volume* and is almost independent of the type of alkali ion." (The effect of type of ion could be implicit, however, in that it can affect the volume.)

In contrast with these interpretations based on vitron theory, the most widely offered explanation of the decreases in viscosity upon the addition of modifier oxides is the concept of broken oxygen bridges. At high modifier contents, especially near 67 mole percent nonsilica where all 4 corner bridges of the tetrahedra are broken and the viscosity is less than one poise, this view is tenable, but the case seems very different for silica-rich glasses. At 16.7 mole percent modifier, where only 10 percent of all oxygen bridges can possibly be broken (even according to conventionally accepted estimates [15]), the viscosity at 1200 °C has decreased from 10^{13} poises for pure silica to 10^{3} poises for a melt of soda silicate glass (fig. 1). The decrease is extremely precipitate for the first few percent of added oxide [16] and relatively very slow after 16.7 percent (fig. 5).

Certain data from infrared studies may be cited here to illustrate the possible bearing of such investigations on structural conditions in glasses. From figure 6 (1400 ° C), the decrease in activation energy of flow at 16.7 percent modification is roughly 90 percent of the total observed decrease for full or maximum modification, and it has here been assumed that the energy of activation is that for the breaking of stressed Si–O bonds. In contrast, for room temperatures it has been shown by Simon and McMahon [9] that the decrease in wave number of the "valence-stretching" peak in the infrared near 1100 cm^{-1} is, for 16.7 percent modification, only about 30 percent of the total observed decrease for very considerable modification. If this evidence is confirmed by similar infrared data at various intermediate temperatures, it will then be shown that 90 percent of the decrease in barriers to flow is realized when about 30 percent of the realizable weakening of the network is effected. Such a result would confirm the idea that the flow depends on a special distribution of the weakened bonds.

3. Conclusion

At some very high molten-glass temperature the units that flow may be very much smaller than vitrons and the process may more nearly resemble those which take place in liquids in general.[17] However, it is here suggested that fissuring at the peripheries of vitrons is a basic phenomenon that provides space for cooperative maneuvers and governs a slip-channel process of vitreous flow in all silicate glasses at all moderately high temperatures where data have been taken.

Near annealing ranges, and in silica-rich glasses at higher temperature, flow is effected primarily by the breaking of tensed and weak Si–O bonds that are found chiefly in thin shell-like peripheral tissues surrounding the vitrons. In modifier-rich glasses, the shell-like tissues at very high temperatures may become channels populated with cations bonded to unshared oxygens and flow be effected primarily by the shearing of weakened cation-to-oxygen bonds. It is noticeable that in this structure range the activation energy for flow in alkaline earth silicates remains appreciably higher than that for the alkali silicates as would be expected if divalent cations, each bonded to two unshared oxygens, can hamper the relative movements of vitrons more than the monovalent cations.

---

[15] The writer has suggested that no bridges are broken until modifier content exceeds "oxide saturation." See Section 2.1 of paper cited in lit. ref. (2). It now seems necessary to modify this by adding, "except possibly in the interconnective or channel fissures, probably a small proportion of total volumes."

[16] It has been noted by C. R. Kurkjian and R. W. Douglas (Physics and Chemistry of Glasses **1**, 19, 1960) that few measurements on dilute solutions of alkali oxides in silica have been made because of the high temperatures involved, but their results with dilute solutions for Na_2O-GeO_2 glasses lead them to conclude that "only of the order two percent alkali is required to produce a complete change in the flow mechanism at high temperatures."

[17] This may be the explanation of the decrease in slope of the curve of log η versus $1/T$ at very high temperatures where such curves tend to converge and where it seems possible that vitrons are formed from discrete tetrahedra.

578970—61——3

For temperatures low in the annealing range it is suggested that viscous movements observable after holding are still between vitrons and surrounding network and that the increased activation energy is necessary for the cooperative movements. The immediately observable viscosity is attributed to volume relaxations, chiefly in the fissures, with the maximum relative travel between neighbors so small that the term flow is questionable and bending and yielding rather than breaking of the weakened bonds may be adequate. Both processes may operate in the intermediate regions of annealing ranges and the observed activation energies there may be sums.

An adequate understanding of vitreous flow in simple silicate glasses in definite terms of structure would involve data taken systematically on several types of glasses at numerous degrees of modification and at many temperatures including those near formation, flow region, softening region, annealing range, strain region, and perhaps lower temperatures.

This preliminary study utilizes ideas concerning fissuring, oxide-volume expansion, steric hindrance, Si–O–Si bond-angle contraction, and locally balanced stress systems (symmetry of smaller units versus vitron growth potential), which are largely developed from vitron theory and used in former applications thereof. These ideas have now been found qualitatively useful for tentative explanations of such salient trends in viscous flow, and in the activation energies therefor, as seem established by existing data.

4. References

[1] L. W. Tilton, J. Research NBS **58,** 139 (1957) RP2782.
[2] L. W. Tilton, J. Research NBS **60,** 351 (1958) RP2854.
[3] L. W. Tilton, J. Soc. Glass Technol. **40,** T338 (1956).
[4] L. W. Tilton, J. Research NBS **61,** 463 (1958) RP2915.
[5] L. W. Tilton, J. Am. Ceram. Soc. **43,** 9 (1960).
[6] Ivan Simon, J. Am. Ceram. Soc. **41,** 116 (1958).
[7] R. J. Callow, J. Soc. Glass Technol. **36,** 137 (1952).
[8] Norbert Neurath, Glastechn. Ber. **28,** 411 (1955).
[9] Ivan Simon and H. O. McMahon, J. Am. Ceram. Soc. **36,** 160 (1953).
[10] J. O'M. Bockris and D. C. Lowe, Proc. Roy. Soc. Lon. **A226,** 423 (1954).
[11] Jack L. White, Ph. D. Thesis, Univ. of Cal. 1955; J. O'M. Bockris, J. W. Tomlinson, and J. L. White, Trans. Faraday Soc. **52,** 299 (1956).
[12] G. Heidtkamp and K. Endell, Glastechn. Ber. **14,** 89 (1936).
[13] N. V. Solomin, Zhur. Fiz. Khim. **14,** 235 (1940).
[14] R. W. Douglas, J. Soc. Glass Technol. **31,** 78 (1947).
[15] S. M. Cox, J. Soc. Glass Technol. **32,** 340 (1948).
[16] F. Hodgdon and D. A. Stuart, J. Appl. Phys. **21,** 1160 (1950).
[17] O. L. Anderson and D. A. Stuart, Ind. and Eng. Chem. **46,** 158 (1954).
[18] H. R. Lillie, Proc. Int. Comm. on Optics **II,** 11 (1955).
[19] G. O. Jones, Report on Progress in Physics **XII,** (a)143, (b)153 (1948–9); J. Soc. Glass Technol. **28,** 432 (1944).
[20] E. Plumat, Silicates Industriels **21,** 454 (1956).
[21] T. G. Fox, S. Gratch, and S. Loshaek, Rheology, p. 431 (Academic Press, 1956).
[22] J. W. Tomlinson, M. S. R. Heynes, and J. O'M. Bockris, Trans. Faraday Soc. **54,** 1822 (1958).
[23] J. E. Stanworth, Physical Properties of Glass, (a)p. 180, (b)p. 188, Oxford 1953; (c) J. Soc. Glass Technol. **21,** 442 (1937).
[24] E. Jenckel and A. Schwittmann, Glastechn. Ber. **16,** 168 (1938).
[25] J. P. Poole, J. Am. Ceram. Soc. **32,** 230 (1949).
[26] M. P. Volarovich and A. A. Leontieva, J. Soc. Glass Technol. **20,** 139 (1936).
[27] N. W. Taylor and P. S. Dear, J. Am. Ceram. Soc. **20,** 296 (1937).
[28] N. W. Taylor and R. F. Doran, J. Am. Ceram. Soc. **24,** 102 (1941).
[29] J. D. MacKenzie, Chemical Reviews **56,** 460 (1956).
[30] E. Preston and E. Seddon, J. Soc. Glass Technol. **21,** T123 (1937).
[31] L. Shartsis, S. Spinner, and W. Capps, J. Am. Ceram. Soc. **35,** 158 (1952).
[32] E. Preston and W. E. S. Turner, J. Soc. Glass Technol. **16,** 331 (1932); *17,* 122 (1933); **18,** 143 (1934).
[33] J. O'M. Bockris, J. D. MacKenzie, and J. A. Kitchener, Trans. Faraday Soc. **51,** 1734 (1955).
[34] S. Pearson, J. Soc. Glass Technol. **36,** 105 (1952).
[35] K. Endell and H. Hellbrügge, Beiheft Nr. 38 zu der Z. VD Gh. 1940; Z. Angew. Chem. **53,** 271 (1940).
[36] J. O. Isard and R. W. Douglas, J. Soc. Glass Technol **39,** 89T (1955).
[37] R. W. Douglas and J. O. Isard, J. Soc. Glass Technol. **35,** 206T (1951); Nature **175,** 747 (1955).

(Paper 65A2–94)

JOURNAL OF RESEARCH of the National Bureau of Standards—A. Physics and Chemistry
Vol. 65A, No. 2, March–April 1961

Tetragermanates of Strontium, Lead, and Barium of Formula Type AB_4O_9

Carl R. Robbins and Ernest M. Levin

(December 13, 1960)

Three new tetragermanates, $SrGe_4O_9$, $PbGe_4O_9$, and $BaGe_4O_9$, of formula type AB_4O_9 were found. $BaTiGe_3O_9$, the germanium analog of the mineral silicate benitoite ($BaTiSi_3O_9$) was prepared for study and comparison. Indexed X-ray powder diffraction patterns of the tetragermanates and of $BaTiGe_3O_9$ and $BaTiSi_3O_9$ show: (1) the tetragermanates are apparently isostructural; (2) the unit cell of $BaTiGe_3O_9$ at room temperature is related to that of the tetragermanates by a doubling of the c-axis of the latter; (3) the tetragermanates and the metastable (room temperature) form of $BaTiGe_3O_9$ are apparently structurally similar to, but not isostructural with benitoite; (4) within its temperature stability range, $BaTiGe_3O_9$ appears to be isostructural with $BaTiSi_3O_9$.

Density, melting point, and partial optical data for the tetragermanates were obtained.

1. Introduction

In the course of a study of the system SrO-GeO_2 [1][1] a new compound, $SrGe_4O_9$, of formula type AB_4O_9 was found.

Although the crystal chemistry of germanium is in many respects similar to that of silicon, no AB_4O_9 silicates are known. The mineral silicate benitoite, $BaTiSi_3O_9$, of formula type ABC_3O_9, one tetrasilicate [2] and three tetragermanates [3] of type $A_2B_4O_9$, and a series of mixed oxides of formula type $AB_2C_2O_9$ [4] have been reported. Barium tetratitanate, $BaTi_4O_9$ [5] was the only example of an AB_4O_9 compound found in the literature.

Accordingly, it was of interest to attempt to synthesize other AB_4O_9 germanates for study and comparison. In addition to $SrO{:}4GeO_2$, mixtures in the ratios $CaO{:}4GeO_2$, $PbO{:}4GeO_2$, and $BaO{:}4GeO_2$ were prepared for study. It was known from previous work [6] that the compound $MgGe_4O_9$ does not exist.

The germanium compositional analog of benitoite, $BaTiGe_3O_9$, had been synthesized previously [7], and natural crystals of $BaTiSi_3O_9$ were obtained for comparison with $SrGe_4O_9$ and any other AB_4O_9 germanates found.

2. Experimental Procedure

2.1. Materials and Methods

Homogeneous starting mixtures were prepared from reagent grade $BaCO_3$, $SrCO_3$, $CaCO_3$, PbO, and GeO_2 (quartz form). Mixtures were pressed into disks under a pressure of 10,000 psi. With the exception of the $PbO{:}4GeO_2$ mixture, the disks were calcined for 2 to 3 hours in platinum crucibles at 1000 °C. The lead mixture was heated at temperatures up to 700 °C. The process of mixing, pressing and calcining was repeated 3 times.

The volatility of GeO_2 and PbO is negligible at the calcining temperatures employed. Samples treated at higher temperatures were enclosed in sealed platinum capsules. Melting point determinations were made by the quenching method. Temperatures were measured with a calibrated Pt-Pt 10 percent Rh thermocouple. Samples were examined with binocular and polarizing microscopes and by X-ray powder diffractometry using Ni-filtered Cu radiation. High temperature X-ray studies were made with equipment described by Mauer and Bolz [8].

2.2. Density Determination

Since large crystals were not obtained in this study, the problem of determining the density of a small amount of fine powder was encountered. Approximate values were obtained with a Berman density balance on fragments of charges heated in sealed capsules for 4 hours. In addition, a theoretical optical density was calculated for each compound by applying the rule of Gladstone and Dale [9] to crystalline materials, as suggested by Larsen [10]. The specific refractivity formula of Gladstone and Dale is:

$$(n-1)/d=K,$$

where

n is the average index of refraction, d represents the density, and K is the sum of products of the weight fractions of the oxides by their respective specific refractivities.

The average index was measured or calculated from measured extreme indices using the relationship $n=(2\omega+\epsilon)/3$, the equation for uniaxial substances.

[1] Figures in brackets indicate the literature references at the end of this paper.

Specific refractivity values were taken from Larsen [10] with the exception of the value of $k=0.165$ for the α-quartz form of GeO_2. The latter was calculated from the data of Laubengayer and Morton [11].

3. Results and Discussion

Three new compounds, $SrGe_4O_9$, $PbGe_4O_9$, and $BaGe_4O_9$, were found. Table 1 lists the density balance, optical and X-ray density values obtained. Melting point data, unit cell dimensions and optical properties are given in table 2.

$CaGe_4O_9$ was not formed at temperatures up to 1,000 °C, the maximum temperature to which the mixture was heated. X-ray diffraction patterns always showed GeO_2 and an unidentified phase richer in CaO than the ratio $CaO:4GeO_2$.

TABLE 1. *A comparison of density values for the* AB_4O_9 *germanates*

Compound	Density Balance	Optical	X-Ray
	(g/cm³)	(g/cm³)	(g/cm³)
$SrGe_4O_9$	[a] 4.84	4.85	4.89
$PbGe_4O_9$	[b] 5.89	5.96	5.94
$BaGe_4O_9$	[a] 5.07	5.11	5.12

[a] Sintered at 1200 °C for 4 hours.
[b] Sintered at 650 °C for 4 hours.

TABLE 2. *Some properties of the* AB_4O_9 *germanates*

Compound	Melting Point	Unit Cell Dimensions	Z	X-Ray Density	Optical Properties		
					Character	Indices	n of glass
	°C	A		(g/cm³)		(±.003)	(±.003)
$SrGe_4O_9$	1298±5 °	Hex. a=11.34 Hex. c=4.75	3	4.89	weakly birefringent	$\bar{\eta}$=1.780	1.735
$PbGe_4O_9$	dissociates at ~700 °.	Hex. a=11.41 Hex. c=4.75	3	5.94	anhedral, birefringent	$\bar{\eta}$=1.800	1.776
$BaGe_4O_9$	1392±5 °	Hex. a=11.61 Hex. c=4.74	3	5.12	anhedral, birefringent, uniaxial negative.	ω=1.797 ϵ=1.783	1.746

3.1. Description of Compounds

$SrGe_4O_9$. The compound $SrGe_4O_9$ melts congruently at 1298 ±5 °C. It crystallizes in plates of irregular outline which show extremely low birefringence. Using the oil immersion method and white light, an average refractive index of 1.780 was observed. The optic sign could not be determined. The X-ray powder diffractometer pattern was indexed on the basis of a hexagonal unit cell with $a=11.34$A, $c=4.75$A, and $c/a=0.4189$. The theoretical X-ray density is 4.89 g/cm³ and there are 3 molecules per unit cell. X-ray data for the compound are given in table 3.

$PbGe_4O_9$. The compound $PbGe_4O_9$ was not observed by Speranskaya [12] in his recent study of the system PbO–GeO_2. It dissociates at approximately 700 °C to GeO_2 (rutile form) and an unidentified crystalline phase. Crystals of $PbGe_4O_9$ obtained were unsuitable for detailed optical study. They were birefringent with an average refractive index of approximately 1.800. The compound was indexed [2] on a hexagonal cell with $a=11.41$A, $c=4.75$A, and $c/a=0.4163$. The X-ray density is 5.94 g/cm³ and Z=3. X-ray powder diffractometer data are given in table 4.

[2] Three very weak diffraction peaks, not indexable on the basis of this cell, were observed. Preliminary studies of the system PbO–GeO_2 suggest that they represent a trace of metastably formed $PbGeO_3$.

TABLE 3. *X-ray* [a] *powder diffraction data for* $SrGe_4O_9$

hkl	dobs	I/I_0 [b]	$\frac{1}{d^2}$ obs	$\frac{1}{d^2}$ cal [c]
	A			
110	5.67	26	0.0311	0.0311
001	4.75	8	.0443	.0443
101	4.28	5	.0547	.0546
111	3.65	92	.0752	.0754
201	3.42	13	.0857	.0858
300	3.27	7	.0933	.0934
211	2.925	55	.1169	.1169
220	2.834	74	.1245	.1245
301	2.695	100	.1377	.1376
221	2.435	21	.1686	.1688
002	2.377	6	.1770	.1770
311	2.364	6	.1789	.1791
102	2.310	8	.1874	.1874
112	2.191	4	.2083	.2082
401	2.182	9	.2101	.2103
410	2.143	7	.2178	.2179
321	2.036	10	.2414	.2414
212	2.002	15	.2495	.2497
411	1.9544	13	.2618	.2621
302	1.9239	6	.2702	.2704
330	1.8960	2	.2799	.2801
222	1.8219	19	.3013	.3015
312	1.7918	8	.3115	.3119
331	1.7568	14	.3240	.3244
402	1.7077	4	.3429	.3430
600	1.6372	14	.3731	.3735
412	1.5923	4	.3944	.3949

[a] Cu Kα Radiation.
[b] I/I_0 represents the intensity of the diffraction peak relative to the strongest peak.
[c] Calculated on the basis of the following unit cell dimensions: $a=11.34$A, $c=4.75$A.

TABLE 4. *X-ray* [a] *powder diffraction data for* $PbGe_4O_9$

hkl	*d*obs	I/I_0 [b]	$\frac{1}{d^2}$ obs	$\frac{1}{d^2}$ cal [c]
	A			
110	5.70	14	0.0308	0.0307
001	4.74	2	.0445	.0444
101	4.28	1	.0547	.0546
---	[d] 4.20	1	-----	-----
210	3.74	2	.0717	.0717
111	3.65	100	.0751	.0751
201	3.42	5	.0855	.0854
---	[d] 3.39	2	-----	-----
300	3.29	23	.0923	.0922
211	2.932	22	.1163	.1161
---	[d] 2.914	4	-----	-----
220	2.851	62	.1230	.1230
301	2.704	79	.1368	.1366
221	2.444	1	.1674	.1674
311	2.373	10	.1777	.1776
102	2.307	4	.1879	.1878
112	2.190	12	.2085	.2083
401				
410	2.155	10	.2153	.2152
321	2.044	4	.2393	.2391
212	2.002	5	.2495	.2493
411	1.9628	25	.2596	.2596
302	1.9255	10	.2697	.2697
330	1.9008	4	.2768	.2767
501	1.8239	21	.3006	.3006
222				.3005
312	1.7934	5	.3109	.3107
331	1.7647	23	.3211	.3211
421	1.7372	1	.3314	.3313
402	1.7113	3	.3415	.3415
511	1.6609	1	.3623	.3621
600	1.6464	14	.3689	.3689

[a] CuKα radiation.
[b] I/I_0 represents the intensity of the diffraction peak relative to the strongest peak.
[c] Calculated on the basis of the following unit cell dimensions: a=11.41A, c=4.75A.
[d] See discussion of $PbGe_4O_9$ in text.

$BaGe_4O_9$. $BaGe_4O_9$ melts congruently at 1392 $\pm$5 °C. Crystals obtained were platy with irregular, rounded shapes. Optical examination showed that the compound is uniaxial negative with ω= 1.797 and ϵ=1.783 ($\pm$.003). The X-ray powder diffraction pattern was indexed on the basis of a hexagonal unit cell with a=11.61A, c=4.74A and c/a=0.4083. The theoretical X-ray density is 5.12 g/cm^3 and there are 3 molecules per unit cell. X-ray powder diffraction data for the compound are given in table 5.

$BaTiGe_3O_9$. Goldschmidt [13] reported the synthesis of the compound $BaTiGe_3O_9$ at 1000 °C and claimed that it has the benitoite ($BaTiSi_3O_9$) structure type at room temperature.

The compound was studied by Robbins [7] who found that $BaTiGe_3O_9$ is stable only from 1132 $\pm$10 ° C to 1255 $\pm$10 ° C. He concluded that the phase described by Goldschmidt as $BaTiGe_3O_9$ was apparently a solid solution of TiO_2 in $BaGe_4O_9$. At room temperature, $BaTiGe_3O_9$ is apparently structurally similar to, but not isostructural with, $BaTiSi_3O_9$, having a=11.73A, c=10.02A and Z=6. Within its temperature stability range, the compound appears to be isostructural with $BaTiSi_3O_9$, having a=6.8A, c=10.0A, and Z=2. Room temperature X-ray diffraction data are given in table 6.

TABLE 5. *X-ray* [a] *powder diffraction data for* $BaGe_4O_9$

hkl	*d*obs	I/I_0 [b]	$\frac{1}{d^2}$ obs	$\frac{1}{d^2}$ cal [c]
	A			
110	5.80	11	0.0298	0.0297
001	4.74	2	.0446	.0446
101	4.28	3	.0546	.0545
111	3.67	100	.0743	.0743
201	3.44	6	.0843	.0842
300	3.35	17	.0893	.0891
211	2.963	25	.1139	.1139
220	2.899	56	.1190	.1188
301	2.733	86	.1339	.1337
221	2.473	9	.1635	.1634
311	2.401	4	.1735	.1733
002	2.368	8	.1783	.1783
320	2.306	9	.1881	.1861
102				.1882
401	2.219	4	.2032	.2029
410	2.192	11	.2081	.2079
112				
202	2.142	2	.2180	.2179
321	2.072	5	.2329	.2326
212	2.010	10	.2475	.2475
411	1.9893	18	.2527	.2524
330	1.9344	11	.2673	.2673
302				
501	1.8499	2	.2922	.2920
222	1.8349	22	.2970	.2970
312	1.8046	6	.3070	.3069
510				
331	1.7905	25	.3119	.3118
402	1.7232	2	.3368	.3366
600	1.6746	17	.3566	.3563

[a] Cu Kα radiation.
[b] I/I_0 represents the intensity of the diffraction peak relative to the strongest peak.
[c] Calculated on the basis of the following unit cell dimensions: a=11.61A, c=4.74A.

TABLE 6. *X-ray* [a] *powder diffraction data for* $BaTiGe_3O_9$ [b] *at room temperature*

hkl	*d*obs	I/I_0 [a]	$\frac{1}{d^2}$ obs	$\frac{1}{d^2}$ cal [d]
	A			
110	5.85	7	0.0292	0.0291
002	5.01	6	.0398	.0398
102	4.49	3	.0496	.0495
112	3.81	65	.0690	.0689
202	3.57	5	.0787	.0786
300	3.39	13	.0872	.0872
301	3.21	28	.0973	.0972
212	3.05	3	.1078	.1077
220	2.928	50	.1166	.1163
302	2.803	100	.1273	.1271
222	2.531	4	.1561	.1561
004	2.505	21	.1594	.1594
312	2.453	2	.1662	.1658
104	2.430	2	.1694	.1691
303	2.378	2	.1769	.1769
114	2.305	16	.1882	.1884
402	2.264	3	.1951	.1949
204	2.247	3	.1981	.1981
410	2.218	13	.2033	.2035
411	2.164	13	.2135	.2135
214	2.097	4	.2274	.2272
412	2.028	14	.2432	.2433
304	2.015	3	.2463	.2466
330	1.956	7	.2615	.2616
224	1.905	15	.2756	.2757
312	1.874	3	.2849	.2853
413	1.848	6	.2928	.2931
332	1.822	11	.3012	.3015

[a] Cu Kα Radiation.
[b] This specimen was prepared by heating a portion of the calcined starting mixture in a sealed platinum capsule at 1150 ° C for 5 days, and quenching it.
[c] I/I_0 represents the intensity of the diffraction peak relative to the strongest peak.
[d] These values were calculated on the basis of the following unit cell dimensions: a=11.73A and c=10.02A.

$BaTiSi_3O_9$. Zachariasen [14] determined the crystal structure of $BaTiSi_3O_9$. He found that the unit cell contained 2 molecules and had the following dimensions: $a=6.60\pm0.01$A, $c=9.71\pm0.01$A. The space group is D^2_{3h} ($P\bar{6}c2$) and the calculated density is 3.73 g/cm³.

The compound was interesting because it was the only known member of the ditrigonal-bipyramidal symmetry class, and because it afforded the only known example of SiO_4 tetrahedra linked in rings of composition Si_3O_9. Subsequently, this structural group has been found in several other silicates. A projection of the structure (after Bragg [15]) on the 0001 plane is shown in figure 1. Both Ba and Ti are surrounded by 6 oxygen atoms. There are two layers of rings in the length of the *c*-axis.

X-ray powder diffractometer data (table 7) were obtained from natural crystals of $BaTiSi_3O_9$ from St. Benito Co., California (USNM #C3938). The compound was indexed on the basis of Zachariasen's unit cell using the cell dimensions obtained in this study.

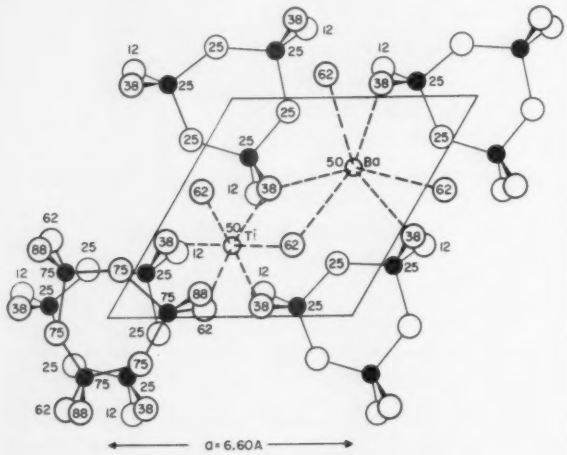

FIGURE 1. *The structure of benitoite,* $BaTiSi_3O_9$ *(after Bragg). Only atoms on either side of the reflection plane at height 25 are shown, except in the bottom lefthand corner.*

Superimposed oxygen atoms are symmetrically displaced. Note the Si_3O_9 rings.

TABLE 7. *X-ray [a] powder diffraction data for benitoite* ($BaTiSi_3O_9$) [b]

hkl	dobs	I/I₀ [c]	$\frac{1}{d^2 obs}$	$\frac{1}{d^2 cal}$ [d]
	A			
100	5.74	18	0.0304	0.0302
002	4.87	5	.0421	.0421
102	3.72	100	.0724	.0723
110	3.32	38	.0909	.0907
111	3.14	14	.1014	.1012
200	2.873	23	.1211	.1210
112	2.742	74	.1330	.1328
202	2.475	8	.1633	.1630
004	2.438	12	.1683	.1683
104	2.245	12	.1985	.1986
210	2.172	25	.2120	.2117
211	2.120	14	.2225	.2222
212	1.984	9	.2540	.2538
114	1.965	28	.2590	.2590
300	1.916	21	.2723	.2722
204	1.859	20	.2894	.2893
302	1.783	17	.3147	.3143
220	1.659	4	.3632	.3629
214	1.622	12	.3801	.3800
310	1.594	4	.3937	.3931
222	1.571	4	.4053	.4050
106	1.567	11	.4072	.4072

[a] Cu Kα radiation.
[b] Data obtained from natural crystals of $BaTiSi_3O_9$ from St. Benito Co., California (USNM #C3938).
[c] I/I_0 represents the intensity of the diffraction peak relative to the strongest peak.
[d] Calculated on the basis of following unit cell dimensions: $a=6.64$A, $c=9.75$A. Zachariasen [14] reported the following values: $a=6.60\pm0.01$A, $c=9.71\pm0.01$A.

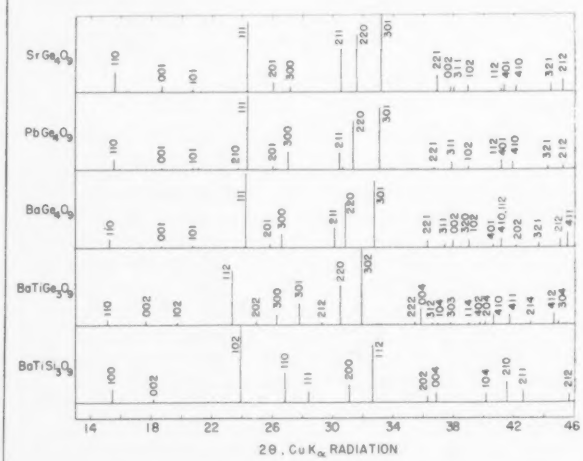

FIGURE 2. *Schematic partial X-ray diffractometer patterns of the* AB_4O_9 *Germanates,* $BaTiGe_3O_9$ *(room temperature form) and* $BaTiSi_3O_9$.

3.2. Structural Considerations

Unit cell dimensions of the AB_4O_9 germanates and of $BaTiGe_3O_9$ and $BaTiSi_3O_9$ are summarized in table 8, and schematic, partial X-ray diffraction patterns are shown in figure 2.

The AB_4O_9 germanates are apparently isostructural, having a *c*-axis of 4.75A and an *a*-axis varying from 11.34A for $SrGe_4O_9$ through 11.61A for $BaGe_4O_9$, with 3 molecules per unit cell. If certain reflections of the powder diffraction patterns are omitted, the 101, 201 and 211 for example, the AB_4O_9 germanates may be indexed on the benitoite ($BaTiSi_3O_9$) cell.

The AB_4O_9 germanates are related to the room temperature form (metastable) of $BaTiGe_3O_9$ by a doubling of the *c*-axis of the former. If certain reflections of the room temperature diffractometer pattern of $BaTiGe_3O_9$ are omitted, the 102, 202, and 212, for example, this form may be indexed on the benitoite cell. However, within its temperature stability range (1132 °±10 °C to 1235 °±10 °C),

TABLE 8. *A comparison of the unit cell dimensions of the* AB_4O_9 *germanates and of* $BaTiGe_3O_9$ *and* $BaTiSi_3O_9$

Compound	a	c	Z
	A	*A*	
$SrGe_4O_9$	11.34	4.75	3
$PbGe_4O_9$	11.41	4.75	3
$BaGe_4O_9$	11.61	4.74	3
$BaTiGe_3O_9$ [a]	11.73	10.02	6
$BaTiGe_3O_9$ [b]	6.8	10.0	2
$BaTiSi_3O_9$ [c]	6.60	9.71	2

[a] Measured at room temperature.
[b] Measured at 1160 °±20 °C.
[c] Zachariasen's values [14].

these reflections are not present, and $BaTiGe_3O_9$ is apparently isostructural with $BaTiSi_3O_9$. Corresponding reflections in the patterns of $SrGe_4O_9$ and $BaGe_4O_9$ did not disappear with heating, and no change was observed in the pattern of $BaTiSi_3O_9$ at temperatures up to 1160 °±20 °C.

Since the AB_4O_9 germanates appear to be structurally very similar to $BaTiSi_3O_9$, rings of GeO_4 tetrahedra of composition Ge_3O_9 are most probably their dominant structural unit. Since germanium may have either 4-fold or 6-fold coordination with respect to oxygen, the fourth germanium atom would occupy the titanium position of $BaTiSi_3O_9$, in octahedral coordination. Thus the formula $BaGe_4O_9$ should, perhaps more correctly, be written as $BaGeGe_3O_9$.

The observed differences between $BaTiGe_3O_9$, $BaTiSi_3O_9$ and the AB_4O_9 germanates result primarily from a difference in size between Ti and Ge (in octahedral coordination) and between Si and tetrahedrally coordinated Ge. In the lower left corner of figure 1 it is seen that the upper Si_3O_9 ring does not lie directly above the lower one, and two units are required in the length of the *c*-axis of $BaTiSi_3O_9$. A similar rotation of a corresponding Ge_3O_9 ring presumably is the reason for the doubling of the *c*-axis of the $BaGe_4O_9$ structure when one Ti is substituted for one Ge to form $BaTiGe_3O_9$. It should be noted that the long diagonal of figure 1 is of the order of magnitude of the 11A *a*-axis of the AB_4O_9 germanates and metastable $BaTiGe_3O_9$. Apparently the substitution of the larger Ge_3O_9 groups for Si_3O_9 groups requires that the diagonal of the silicate cell become the *a*-axis of the germanate cell. Within the temperature stability range of $BaTiGe_3O_9$ this distortion is relieved, and the compound has the 6A *a*-axis of the silicate.

Preliminary intensity calculations indicate that the preceding structural assumptions for the AB_4O_9 germanates are correct. Suitable single crystals of $BaGe_4O_9$ have been obtained, and a detailed study of the structure of the compound is in progress.

(Paper 65A2–95)

4. Summary

Three new compounds, $SrGe_4O_9$, $PbGe_4O_9$ and $BaGe_4O_9$, of formula type AB_4O_9, have been synthesized. These tetragermanates appear to be isostructural. They are apparently structurally similar to, but not isostructural with, $BaTiSi_3O_9$.

The compound $BaTiGe_3O_9$ is metastable at room temperature. The metastable form is related to the AB_4O_9 germanates by a doubling of the *c*-axis of the latter. Metastable $BaTiGe_3O_9$ is apparently structurally similar to, but not isostructural with, $BaTiSi_3O_9$. It appears to be a structural link between the AB_4O_9 germanates and $BaTiSi_3O_9$, having the 11A *a*-axis of the former, and the two layers of rings in the length of the *c*-axis of the latter.

Within its temperature stability range, $BaTiGe_3O_9$ is apparently isostructural with $BaTiSi_3O_9$.

The authors are grateful to H. F. McMurdie for helpful discussions of the work, and to Helen Ondik and Alvin Perloff for assistance with the intensity calculations.

6. References

[1] C. R. Robbins and E. M. Levin, The System SrO-GeO_2, paper in preparation.
[2] F. C. Kracek, N. L. Bowen, and G. W. Morey, Equilibrium relations and factors influencing their determination in the system K_2SiO_3-SiO_2, J. Phys. Chem. **41,** 1183–1193 (1937).
[3] Gmelins Handbuch **30,** 332 (1931).
[4] Bengt Aurivillius, Mixed bismuth oxides with layer lattices, ARKIV Für Kemi, **1,** [No. 54] 463–480 (1950).
[5] D. E. Rase and R. Roy, Phase equilibrium in the system BaO-TiO_2, J. Am. Ceramic Soc., **38,** [No. 3] 110 (1955).
[6] C. R. Robbins and E. M. Levin, The system magnesium oxide-germanium dioxide, Am. J. Sci. **257,** 63–70 (1959).
[7] C. R. Robbins, The compound $BaTiGe_3O_9$, J. Am. Ceramic Soc., in press.
[8] F. A. Mauer and L. H. Bolz, Thermal expansion of Cermet components by high temperature X-ray diffraction, NBS Report 3148 (1953).
[9] J. H. Gladstone and T. P. Dale, Researches on the refraction, dispersion, and sensitiveness of liquids, Roy. Soc. London Philos. Trans., **153,** 337 (1864).
[10] E. S. Larsen and H. Berman, The microscopic determination of the nonopaque minerals, U.S. Geological Survey Bull, 848, p. 31 (U.S. Government Printing Office, 1934).
[11] A. W. Laubengayer and D. S. Morton, The polymorphism of germanium dioxide, J. Am. Chem. Soc. **54,** 2303–2320 (1932).
[12] E. I. Speranskaya, System PbO-GeO_2, Izvest. Akad. Nauk S.S.S.R., Otdel. Khim. Nauk, 162–3 (1959).
[13] V. M. Goldschmidt, Zur Kristallchemie des Germaniums, Nachr. Ges. Wiss. Göttingen, Math.-Phys. Klasse, 184–190 (1931).
[14] W. H. Zachariasen, The crystal structure of benitoite, $BaTiSi_3O_9$, Z. Krist., **74,** 139–146 (1930).
[15] W. L. Bragg, Atomic Structure of Minerals, p. 181 (Cornell University Press, Ithaca, New York, 1937).

JOURNAL OF RESEARCH of the National Bureau of Standards—A. Physics and Chemistry
Vol. 65A, No. 2, March–April 1961

Publications of the National Bureau of Standards

Selected Abstracts

On Stokes flow about a torus, W. H. Pell and L. E. Payne, *Mathematika* **7,** *78–92 (1960).*

This is the third of a series of papers on the Stokes (slow viscous) flow about axially symmetric bodies immersed in a uniform flow parallel to the axis of symmetry. The flow itself then has axial symmetry and is amenable to attack by the generalized axially symmetric potential theory of A. Weinstein. In this particular paper the flow in multiply connected regions is considered and, in particular, the problem of flow about a torus is solved. The mathematical problem which characterizes the flow does not have a unique solution. Uniqueness is insured by the physical condition that the pressure be continuous throughout the flow field.

The Stokes flow about a spindle, W. H. Pell and L. E. Payne, *Quart. Appl. Math.* **18,** *257–262 (1960).*

This is a continuation of earlier work by the same authors. The methods of the generalized axially symmetric potential theory of A. Weinstein and certain representation theorems of L. Payne for the solution of repeated operator equations are applied to the solution of the Stokes (slow) flow about a spindle-shaped body. The stream function of the flow is found and an expression is given for the drag of the body.

A quantitative formulation of Sylvester's law of inertia, A. M. Ostrowski, *Natl. Acad. Sci. Proc.* **45,** *No. 5, 740–744 (May 1959).*

If an Hermitian form is transformed by a general linear transformation, bounds for the factors by which the eigenvalues are multiplied, can be indicated that depend only on the transformation used.

A comparison of atomic beam frequency standards, R. E. Beehler, R. C. Mockler, and C. S. Snider, *Nature* **187,** *681–682 (August 20, 1960).*

Standard frequencies obtained from various cesium atomic beam frequency standards have been compared in a number of instances. The results of Holloway, et al, showed agreement to about 2×10^{-10} between the commercial beam standards developed and manufactured by the National Company and the atomic standards at the National Physical Laboratory, Teddington, England.
Two dissimilar beam standards at the National Bureau of Standards have been compared over the last several months. Their frequencies agree to within $\pm1.5\times10^{-11}$ (standard deviation of the mean for the comparisons and estimated uncertainty due to effects of pertinent parameters).

Maser frequency stability, R. C. Mockler and J. A. Barnes, *Proc. 13th Annual Frequency Control Symp., 583–595 (May 12–14, 1959).*

The effort of the Bureau of Standards in maser work has been directed toward the attainment of high frequency stability for extended periods of time. A maser stabilized frequency multiplier chain has been controlled to 1×10^{-11} for periods of 6 hours. These preliminary measurements and tests indicate that the maser can be held within narrow frequency limits for periods of weeks with simple modifications. The masers have been employed to study frequency multiplier and crystal oscillator stability. The data have enabled us to make some predictions of the behavior of extremely long atomic beam machines.

Thermal voltage converters for accurate voltage measurements to 30 megacycles per second, F. L. Hermach and E. S. Williams, *Commun. Electron, AIEE, No. 49, 200–206 (July 1960).*

Thermal voltage converters, each consisting of a deposited carbon resistor in series with a thermoelement in a coaxial line, have been developed for measurements of rms voltages from 1 to 200 volts. Their configuration permits an extended frequency range and makes it possible to compute the effect of residual reactances. Extensive tests indicate satisfactory agreement with computed ac-dc differences to 40 mc.
These voltage converters are ordinarily used to make ac-dc tests of other thermocouple instruments, but can be used for a-c measurements as well. They are inexpensive and easy to construct. An accuracy of 0.1% or better is possible to at least 10 mc and 0.2% at 30 mc.

Influence of earth curvature and the terrestrial magnetic field on VLF propagation, J. R. Wait and K. Spies, *J. Geophys. Research* **65,** *2325–2331 (Aug. 1960).*

An account is given of some recent work on the mode theory of V.L.F. ionospheric propagation. Attention is confined to the behavior of the attentuation coefficient of the dominant mode. The ionosphere is assumed to be a sharply bounded and homogeneous ionized medium. It is indicated that earth curvature increases the attenuation rate by as much as a factor of 2 as compared with corresponding attenuation for a flat earth. The influence of the earth's magnetic field is also shown to be important. In fact propagation paths from east-to-west suffer much greater attenuation than for west-to-east paths. The theoretical results in the present paper appear to agree quite well with the experimental data of W. L. Taylor.

Charge transfer and electron production in H+H collision, D. G. Hummer, R. F. Stebbings, W. L. Fite, and L. M. Branscomb, *Phys. Rev.* **2,** *668–670 (July 1960).*

The cross sections for charge transfer and electron production in collisions between hydrogen atoms and hydrogen negative ions (H^-) have been measured over the energy range 100 ev to 40,000 ev using modulated atomic beam techniques in a cross beam experiment. Agreement of the experimental results with the perturbed stationary states calculation of Dalgarno and McDowell for charge transfer is quite satisfactory. Considerable discrepancy between available theory and experimental results occurs for the electron production cross section.

Variational treatment of electron-hydrogen atom elastic scattering, S. Geltman, *Phys. Rev.* **119,** *No. 4, 1283–1290 (Aug. 1960).*

The Hulthén-Kohn variational method is applied to the elastic scattering of electrons by hydrogen atoms. The trial function used is of a non-separable form, allows for the virtual excitation of the 2s and 3s states, and contains a scaling parameter which is allowed to vary. The resulting scattering lengths and S, P, and D singlet and triplet phase shifts are compared with the results of other calculations, and reasons are given for expecting them to be of greatly improved accuracy.

Thermodynamic structure of the outer solar atmosphere. VI. Effect of departures from the Saha equation on inferred properties of low chromosphere, S. R. Pottasch and R. N. Thomas, *Astrophys. J.* **132,** *195–201 (July 1960).*

We apply the methodology of our preceding treatment of the Saha equation under conditions of high Lyman continuous opacity, to a re-analysis of the continuous emission from the lowest chromosphere. The result is a greatly-steepened T_e-gradient, relative to the results of an earlier analysis based on the neglect of non-LTE effects.

Relationship between red auroral arcs and ionospheric recombination. G. A. M. King and F. E. Roach, *J. Research NBS* **65D,** *No. 2, 32 (1960).*

A "monochromatic" (6300 A) auroral arc, observed photometrically to be north of Boulder, Colo., has been identified with oblique echoes on ionograms taken near Boulder. The auroral emission is explained in terms of a great enhancement of ionospheric recombination. The recombination process is shown to depend on the density of molecular nitrogen in the ionospheric *F* region; the change in nitrogen density during and after auroral activity, responsible for the change in recombination rate, is ascribed to the combined effects of heating and mixing of the atmosphere at the lower ionospheric heights.

The characteristic energy losses of electrons in carbon, L. B. Leder and J. A. Suddeth, *J. Appl. Phys.* **8,** *1422–1426 (August 1960).*

The values reported for the characteristic energy losses of electrons in carbon vary by as much as 50%. In an attempt to resolve this discrepancy the electron energy losses have been remeasured for evaporated carbon and natural graphite, and it is found that there is a large difference for these two forms of carbon. Electron diffraction patterns of evaporated carbon show it to be highly amorphous. Annealing of the films causes growth of the crystallites, and also an increase of the energy loss toward the loss values for graphite. It is shown by calculation that the difference in the energy losses for the two forms is due to a difference in density, and that annealing increases the density of the evaporated carbon and, therefore, the energy loss value.

Calibration of five gamma-emitting nuclides for emission rate, J. M. R. Hutchinson, *NBS TN71 (PB161572) (1960) 75 cents.*

Mercury-203 and Niobium-95 were calibrated by a $4\pi\beta$-γ coincidence method for γ-emission rate, Zinc-65 by comparison with the 1.12 Mev peak of Scandium-46, Sodium-22 by a γ-annihilation-quanta coincidence method and by a triple coincidence method, and Strontium-85 by x-γ coincidence counting. The accuracy of the calibration in all cases was ± 2 percent. The half-life of the isomeric state of Rubidium-85 was measured and found to be .98 microseconds.

Fast counting of alpha particles in air ionization chambers, Z. Bay, F. D. McLernon, and P. A. Newman. J. Reseacrh NBS **65C,** No. 1, 51 January–March 1961.

It was assumed in the past that counting of alpha particles in air ionization chambers could only be based on the collection of ions since electrons produced in the alpha track quickly form negative ions in electronegative gases. This leads to time resolutions of the order of a millisecond. It is shown in the present work that the motion of the electrons before attachment produces a sharp initial rise in the pulse profile which, although small, can be detected and utilized for high speed counting. Time resolutions of the order of a few microseconds with good signal-to-noise ratios are realized in atmospheric air, and therefore counting speeds similiar to those in nonelectronegative gases are obtained.

Neutron-insensitive proportional counter for gamma-ray dosimetry, R. S. Caswell, *Rev. Sci. Instr.* **31,** *No. 8, 869–871 (August 1960).*

A gamma-ray dosimeter with low sensitivity to neutrons has been developed for radiation dosimetry in mixed fields of neutrons and gamma rays. Neutron sensitivity in a 2.5—3 Mev H^2(d, n) He^3 neutron field has been shown experimentally to be $\leq$1.2 percent on the basis of first collision dose in tissue. Gamma-ray sensitivity is independent of energy to within ± 5 percent from 1.25 Mev (Co^{60}) to 200 kev and to within ± 20 percent down to 47 kev. The instrument is a proportional counter which may be used as a dosimeter for gamma rays in the presence of neutrons by pulse-height integration of the small pulses due to secondary electrons produced by gamma rays and rejection of the large pulses due to heavy particle recoils from neutrons.

Scattering of cobalt-60 gamma radiation in air ducts, C. Eisenhauer, *NBS TN74 (PB161575) (1960) 75 cents.*

The exposure dose rates due to Cobalt-60 gamma radiation scattered in small air ducts in concrete has been measured for ducts with one and two right angle bends. The inside corner of a right angle bend has been found to be an important source of scattered radiation. Results are analyzed in terms of solid angle relationships and attempts are made to extrapolate experimental results to other duct configurations.

Spatial distribution of energy dissipated by fallout beta rays, A. E. Boyd and E. E. Morris, *Health Phys.* **2,** *321–325 (1960).*

Calculations are described of the spatial distribution of energy dissipated in air by the delayed beta rays from products of slow neutron U^{235} fission. Results are given for both plane isotropic and point isotropic sources for times after fission of 1.12 and 23.8 hr.

On the nature of the crystal field approximation, H. Goldberg and C. Herzfeld, *NBS TN67 (PB-161568) (1960) $2.50.*

A new method is developed for the treatment of molecular interactions, and is applied to a system consisting of a hydrogen atom in a 2p state and a hydrogen molecule in the ground state. The interaction of these two species is calculated using ordinary crystal field theory and also the new method. A comparison of the results shows some of the shortcomings of the conventional crystal field theory, and provides corrections to it. The new method consists of (1) expanding all electron terms of the total Hamiltonian for the system which involve interactions between the atom and the molecule, thus transforming the interaction Hamiltonian into sums of products of one-electron operators, and (2) of using properly antisymmetrized wave functions made up of products of atom and molecule eigenfunctions. The calculations show the effect of the neglect of overlap and exchange in ordinary crystal field theory.
All calculations and results are presented in full detail. Transformations of three-center to two-center integrals are given explicitly.

Some experiments on the deposition of gases at 4.2 °K, T. Baurer, *NBS TN73 (PB161574) (1960) $1.00.*

In order to develop some preliminary information concerning the very basic problems of gaseous deposition at extremely low temperatures, samples of argon, nitrogen, oxygen, and hydrogen were deposited at 4.2 °K, and variations in some of the parameters associated with these depositions were observed. In addition, samples of the same gases were passed through an excitation zone prior to deposition, and differences in the deposition behavior were recorded. The pressure downstream of the deposition region and the temperature

within the deposited solids were found, in general, to increase with flow rate of the depositing substances, and to vary with time in a manner depending on the density, flow rate, and state of excitation of the incoming gases. Arrhenius curves were plotted using warmup data observed in these experiments and solid-phase transition data determined elsewhere. Variations in the positions of these plots were sometimes the result of differences in the conditions of deposition, and at other times an effect of the chemical nature of the gas studied. The experimental behavior of hydrogen, relative to that of the other gases studied, was observed to be strongly dependent upon its much higher thermal conductivity.

A comment on a paper of Mori on time-correlation expressions for transport properties, M. S. Green, *Phys. Rev.* **119,** *No. 3, 829–830 (August 1960).*

An auto-correlation expression given by Mori for the thermal conductivity of a fluid is shown to be only apparently different from an expression previously derived by the author.

An optical study of the boundary layer transition processes in a supersonic air system, W. Spangenberg and W. R. Rowland, *Phys. of Fluids* **3,** *No. 5 667–684 (Sept.–Oct. 1960).*

A sequential-spark schlieren system with cylindrical-lens camera was used to trace the history of transition from laminar to turbulent flow on a cylindrical model in a Mach number 1.96 air stream. Both smooth and rough models were tested at several Reynolds numbers per unit length. The results showed that transition in a supersonic stream starts with high-frequency disturbances in the laminar boundary layer which degenerate into areas of turbulent flow. These spots erupt independently near the trailing face of the turbulent-flow region which is always moving downstream. The addition of the newly-turbulent areas of finite size to the trailing face of the turbulent-flow region causes it to jump upstream discontinuously. Spots are traveling at a very low velocity when they first become visible, and accelerate to continue downstream at a velocity of about 0.7 times free-stream speed at their trailing face. The origin of the fresh areas of breakdown to turbulence is apparently in amplified Tollmien-Schlichting waves. The frequency of spot production lies within the region where stability theory predicts that disturbances within the boundary layer will be amplified. It is concluded that transition mechanisms in supersonic flow are similar to those in a subsonic air stream.

Temperature stratification in a non-venting liquid helium dewar, L. E. Scott, R. F. Robbins, and B. W. Birmingham, *Proc. 1959 Cryogenic Engr. Conf.* **5,** *(Sept. 2–4, 1959).*

Large temperature gradients were observed in experiments conducted with a 40-liter stainless steel dewar. A method is shown for calculating the pressure rise in the non-stratifying condition and the results are compared with the observed pressure rise. An intersection of these two curves is observed and a possible explanation is given. The destratifying effects of both a concentrated heat input and of copper rods is shown.

Pressure dependence of rotationally perturbed lines in the ultraviolet band spectrum of CN, H. P. Broida and S. Golden, *Can. J. Chem.* **38,** *1666–1667 (1960).*

Intensity measurements of the components of rotationally perturbed lines (K′=4, 7, 11, and 15) in the 0, 0 transition of the violet system ($B^2\Sigma^+$—$X^2\Sigma^+$) of the CN formed in an "active" nitrogen flame have been made at pressures from 0.1 to 100 mm Hg. A simple kinetic model considering competition between formation, radiation, and collisional interchange of states gives a reasonable fit to the data over the entire range of measured pressures. At high pressures the intensity ratios of the component rotationally perturbed lines depend only upon the radiative transition probabilities and at low pressures only upon the relative rates at which they are populated. At intermediate pressures, the intensity ratios depend upon the collision frequency for the interchange of the rotationally perturbed states. The collision frequency determined in this manner is the same order of magnitude as the gas kinetic collision frequency.

Absolute isotopic abundance ratio and the atomic weight of silver, W. R. Shields, D. N. Craig, and V. H. Dibeler, *J. Am. Chem. Soc.* **82,** *5033–5036 (1960).*

An absolute value for the isotopic abundance ratio of natural silver is obtained by the use of isotopic standards prepared from nearly pure separated silver isotopes. Mass spectrometric data result in a value for the ratio, Ag^{107}/Ag^{109}= 1.07540.0013. Within the stated limits, no variation in natural abundance is found among six samples of native silver and commercial silver nitrate. A seventh native silver sample, obtained from Cobalt, Ontario, shows a statistically significant variation. The calculated physical and chemical atomic weights of silver are 107.9028±0.001 and 107.8731± 0.0016, respectively, where the indicated uncertainties are over-all limits of error based on a 95% confidence limits the mean and allowances for effects of known sources of possible systematic error.

The dynamic compressibility of a rubber-sulfur vulcanizate and its relation to free volume, J. E. McKinney, H. V. Belcher, and R. S. Marvin, *Trans. Soc. Rheology* **IV,** *347–362 (1960).*

The dynamic bulk compliance of natural rubber-12% sulfur was measured for varying static pressure (0 to 1000 bar), temperature (−30 to +70° C), and frequency (50 to 1000 cps). The data can be represented by reduced frequency or temperature plots, assuming viscosity is proportional to exp $(1/\phi)$, ϕ a fractional free volume which is a linear function of temperature and pressure. The temperature-frequency reduction fits the "universal" WLF constants, and the temperature-pressure reduction term is practically the same as that found by Singh and Noll for polyisobutylene.

The ionization constants of 2-chloro-4-nitrophenol and 2-nitro-4-chlorophenol, V. E. Bower and R. A. Robinson, *J. Phys. Chem.* **64,** *1078 (1960).*

Spectrophotometric measurements of 2-chloro-4-nitrophenol in succinate buffers and of 2-nitro-4-chlorophenol in phosphate buffers have been used to determine the ionization constants in aqueous solution at 25°. Values of $pK=5.44_9$ and $pK=6.45_9$ were respectively found.

Acid-base equilibria in benzene at three temperatures. The comparative reactivities of a phenolic acid and a carboxylic acid with triethylamine with 1,3-diphenylguanidine, M. M. Davis and M. Paabo, *J. Am. Chem. Soc.* **82,** *5081–5084 (1960).*

Equilibrium constants for the association of the phenolic indicator, bromophthalein magenta E (3′, 5′, 3″, 5″-tetrabromophenolphthalein ethyl ester), with 1,3-diphenylguanidine and with triethylamine in benzene have been determined spectrophotometrically at 20°, 25°, and 30° C.; and the association of benzoic acid with the same two bases has also been determined, using bromophthalein magenta E as the indicator. In all four cases the association has been assumed to conform to the equation:

$$B\ (\text{base}) + HA\ (\text{acid}) \rightleftharpoons BH^+ \ldots A^-\ (\text{hydrogen-bonded ion-pair}).$$

Electron spin resonance studies of free radicals in irradiated materials, L. A. Wall, *Symp. on Materials in Nuclear Application, Am. Soc. Testing Materials Spec. Tech. Publ. No. 276, 208–223 (1959).*

Trapped free radicals are very often responsible for post-irradiation effects. Such effects are, for example, thermal luminescence, bleaching sensitivity to oxidation and depolymerization, crosslinking, and degradation. The identification and measurement of free radicals produced by irradiation can most readily be carried out by making use of electron spin resonance (ESR). In general, the detection of simple atoms requires operation at low temperature, often as low as 4.2 ° K, i.e., liquid helium. At such temperatures, atoms of hydrogen, deuterium, and nitrogen and also alkyl radicals have been found by ESR methods. On the other hand, quite high concentrations of polymer radicals with long lifetimes are found at room temperature. While the interpretation of the spectra for simple atoms is relatively simple, that of the more complex polymer radicals is much more complicated. In polymeric systems steric effects and hindrance of rotation about bonds influence the various interactions to such an extent that comparisons with model compounds of low molecular size are of little value in establishing radical structures. With all polymeric systems studied thus far, full understanding and interpretation of the ESR spectra and their behavior with temperature have not yet been achieved.

Polymer decomposition: Thermodynamics, mechanisms, and energetics, L. A. Wall, *Soc. Plastic Engrs. Pt. I, 810–814 (Aug. 1960); Pt. II, 1031–1035 (Sept. 1960).*

The mechanism of polymer decompositions is now at a stage where a partial understanding exists for a rather large series of polymers. However, only a few polymers have been investigated in sufficient detail to permit estimation of the activation energies and steric factors for the elementary processes. Since polymer decompositions occur in the condensed phase, assumptions that are made in gas-phase studies are not, in general, valid. Radical terminations are likely to be controlled by diffusion and hence will have relatively high activation energies. Dissociation energies for bonds in polymeric substances cannot be studied by the same techniques applicable to studies of small molecules. The "ceiling temperature" concept or thermodynamic approach, while of value for the production of polymers, is not of primary importance for thermal stability. It may be pointed out that under normal conditions polymers are metastable, and that the most thermally stable one, polytetrafluoroethylene, is the most metastable.

Heat treatment and properties of iron and steel, T. G. Digges and S. J. Rosenberg, *NBS Mono.* **18** *(1960) 35 cents. (Supersedes C495.)*

This Monograph has been prepared to give an understanding of heat treatment principally to those unacquainted with this subject. To this end, the basic theoretical and practical principles involved in the heat treatment of iron and steel are presented in simplified form.

The role of surface tension in determining certain clay-water properties, W. C. Ormsby, *Bull. Am. Ceramic Soc.* **39,** *No. 8, 408–432 (August 1960).*

The importance of the surface tension of the liquid phase in controlling the plasticity and related properties of clay-water systems is critically reviewed. The experimental evidence supporting the so-called stretched membrane theory of plasticity is re-examined in some detail and is found to be incomplete. Generalizations based on this evidence are therefore open to question. Recent literature on the deformation behavior and related properties of clay-water systems suggests that wetting agents may produce ionic effects not unlike those produced by many inorganic electrolytes. The conclusion reached is that surface tension is of secondary importance in controlling many of the properties of clay-water systems and that, when considering wetting agents or similar types of materials, specific ionic effects are of greater importance.

Comparative fixation of calcium and strontium by synthetic hydroxyapatite, R. C. Likins, H. G. McCann, A. S. Posner, and D. B. Scott, *J. Biolog. Chem.* **235,** *No. 7, 2152–2156 (July 1960).*

Samples of hydroxyapatite with different crystal sizes were prepared from solutions containing radioactive calcium and strontium. Analysis of these preparations and the results of exchange studies showed a discrimination against strontium in the formation of apatite crystals which increased with crystal perfection.

Other NBS Publications

Journal of Research, Section 65B, No. 1, January–March 1961. 75 cents.

On transient solutions of the "baffled piston" problem, F. Oberhettinger.
Special types of partitioned matrices, E. V. Haynsworth.
Bound for the *p*-condition number of matrices with positive roots, P. J. Davis, E. V. Haynsworth, and M. Marcus.
Some computational problems involving integral matrices, O. Taussky.
Computational problems concerning the Hilbert matrix, J. Todd.
Index to the distributions of mathematical statistics, F. A. Haight.
Selected bibliography of statistical literature, 1930 to 1957: IV. Markov chains and stochastic processes, L. S. Deming and D. Gupta.

Journal of Research, Section 65C, No. 1, January–March 1961. 75 cents.

Electronic scanning microscope for a spectrographic plate comparator, M. L. Kuder.
Viscoelastometer for measurement of flow and elastic recovery, R. J. Overberg and H. Leaderman.
An ultra low frequency bridge for dielectric measurements, D. J. Scheiber.
The ephi system for VLF direction finding, G. Hefley, R. F. Linfield, and T. L. Davis.
Fast counting of alpha particles in air ionization chambers, Z. Bay, F. D. McLernon, and P. A. Newman. (See above abstract.)
X-ray diffraction measurement of intragranular misorientation in alpha brass subjected to reverse plastic strain, C. J. Newton and H. C. Vacher.
Enthalpy and specific heat of nine corrosion-resistant alloys at high temperatures, T. B. Douglas and A. C. Victor.
Determination of minor constituents in low-alloy steels by X-ray fluorescence, R. E. Michaelis, R. Alvarez, and B. A. Kilday.

Journal of Research, Section 65D, No. 2, March–April 1961. 70 cents.

Ionospheric motions observed with high-frequency backscatter sounders, L. H. Tveten.
Relationship between red auroral arcs and ionospheric recombination, G. A. M. King and F. E. Roach. (See above abstract.)
Fresnel region fields of circular aperture antennas, Ming-Kuei Hu.
Free-balloon borne meteorological refractometer, J. F. Theisen and E. E. Gossard.
Weather and reception level on a troposphere link—annual and short-term correlations, L. G. Abraham, Jr., and J. A. Bradshaw.

Initial results of a new technique for investigating sferic activity, G. Hefley, R. H. Doherty, and R. F. Linfield.

Effect of antenna radiation angles upon HF radio signals propagated over long distances, W. F. Utlaut.

Graphic determination of radio ray bending in an exponential atmosphere, C. F. Pappas, L. E. Vogler, and P. L. Rice.

A formula for radio ray refraction in an exponential atmosphere, G. D. Thayer.

The impedance of a monopole antenna with a circular conducting-disk ground system on the surface of a lossy half-space, S. W. Maley and R. J. King.

Radio-wave propagation in the earth's crust, Harold A. Wheeler.

Specific heats and enthalpies of technical solids at low temperatures. A compilation from the literature, R. J. Corruccini and J. J. Gniewek, NBS Mono. **21** (1960) 20 cents.

Amplitude-probability distributions for atmospheric radio noise, W. Q. Crichlow, A. D. Spaulding, C. J. Roubique, and R. T. Disney. NBS Mono. **23** (1960) 20 cents.

Household weights and measures, NBS Misc. Publ. **234** (1960) (Supersedes M39) 5 cents.

Screw-thread standards for federal services, 1957. Amends in part H28 (1944) (and in parts its 1950 Supplement), NBS Handb. H28 (1957)—Part III (1960) 60 cents.

Building code requirements for reinforced masonry, NBS Handb. H74 (1960) 15 cents.

Quarterly radio noise data—June, July, August 1959, W. Q. Crichlow, R. D. Disney, and M. A. Jenkins, NBS TN18–3 (PB151377–3) (1960) $1.00.

Quarterly radio noise data—September, October, November 1959, W. Q. Crichlow, R. D. Disney, and M. A. Jenkins, NBS TN18–4 (PB151377–4) (1960) $1.50.

Quarterly radio noise data—December, January, February 1959–60, W. Q. Crichlow, R. D. Disney, and M. A. Jenkins, NBS TN18–5 (PB151377–5) (1960) $1.75.

Quarterly radio noise data—March, April, May 1960, W. Q. Crichlow, R. D. Disney, and M. A. Jenkins, NBS TN18–6 (PB151377–6) (1960) $1.75.

Transistorized building blocks for data instrumentation, J. A. Cunningham and R. L. Hill, NBS TN68 (PB161569) (1960) $2.00.

Table of magnitude of reflection coefficient versus return loss ($L_R = 20 \log_{10} 1/|\Gamma|$), R. W. Beatty and W. J. Anson, NBS TN72 (PB161573) (1960) $1.25.

Soviet research in field electron and ion emission, 1955–1959; an annotated bibliography, T. W. Marton and R. Klein, NBS TN75 (PB161576) (1960) $1.25.

VHF and UHF power generators for RF instrumentation, A. H. Morgan and P. A. Hudson, NBS TN77 (PB161578) (1960) 75 cents.

Oblique incidence receiving antenna array for a relative ionospheric opacity meter, A. C. Wilson, NBS TN78 (PB161579) (1960) 50 cents.

Our measurement system and national needs, A. V. Astin, Sperryscope **15,** No. 6, 16 (1960).

Standards of heat capacity and thermal conductivity, D. C. Ginnings, Book Thermoelectricity (Including Proc. Conf. Thermoelectricity, Sponsored by the Naval Research Lab., September 1958), p. 320 (1960).

A study of 2-Mc/s ionosphreic absorption measurements at high altitudes, K. Davies, J. Geophys. Research **65,** 2285 (August 1960).

Carrier-frequency dependence of the basic transmission loss in tropospheric forward scatter propagation, K. A. Norton, J. Geophys. Research **65,** 2029 (July 1960).

Closed circuit liquid hydrogen refrigeration system, D. B. Chelton, J. W. Dean, and B. W. Birmingham, Rev. Sci. Instr. **31,** 712 (July 1960).

Infrared transmission of clouds, D. M. Gates and C. C. Shaw, J. Opt. Soc. Am. **50,** 876 (September 1960).

VI. Microscopic and macroscopic energy loss distributions. 1. Theoretical reviews: A summary, U. Fano, Natl. Acad. Sci., Natl. Research Council Publ. **752,** Report 29, p. 24 (Aug. 1960).

The mechanical properties of ceramics and their measurement at elevated temperatures, S. J. Schneider, Book Thermoelectricity, Chapter **21,** 342 (1960).

A rating method for refrigerated trailer bodies hauling perishable foods, C. W. Phillips, W. F. Goddard, Jr., and P. R. Achenbach, ASHRAE J. **2,** No. 5, 45 (May 1960).

Reply to On the structure of trimethylamine-trimethylboron, D. R. Lide, Jr., J. Chem. Phys. **32,** No. 5, 1570 (May 1960).

Dimensional changes occuring in dentures during processing, J. B. Woelfel, G. C. Paffenbarger, and W. T. Sweeney, J. Am. Dental Assoc. **61,** No. 4, 413 (Oct. 1960).

Teeth, artificial, G. C. Paffenbarger and G. B. Denton, Encyclopaedia Britannica **21,** 878 (Jan. 1960).

A method of improving isolation in multi-channel waveguide systems, G. F. Engen, IRE Trans. Microwave Theory and Tech. Letter **MTT–8,** 460 (July 1960).

The characteristic energy losses of electrons in carbon, L. B. Leder and J. A. Suddeth, J. Appl. Phys. **8,** 1422 (Aug. 1960).

Note historique sur les premieres annees de la microscopie electronique, L. Marton, Extrait Bull. Acad. Roy. Belg. (Classes des Sciencies) **5,** 119 (Mar. 1959).

Procedure for the determination of the noble metal content of dental gold alloys, H. J. Caul., W. S. Clabaugh and M. E. Susa, J. Am. Dental Assoc. **61,** No. 4, 339 (Oct. 1960).

Theory of anisotropic fluids, J. L. Ericksen, Trans. Soc. Rheology IV, 29–39 (1960).

Rapid frequency analysis of fading radio signals, J. M. Watts and K. Davies, J. Geophys. Research **65,** No. 8, 2295 (Aug. 1960).

Reply to criticisms concerning Ireland contained in article "Basic research in Europe," D. M. Gates, Science **128,** No. 3318, 1–9 (Aug. 1, 1958).

Modern theories of materials, C. Truesdell, Trans. Soc. Rheology IV, 9–22 (1960).

Use of the incoherent scatter technique to obtain ionospheric temperatures, T. E. VanZandt and K. L. Bowles, J. Geophys. Research **65,** 2627 (Sept. 1960).

Highlights of the consultative committee on international radio (CCIR) activities in the field of radio propagation, J. W. Herbstreit, 9th Plenary Assembly of CCIR Proc. IRE **48,** No. 1, 45 (Jan. 1960).

Graphs for bivariate normal probabilities, M. Zelen and N. C. Severo, Ann. Math. Stat. **31,** No. 3, 619 (Sept. 1960).

A microwave impedance meter capable of high accuracy, R. W. Beatty, IRE Trans. Microwave Theory and Tech. **MTT–8,** No. 4 (July 1960).

Relaxation processes in multistate systems, K. E. Shuler, Phys. Fluids **2,** No. 4, 442 (July–Aug. 1959).

Comment on models of the ionosphere above h_{max} F2, J. W. Wright, J. Geophys. Research **65,** 2595 (Sept. 1960).

Some magnetoionic phenomena of the Arctic E-region, J. W. Wright, J. Atmospheric and Terrest. Phys. **18,** 276 (Aug. 1960).

Tables of thermodynamic and transport properties of air, argon, carbon dioxide, carbon monoxide, hydrogen, nitrogen, oxygen and steam, J. Hilsenrath, C. W. Beckett, W. S. Benedict, L. Fano, H. J. Hoge, J. F. Masi, R. L. Nuttall, Y. S. Touloukian, and H. W. Woolley, 478 pp. (Pergamon Press, Oxford, London, New York, and Paris, 1960).

Methods of nuclear orientation, E. Ambler, Progress in Cryogenics **2,** 235–280 (Heywood & Co., Ltd., London, England, 1960).

A conference on the propagation of ELF electromagnetic waves, J. R. Wait, Proc. IRE **48,** 1648 (Sept. 1960).

The strength of ten structural adhesives at temperatures down to minus 424 F., W. M. Frost, Proc. 1959 Cryogenic Engr. Conf. **5,** 375 (Sept. 2–4, 1959).

Possibility of detecting ionospheric drifts from the occurrence of spread F echoes at low latitudes, R. W. Knecht, Nature Letter **187,** 927 (Sept. 1960).

Some mechanical properties of magnesium alloys at low temperatures, R. P. Reed, R. P. Mikesell and R. L. Greeson, Proc. 1959, Cryogenic Eng. Conf. **5,** 397 (Sept. 2–4, 1959).

A compilation and correlation of the PVT data of normal hydrogen from saturated liquid to 80 degree K., R. B. Steward and V. J. Johnson, Proc. 1959 Cryogenic Engr. Conf. **5,** 548 (Sept. 2–4, 1959).

Neighbor interactions and internal rotations in polymer molecules. IV. Solvent effect on internal rotarions, S. Lifson and I. Openheim, J. Chem. Phys. **33,** No. 1, 109 (July 1960).

Improvements in radio propagation prediction service, W. B. Chadwick, Elec. Engr. 1–4 (Sept. 1960).

Carbon resistance thermometry with mixed dc and rf currents. J. J. Gniewek and R. J. Corruccini, Rev. Sci. Inst. **31**, No. 8, 899 (Aug. 1960).

Some SEAC computations of subsonic flows, P. Davis and P. Rabinowitz. Book Bergman's Linear Integral Operator Method in the Theory of Compressible Fluid Flow, by M. Z. Krsywoblocki, p. 148 (Wien. Springer-Verlag, Berlin, Germany, 1960).

Publications for which a price is indicated (except for NBS Technical Notes) are available only from the Superintendent of Documents, U.S. Government Printing Office, Washington 25, D.C. (foreign postage, one-fourth additional). Technical Notes are available only from the Office of Technical Services, U.S. Department of Commerce, Washington 25, D.C. (order by PB number). Reprints from outside journals and the NBS Journal of Research may often be obtained directly from the authors.

UNITED STATES
GOVERNMENT PRINTING OFFICE
DIVISION OF PUBLIC DOCUMENTS
WASHINGTON 25, D.C.

OFFICIAL BUSINESS

PENALTY FOR PRIVATE USE TO AVOID
PAYMENT OF POSTAGE, $300
(GPO)

JOURNAL OF RESEARCH of the National Bureau of Standards Vol. 65A, No. 2 March–April 1961
A. Physics and Chemistry

Contents

Page

Mass spectra of some deuteroethanes. Edith I. Quinn and Fred L. Mohler 93

Heats of hydrolysis and formation of potassium borohydride. Walter H. Johnson, Richard H. Schumm, Isa H. Wilson, and Edward J. Prosen. 97

Heat of combustion of borazine $B_3N_3H_6$. Marthada V. Kilday, Walter H. Johnson, and Edward J. Prosen 101

Thermodynamic properties of thorium dioxide from 298 to 1,200 °K. Andrew C. Victor and Thomas B. Douglas 105

Calculated energy dissipation distribution in air by fast electrons from a gun source. John E. Crew 113

Vitrons as flow units in alkali silicate binary glasses. Leroy W. Tilton. 117

Tetragermanates of strontium, lead, and barium of formula type AB_4O_9. Carl R. Robbins and Ernest M. Levin 127

Publications of the National Bureau of Standards 133

For sale by the Superintendent of Documents, U.S. Government Printing Office, Washington 25, D.C. Price 70 cents (single copy)
Subscription price: $4.00 a year; 75 cents additional for foreign mailing.
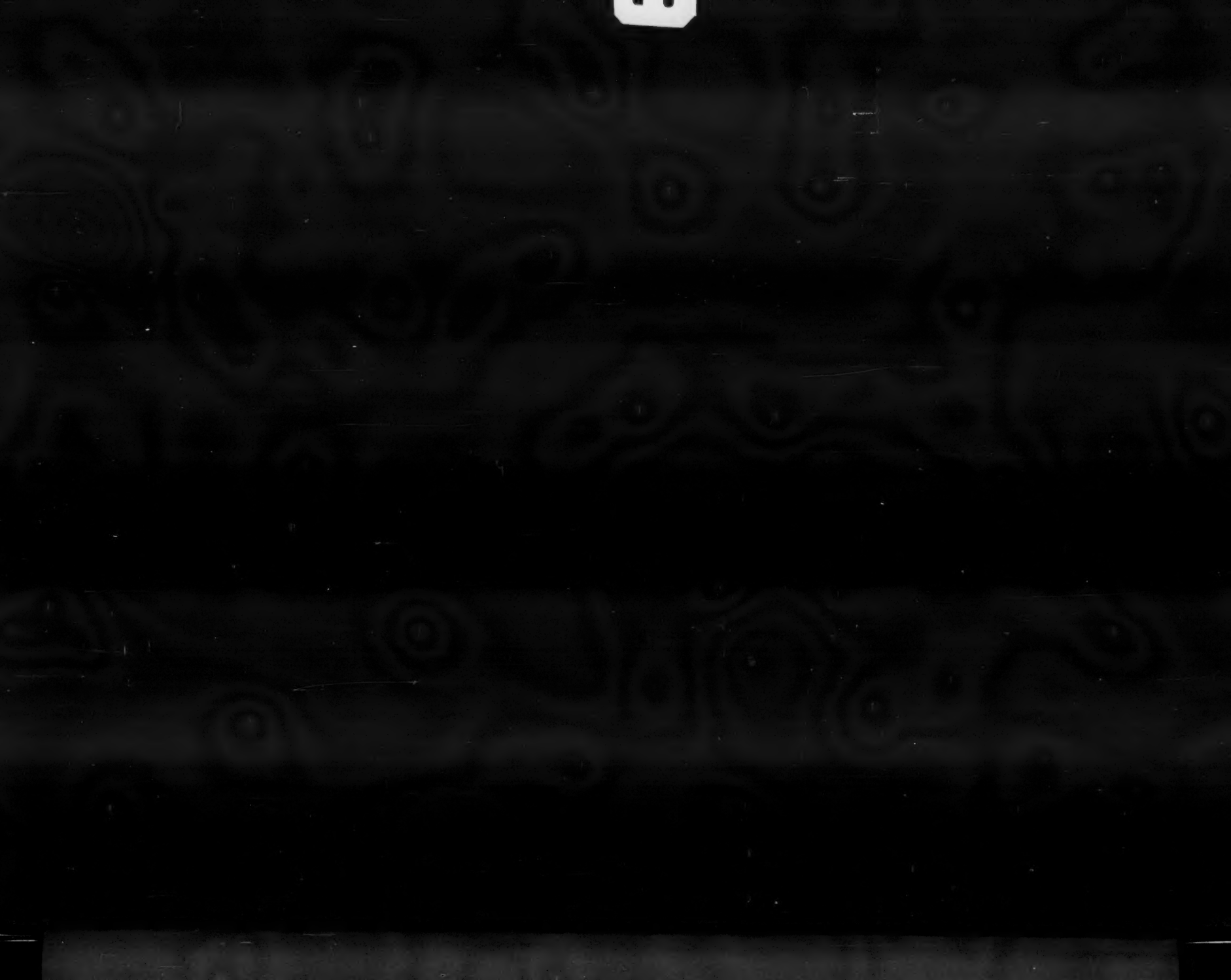
UNITED STATES GOVERNMENT PRINTING OFFICE, WASHINGTON : 1961